

Traffic Calming Radar for Low Traffic Density Roads



Prepared by:
Carl Jacob Wesselink
WSSCAR008

Prepared for:
Dr M. Y. Abdul Gaffar
Dept. of Electrical and Electronics Engineering
University of Cape Town

October 23, 2024

Submitted to the Department of Electrical Engineering at the University of Cape Town in partial fulfilment of the academic requirements for a Bachelor of Science degree in Mechatronic Engineering

Key Words: Traffic Calming Radar

Declaration

1. I know that plagiarism is wrong. Plagiarism is to use another's work and pretend that it is one's own.
2. I have used the IEEE convention for citation and referencing. Each contribution to, and quotation in, this report, Traffic Calming Radar for Low Traffic Density Roads, from the work(s) of other people has been attributed, and has been cited and referenced. Any section taken from an internet source has been referenced to that source.
3. This report, Traffic Calming Radar for Low Traffic Density Roads, is my own work and is in my own words (except where I have attributed it to others).
4. I have not paid a third party to complete my work on my behalf. My use of artificial intelligence software has been limited to the use of ChatGPT for the following purposes:
 - Generation of BibTeX for referencing sources.
 - Summarizing sources and extracting key information therefrom.
 - Generation of Latex code, specifically equations and image inserts.
 - Identification of errors concerning latex code when the document did not compile.
 - Explanation of some topics if needed.
 - Correcting Matlab code.
5. I have not allowed and will not allow anyone to copy my work with the intention of passing it off as his or her own work.
6. I acknowledge that copying someone else's assignment or essay, or part of it, is wrong, and declare that this is my own work.

Word Count = 18 300



October 23, 2024

Jake Wesselink

Date

Acknowledgements

Now that I sit here, in the seat that I have sat for the last four years completing all the work that this Engineering degree had me do, I am truly grateful for the people who have guided me along the way.

First and foremost, to my parents, Dot and Carl, I love you. Thank you for everything that you have done. I know my path to this degree took a few detours but we made it. I owe it all to you.

Second, to my supervisor for this project, Dr Abdul Gaffar, you have been a pillar of stability throughout this semester. I can still recall your voice echoing around Snape LT1 during your second-year electronics course. I am so glad that our relationship was formed then, and that we managed to continue it this year with this project. Our weekly meetings were a highlight, and your company so inviting. Thank you for all the effort you put in, I could never repay you.

Next to my other lecturers, thank you all for teaching me the bits and bobs needed to be considered an Electrical Engineer.

To my sisters, Ella and Ruth, thank you for always having my back. Know that I always have yours. I love that we have all taken such different paths, and I am so lucky to call you family.

To my friends, you are all legends. I would not have been able to get through some of the days without that joke that made me smile just a little, or the cup of tea you brought to my room, or that hug when I needed it most. I see the value you have in my life and I will never forget that.

To Meysie Meys, Tayla and Nick, thank you for helping me record my data. I know it wasn't what you felt like doing on a beautiful Saturday but I couldn't have done it without you.

To Tinashe, Ankush, Murray, Dylan, Dylan and Dan, the Con-Men, thank you for the laughs, late-night study sessions, worked solutions and (bunked) lectures. I could not have asked to have made better friends at Uni.

To myself - you did it!

Abstract

This report details the testing and evaluation of two low-cost radar systems, the MIT Coffee-Can radar and the IPM-165 radar chip, for vehicle speed monitoring in low-traffic-density urban areas. The investigation aimed to contribute to the development of modernised traffic-calming devices by assessing the performance of low-cost radar systems. Existing commercial system's prices can exceed R 50 000, making them undesirable for use in low-traffic areas such as housing complexes, school and university campuses or shopping centres.

The project involved performing speed detection tests on both devices, and analysing the data in order to evaluate performance. It then went on to advise if either system was suitable for integration into a comprehensive traffic-calming solution. In general, it demonstrated that there was a trade-off between performance and cost-effectiveness. However, the MIT Coffee-Can system did perform adequately enough, when compared to similar commercial systems, to warrant continued investigation.

Contents

List of Figures	viii
List of Tables	xi
Abbreviations	xii
1 Introduction	1
1.1 Subject of Report	1
1.2 Application Area and Motivation	2
1.3 Background of Investigation	2
1.4 Problem Statement	4
1.5 Objectives	5
1.6 Project Scope	5
1.7 Methodology Overview	6
1.8 Plan of Development	6
2 Literature Review	8
2.1 Introduction	8
2.1.1 Contextual Background	8
2.1.2 Radar Today	9
2.1.3 Application to the Automotive Industry	10
2.1.4 Vehicle Speed Detection	10
2.1.5 Experimental Low-Cost Solutions to Traffic-Calming	10
2.2 Discussion	11
2.3 Theory Development	11
2.3.1 Overview	11
2.3.2 Radar Theory	14
2.3.3 Signal Theory	18
2.4 Conclusion	23
3 Processing Pipeline	24
3.1 Overview	24
3.2 Recording Import and Analysis	24
3.3 STFT	25
3.4 Conversion From Doppler Frequencies to Speed	26
3.5 Normalisation and Plotting	26
3.6 CFAR	29
3.7 Simulated Results	32

3.7.1	Code Alterations for Simulated Data	32
3.7.2	Results	33
4	Experiments and Testing Plan	36
4.1	Systems Overview	36
4.2	MIT Coffee-Can	36
4.2.1	Working Principles	36
4.2.2	Block Diagram	36
4.2.3	System Specifications	37
4.3	IMP-165	37
4.3.1	Working Principles	39
4.3.2	Block Diagram	39
4.3.3	System Specifications	39
4.4	Test Procedure	40
4.4.1	Test Plan	40
4.4.2	Experimental Methodology and Setup	42
5	Results and Discussion	44
5.1	Controlled Tests	44
5.1.1	Constant Speed Tests	44
5.1.2	Varying Speed Tests	46
5.1.3	Range Tests	47
5.1.4	Two Car Tests	47
5.2	Uncontrolled Tests	49
5.2.1	Large Vehicle Test	49
5.2.2	Multiple Vehicle Tests	50
5.3	CA-CFAR	50
5.3.1	Setting the PFA	51
5.3.2	Setting the Number of Reference and Guard Cells	52
5.3.3	CA-CFAR Comparison Between Systems	53
5.4	Discussion	55
5.4.1	Speed Estimation Performance	56
5.4.2	Detection Range Comparison	56
5.4.3	CFAR Comparison	57
6	Conclusion	59
6.1	Coffee-Can	59
6.2	IPM-165	60
6.3	Performance Comparison	60
6.4	Practical Implications	60
6.5	Limitations and Recommendations	61
6.6	Summary	61
	Bibliography	62

.1	Appendix A	68
.2	Appendix B	69
.2.1	MIT Coffee-Can Spectrograms	69
.2.2	IPM-165 System Spectrograms	69
.3	Appendix C	73
.4	GitHub	76

List of Figures

1.1	Common Traffic Calming Techniques.	1
1.2	Images of Two Common Types of Speed Monitoring Devices.	3
1.3	Digital Traffic Calming Device	3
1.4	Example Spectrogram of Simulated Data Displaying Different Ranging Abilities	6
2.1	Dowding Radar System	8
2.2	AN/MPQ-39 Continuous-Wave (CW) Hawk Missile System	9
2.3	AN/FPS-16 Precision Tracking Radar	9
2.4	Modern Applications of Radar in Warfare	9
2.5	Basic Radar Concepts	12
2.6	Overview of Electromagnetic Radiation and Radar Frequencies	13
2.7	The Doppler Effect	13
2.8	Test Scenario and Associated Simulated Spectrogram	14
2.9	Basic Radar Block Diagram	14
2.10	Radar Modulation Techniques	16
2.11	Comparison of Radiation Patterns	16
2.12	Comparison of Radar Antennas	17
2.13	Simulation of Various Forms of Continuous Time Domain Return Signals	18
2.14	Example Time-Domain Recording of Cars Travelling Passes a Radar Device	19
2.15	Discrete Time Fourier Transforms of Simulated Return Signal	19
2.16	Plot of Three Types of Window Functions	20
2.17	Visual Representation of Spectral Leakage on Spectrogram Plot	21
2.18	CA-CFAR Cell Diagram	22
2.19	CA-CFAR Detection Threshold Example	22
2.20	Example of CA-CFAR Applied to a Spectrogram	23
3.1	Full Code Process	24
3.2	Flow Diagram of STFT Function	25
3.3	Comparison of Scaling Techniques for Plotting Spectrograms	27
3.4	Spectrogram of Car Using N1 Normalisation	27
3.5	Spectrogram of Car Using N2 Normalisation	28
3.6	Spectrogram of Car Using N3 Normalisation	29
3.7	Flow Diagram of CA-CFAR Algorithm	30
3.8	Optimal Target Detection with High Probability of Detection $P_{FA} = 10^{-7}$, $N = 20$, $N_G = 6$	30
3.9	Comparison of Different P_{FA} Values $N = 20$, $N_G = 6$	31
3.10	Comparison of Different Numbers of Reference Window Cells $P_{FA} = 10^{-7}$, $N_G = 6$	31
3.11	Comparison of Different Numbers of Guard Cells $P_{FA} = 10^{-7}$, $N_G = 6$	32

3.12	Simulated Spectrogram of a Car at a Constant Velocity	33
3.13	Simulated Spectrogram of a Car at a Constant Acceleration	33
3.14	Simulated Spectrogram of Two Cars Travelling at Different Speeds	34
4.1	MIT Coffee-Can System	37
4.2	MIT Coffee-Can Block Diagram	37
4.3	IPM-165 System	38
4.4	IPM165 Radar Module Block Diagram	39
4.5	Comparison of the Three Vehicle Classes Used	41
4.6	Maps of the Test Sites Used	42
4.7	Images from Testing	43
5.1	MIT Coffee-Can System Tracking the Bakkie at Set Speeds	45
5.2	IPM-165 System Tracking the Bakkie at Set Speeds	45
5.3	IPM-165 System Tracking the Car at Changing Speeds	46
5.4	MIT Coffee-Can System Tracking the Car at Changing Speeds	46
5.5	Comparison of the Two Systems at a Height of 1 m, Tracking a Car	47
5.6	Comparison of the Two Systems at a Height of 1 m, Tracking a Car	48
5.7	MIT Coffee-Can System Tracking Two Cars	48
5.8	IPM-165 System Tracking Two Cars	49
5.9	Comparison of Both Systems Tracking a Large Vehicle	49
5.10	Comparison of Both Systems Recording a Busy Road with Multiple Targets	50
5.11	Comparison of Different PFA Values on an IPM-165 Spectrogram Plot	51
5.12	Comparison of Different PFA Values on an MIT Coffee-Can Spectrogram Plot	52
5.13	Comparison of the Thickness of the Visible Target in Both Radar Systems	53
5.14	Comparison of the CA-CFAR Algorithm Performed on Various Speed Recording from the MIT Coffee-Can System	54
5.15	Comparison of the CA-CFAR Algorithm Performed on Various Speed Recording from the IPM-165 System	54
5.16	Comparison of the CA-CFAR Algorithm Performed on Recordings of Multiple Targets from Both Systems	55
1	MIT Coffee-Can System Tracking the Car at Set Speeds	69
2	MIT Coffee-Can System Tracking the Car at Set Speeds	69
3	MIT Coffee-Can System Tracking the Bakkie Under Braking	70
4	MIT Coffee-Can System Tracking the Bakkie While Accelerating	70
5	MIT Coffee-Can System Tracking Multiple Targets	70
6	MIT Coffee-Can System Range Test Using the Car	71
7	IPM-165 System Tracking the Car at Set Speeds	71
8	IPM-165 System Tracking the Car at Set Speeds	71
9	IPM-165 System Tracking the Bakkie Under Braking	72
10	IPM-165 System Tracking the Bakkie While Accelerating	72
11	IPM-165 System Range Test Using the Car	72
12	Use of ChatGPT	73

13	Use of ChatGPT	74
14	Use of ChatGPT	74
15	Use of ChatGPT	75
16	Use of ChatGPT	75
17	Use of ChatGPT	76

List of Tables

1.1	Comparison of Commercially Available Speed Guns and Camera Systems	3
4.1	MIT Coffee Can Radar System Specifications	38
4.2	5V Regulator Specifications	39
4.3	LM358 Weak Signal Amplifier Module Specifications	40
4.4	IPM-165 Radar Module Specifications	40
5.1	Comparison of CA-CFAR Parameters for MIT Coffee-Can and IPM-165 Systems . .	53
1	Appendix A - GA Requirements	68

Abbreviations

ADC Analogue-To-Digital Converter

BPSK Bipolar Phase Shift Keying

CA-CFAR Cell-Averaging Constant False Alarm Rate

CUT Cell Under Test

CW Continuous-Wave

dB Decibel

DTFT Discrete-Time Fourier Transform

EM Electromagnetic

FM Frequency Modulation

FMCW Frequency-Modulated Continuous-Wave

ITS Intelligent Transportation System

lidar Light Detection and Ranging

LNA Low-Noise Amplifier

PFA Probability of False Alarm

RAF British Royal Air Force

RCS Radar Cross Section

SAR Synthetic Aperture Radar

SIMMWIC Silicon Monolithic Microwave Integrated Circuits

SMT Surface-Mounted Technology

SNR Signal-to-Noise Ratio

STFT Short-Time Fourier Transform

ZCD Zero-Crossing Detector

Chapter 1

Introduction

1.1 Subject of Report

This report details the testing and assessment of two low-cost radar systems in the application of vehicle speed monitoring in low-traffic urban residential areas. This investigation was driven by a desire to progress research into modernised traffic-calming devices to promote more responsible driving practices. According to Arrive Alive[1], traffic calming techniques are intended to slow or reduce motor-vehicle traffic to improve road users' safety. These techniques range from physical barriers such as speed bumps seen in Fig. 1.1a to visual warnings such as signs and speed displays shown in Fig. 1.1b. Current digital commercial speed detection systems are expensive, with a price range ranging from R 6 500 to R 55 000, and are tailored to highway traffic control and monitoring, as seen in Table 1.1 in Sec 1.3 below. Specialised traffic calming devices are more expensive still, costing between R 50 000[2] and R 120 000[3]. This report outlines the successes and shortfalls of two radar systems in estimating vehicle speeds. It goes on to assess the feasibility of further integration of these systems into a complete traffic-calming device that could be deployed to alert drivers of their speeds in urban residential low-car-density areas, such as small residential communities, academic campuses and roads with low-traffic densities.



(a) Speed Bump[4]



(b) Speed Limit Warning Sign[5]

Figure 1.1: Common Traffic Calming Techniques.

The broader area of research is aimed at creating a self-sustaining unit capable of being deployed in the specified urban environment to accurately detect and display, in real-time, the speeds of the cars travelling past it. This is to be done in such a way as to minimise costs while still having the desired effect of promoting good driver behaviour. To this end, the report's focus is on testing and quantifying

the performance of the two radar systems in a low-car-density environment. In addition, work was done to assess their functional abilities, advantages, and disadvantages and provides a recommendation for which system to continue to use in developing a radar-based, traffic-calming device.

1.2 Application Area and Motivation

Radar technology has in recent times become so widely usable and commercially available that one hardly considers the means behind a police officer's speed enforcement camera trap, the visualisations of weather patterns on the news, or even the speed of a tennis player's serve displayed on a big screen at Wimbledon[6]. However, these are all to some extent made possible through the plethora of radar applications in the modern world.

For the purpose of this report, radar technology was chosen as the means of experimental implementation due to a few defining characteristics. Firstly, radar is non-contact and non-invasive involving only the transmission of electromagnetic radiation in the radio-wave range. At this relatively low frequency, radar waves contain a fraction of the energy contained in, for example, X-rays. This makes radar safe for use in this application. Radar is also not a new concept, having first been experimented with in the 1880s [7]. Because of this, modern radar concepts and technologies are well-understood and accurate. Further, radar can operate at long ranges, and in almost any weather conditions, and is resilient against interference[8]. To this end, radar perfectly complements the basic car speed monitoring requirements as it is non-contact and acts over a practical range. To ensure ethical implementation, the technology must be safe for all parties involved, and to produce accurate results it needs to be reliable and able to perform in adverse weather and environmental conditions.

It is for this reason that a low-cost radar module could have multiple applications in the automotive industry other than just traffic calming. Most notably, the continued development of a radar 'gun' has - and could further - be used by police services globally to detect and penalise speeding motorists. This application concept could be extended to racing teams eager to determine the speeds of their cars on track. A slightly different implementation could benefit local governments in creating 'smart cities' where traffic flow can be monitored allowing for real-time monitoring, and also traffic light timing optimisation for reduced congestion. The likes of which can be seen in several applications as outlined in papers by Sánchez-Oro et al. in[9], Gómez-del-Hoyo et al. in [10], and Samczynski et al. in [11].

1.3 Background of Investigation

As vehicle speed detection is not a novel application of radar technology, especially in urban settings, many systems have already been developed and are in use. Most of these systems are designed and manufactured for the commercial markets with only a few catering to the experimental side of radar research and development.

The commercial systems in place that offer real-time speed detection, range from handheld devices often referred to as 'Speed Guns'[12] to mobile or fixed radar camera systems able to capture images as well as detect speeds[13]. Table 1.1 outlines some of these systems, and Fig. 5.5 provides pictures for reference.

1.3. Background of Investigation

Type	Name	Functionality	Price (R)
Speed Guns	PR1000-TA[14]	Vehicle and Athlete Speed Detection	13 900.04
	Speedster 3[15]	Traffic Control	29 810
	Bushnell Velocity Radar[16]	Vehicle Speed Detection	7 199
	Decatur Scout 2[17]	Vehicle Speed Detection	55 000
Camera Traps	ST-PSR-60T[18]	Speed Detection and Imaging	N/A
	Q1656-DLE Radar-Video Fusion[19]	Speed Detection and Surveillance	52 649
	Signalway Radar Speed Camera[20]	Traffic Monitoring	\$ 6 500

Table 1.1: Comparison of Commercially Available Speed Guns and Camera Systems



(a) Mobile Speed Camera[21]



(b) Handheld Speed Gun[22]

Figure 1.2: Images of Two Common Types of Speed Monitoring Devices.

Some companies have also focused radar applications specifically towards traffic calming. This process involves both speed determination and a real-time display of that speed to alert the driver. International companies such as Via[23] and Trafficalm [24] already produce commercial systems like this for use in urban settings in an attempt to improve road user safety. Such a device can be seen in Fig. 1.3 below.

Amongst these commercial systems lie experimental systems that have been developed to further research into radar used for speed detection and monitoring. Hagargund et al. present a technique for vehicle speed detection which utilises a **Zero-Crossing Detector (ZCD)** algorithm[25]. In this process, they estimate speed information based on the Doppler Shift Frequency passed through the **ZCD**. The benefit of this technique is that there is no need for expensive digital signal processors as there would be in other similar devices. Further, Fang et al. in [26], proposed a system capable of classifying



Figure 1.3: Digital Traffic Calming Device

vehicles through using a cost-effective K-band unmodulated CW radar. This device was shown to be capable of measuring traffic parameters such as vehicle speed, traffic flow rate and vehicle classification for application in an Intelligent Transportation System (ITS)[26]. Finally, Xu et al. addressed the challenges of high-speed vehicle detection through the use of an innovative Doppler-Range Processing Algorithm[27].

These papers have contributed towards the development of radar in the use of vehicle speed detection, all addressing different areas that need continued research. Through published research, a greater understanding is developed allowing for more advanced systems to be developed which in turn makes way for more reliable results and specialised applications. However, some areas still required investigation, as identified in Section 1.4 below.

1.4 Problem Statement

As this report assesses the performance abilities of two low-cost radar systems, it is necessary to investigate the literature already published in this field to gauge the areas where challenges may lie and how they might be solved. A key aspect of this, as seen in the papers discussed below, is the trade-off between cost-saving and performance.

When systems are engineered to ensure minimum cost implications, innovative ways to achieve optimal performance are utilised. For instance, the authors involved in designing a low-cost Doppler radar sensor for traffic monitoring[28] were able to obtain a vehicle detection range of 300 metres when deploying their cost-effective device constructed from a multilayered PDB and discrete components. Rasshofer and Biebl in [29] managed to distinguish between approaching and receding vehicles in a similarly cost-effective manner. Further, Heide et al. produced a highly sensitive radar device, and discussed the suitability for large-scale deployment[30].

However, these systems did not come without their own challenges. Most notably, the use of commonly available surface mount components induced noise into two of the systems[28] [29]. Even though the device from Rasshofer and Biebl [29] produced promising results, it only did so at a range of 3 metres or less which is not suitable for many applications. The device developed by Heide et al.[30] needed to be meticulously calibrated to achieve the desired results. This is all compounded by the fact that the newest of these systems[28], was developed in 2007, whereas the others [29] and [30] were developed before the turn of the 21st century, possibly rendering these systems obsolete when compared to newer technology.

As can be seen in the three systems discussed above, cost-effective solutions to vehicle speed estimation have been researched. However, here lies the disparity, because, as seen in the prices of the systems in Table 1.1, these systems would not be considered 'low-cost'. In addition, these are commercially available they do not contain detailed reports on their functionality or operating algorithms. This gap in relevant available resources is further emphasised by the fact that all of the experimental systems outlined above were published more than 17 years ago. This indicated a potential disparity between the commercial systems available today and the research-driven low-cost systems developed many years ago, a disparity that this report sought to address.

This project was undertaken to fill a gap in the current literature. The problem statement for this report is as follows:

This project aims to investigate the performance capabilities of two modernised low-cost radar devices in a low-car-density environment to evaluate whether their functionality is adequate enough to warrant widespread integration compared to, commercially available systems. In this, a critical evaluation of the trade-offs made between low cost and performance (specifically speed determination and range detection) was addressed. In doing so, this report gave insight into how experimental systems have developed, bridging a gap between past and present and providing a guide for future innovations.

1.5 Objectives

Based on the problem statement defined above, the following objectives were outlined:

- Objective 1: Plan and execute experiments to test two low-cost radar systems, the MIT Coffee-Can radar system and the IPM165_F radar chip, in their ability to estimate the speed of moving vehicles.
- Objective 2: Compare the performance of these devices to that of commercially available alternatives.
- Objective 3: Assess the feasibility of both devices for use in the required application of low-speed traffic calming in urban residential areas.

1.6 Project Scope

Based on the objectives defined above, the scope of this project is limited to:

- Work on the MIT Coffee-Can radar device and IPM-165_F radar chip, and relevant components.
- The area of testing is focused on low-car-density urban areas such as schools, university campuses, and housing complexes.
- The data will be recorded using the Asus Xonar U5 Sound Card for later processing on Matlab.
- The evaluation of low-cost systems in vehicle speed detection, and comparison to similar, commercially available products.

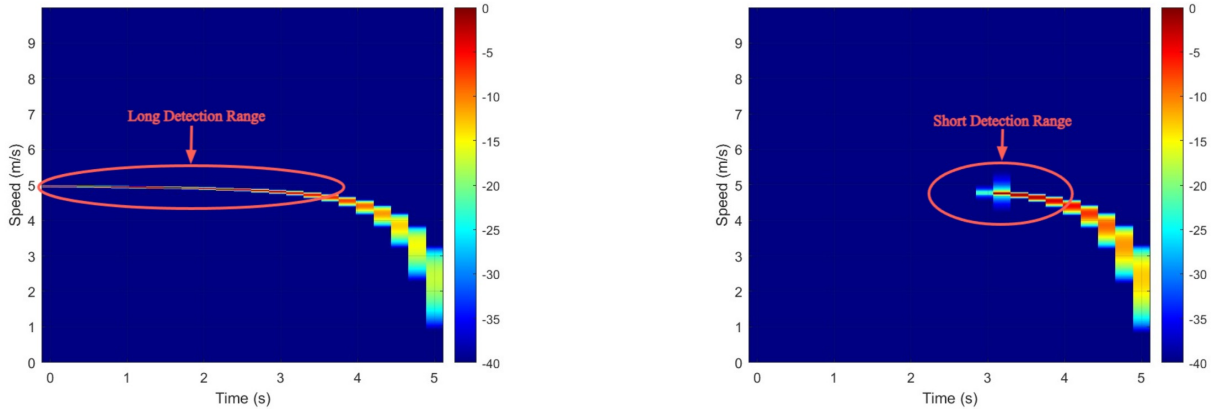
The scope of this project excludes:

- The use of other radar types or processes.
- The real-time implementation of these systems and integrated, automatic speed displays.
- The use on pedestrians or non-vehicles.
- The evaluation of the system's effectiveness in slowing traffic in the areas defined.

1.7 Methodology Overview

A high-level overview of the methodology can now be drawn from the project's objectives and scope defined in Sections 1.5 and 1.6 above.

1. Design and implement Matlab code capable of importing Radar recordings and processing them to be able to produce a Spectrogram which displays the target's velocity over time on a heat intensity map.
2. Test the code on simulated data in Matlab to ensure the correct functionality.
3. Design a test procedure to collect radar data of vehicles to comprehensively test the functional abilities of both the systems in question.
4. Carry out this test procedure to obtain the necessary results.
5. Analyse these results, comparing them to the performance of commercially available products. The radar performance of these systems was judged on the length of time a given radar device was able to detect the speed of a vehicle. Examples of long and short detection ranges can be seen in Fig. 1.4a and Fig. 1.4b below respectively, where a car was travelling at 5 m/s towards the radar, starting at an initial distance of 25 m.



(a) Spectrogram Displaying Long Range Abilities

(b) Spectrogram Displaying Short Range Abilities

Figure 1.4: Example Spectrogram of Simulated Data Displaying Different Ranging Abilities

6. Finally comment on the feasibility of integrating these low-cost systems into a fully functioning device capable of performing real-time speed detection for traffic calming purposes in low-traffic residential areas.

1.8 Plan of Development

This report begins in Chapter 2 with a detailed literature review of the current vehicle speed detection techniques and systems. This also includes an in-depth explanation of the signal and radar theory needed to understand the workings of the systems evaluated in this report. The following chapter, Chapter 3, defines the methodology used during this project, detailing the coding algorithms developed

and the simulated results they produced. The test plan comes next in Chapter 4 where all the experiments performed are fully defined. This chapter includes a breakdown of both the systems used, namely the MIT Coffee-Can radar device and the IPM165_F radar chip, defining their key features and implementation strategies. Following this, Chapter 5 presents the results obtained from the conducted experiments, accompanied by a comprehensive discussion and analysis of these findings. Finally, the conclusion in Chapter 6 provides the verdict on the abilities of these systems to accomplish the tasks at hand specifying their successes and shortcomings and then providing recommendations for future work and necessary research.

Chapter 2

Literature Review

Why did the rookie technician allow a German zeppelin to fly over Allied airspace?

-It was just a blimp on the radar!

2.1 Introduction

2.1.1 Contextual Background

Although Radio Detection and Ranging (radar) was first experimented on in the late 1880s by Heinrich Hertz, it would have to wait until the mid-1930s to gain attention beyond the minds of just scientists and physicists[7]. It was at this point, when the prospect of a new war in Europe seemed inevitable that many countries began work developing radar systems for their own military capabilities. The most notable of these became the Chain Home stations, as seen in Fig. 2.1[31], in Britain that were integrated into the Dowding System to alert the [British Royal Air Force \(RAF\)](#) of incoming Nazi German air raids and bombing runs during the second world war[32]. This early use of the technology gave the [RAF](#) an early warning system, allowing for time to launch aircraft to intercept the bombers and defend their territory, eventually helping them win the Battle of Britain[33].

Following the Second World War, radar systems continued to be refined and improved, leading to some major new innovations such as Coherent radars, pulse compression, and monopulse tracking.



Figure 2.1: Dowding Radar System

Coherent system technology, utilising klystron and amplitron tubes for the amplification stage of the radar system, allowed radar systems to better distinguish between stationary and moving targets, as well as improved clutter rejection. These developments were integrated into air and missile defence systems such as the Hawk Missile System seen in Fig. 2.2[34] below, developed by the United States of America (USA). Pulse compression, on the other hand, was an adaptation to the format of the signal that was transmitted from the radar device. Here, Linear FM (chirp) or phase-coded pulses were emitted containing more energy which improved the detection range available. Monopulse radar was developed to improve tracking accuracy by allowing for the measurement of the trajectory of the target to be made using only a single pulse rather than multiple pulses. The AN/FPS-16 was a notable example of a precision monopulse tracking radar developed in the 1950s for guided missile tracking and can be seen in Fig. 2.3[35] below.



Figure 2.2: AN/MPQ-39 CW Hawk Missile System



Figure 2.3: AN/FPS-16 Precision Tracking Radar

Figure 2.4: Modern Applications of Radar in Warfare

2.1.2 Radar Today

Today radar still plays a critical role in many applications that serve the public at large. It has become synonymous with air traffic control[36], providing precise aircraft location and altitude information[8]. It also still remains a critical component of modern warfare[8], being used for missile guidance[8], early warning systems[8], and surveillance[8]. Phase-array radars[37] have been developed to this end to provide faster scanning abilities in target acquisition[37]. Other functionalities include weather monitoring where Doppler radar is used in meteorology for forecasting and storm prediction[8]. Synthetic Aperture Radar (SAR)[6] is also extensively used in geological studies due to its high-resolution imaging capabilities[6], and satellites use radar to map Earth's terrain and monitor ground deformation[38].

The long list of reasons why radar is so effective underlines its ongoing wide use. Radar has the ability to perform well in almost all weather and lighting conditions, making it more versatile than optical systems such as cameras or infrared sensors[6]. The radio waves it emits are not hindered in the same way that say smoke or fog would obscure a camera's view. It can also detect and track targets over very long distances, outperforming Light Detection and Ranging (lidar) devices that use laser light rather than radio waves to obtain similar target information but struggle in rain and poor weather[39].

2.1.3 Application to the Automotive Industry

The miniaturisation of radar chips has allowed them to be integrated into the automobile industry for accurate and reliable target detection[40]. For this, phase and Frequency-Modulated Continuous-Wave (**FMCW**) radar systems are utilised[40]. To this end, radar has been used for adaptive cruise control[41], ensuring a safe distance to the vehicle in front, and for pre-collision warnings, avoidance, and mitigation through reactive measures. According to a study done by Eichelberg (2016), around 90% of drivers would want adaptive cruise control and forward collision avoidance stating that it made driving ‘less stressful’[42].

Radar has also found applications in the automotive industry from outside of the vehicle. In an effort to reduce the energy consumption of street lights, researchers in [43] propose a radar-based detection system capable of only turning on the lights when a vehicle is approaching. This study showed that the energy savings could amount to as much as 60% [43]. Further adaptations for radar include a pedestrian traffic-light triggering mechanism, used to improve traffic flow and pedestrian safety[44]. Both these systems act as a step towards ‘Smart Cities’, with the aim of utilising infrastructure based around technological adaptations to improve overall efficiency[45]. Further, and possibly most familiarly, radar has found a common place in vehicle speed detection and monitoring.

2.1.4 Vehicle Speed Detection

As seen in Table 1.1, many modern-day systems exist and are used to determine the speeds of vehicles in moving traffic. For law enforcement, this is often used to issue fines to non-law abiding citizens, whereas, other applications in traffic calming devices only look to improve road user safety by encouraging slower driving speeds. The radar gun systems tend to have a range of around 500 m [16] [15] [14], and have a large speed detection window ranging from close to 0 km/h to well over 150 km/h. Commercial traffic calming devices, on the other hand, have been shown to offer slightly shorter-ranging abilities, offering only around 360 m [46] for a similar speed window. These systems often come with supporting equipment such as the LED display, battery system and solar panels which can inflate the price to over R 50 000[2], or even beyond R 120 000[3]. This price tag may present a barrier to uptake and suggests that there is a need for a lower-cost solution to traffic-calming radar devices.

2.1.5 Experimental Low-Cost Solutions to Traffic-Calming

As noted, there exists a gap in the commercial market for low-cost traffic-calming radar devices. Researchers from the following papers have attempted to fill this gap through innovative, cost-saving techniques.

The authors in [28] were able to reduce overall costs by using standard Surface-Mounted Technology (**SMT**) components when developing their traffic monitoring radar system. Being widely available, these components are cheaper than alternatives. They also opted to use a fibreglass-reinforced multi-layer PCB, which is cheaper than the standard PTFE-based substrates[28]. However, the use of these **SMT** components introduced noise into the system resulting in the need for a Low-Noise Amplifier (**LNA**) with a 10 dB gain and a noise figure of 1.5 dB to be included in the design. This system was able to produce reliable speed detection results at a maximum range of 300 m and under 3% error when used in vehicle length-measurement mode[28].

In a paper by Rasshofer and Biebl[29], an innovative mechanism to obtain direction-sensitive velocity information is outlined. The radar sensor employs a homodyne I/Q detection method to distinguish between approaching and receding targets, using a combination of active integrated antennas and rectennas[29]. **Silicon Monolithic Microwave Integrated Circuits (SiMMWIC)** were used to ensure low production costs by allowing for the entire system to be deployed on a single chip. The homodyne I/Q detection system allowed for direction-sensitive information to be captured. This was done by ensuring the rectenna was placed correctly in relation to the antenna to obtain a 90-degree phase shift between the in-phase (I) and quadrature (Q) signals. Additionally, Schottky rectennas were utilised to ensure low noise and high sensitivity.

Finally, the authors, Heide et al. in [30] have outlined the design for a high-precision vehicle speed and position measurement system which uses spread-spectrum coding to enhance its sensitivity and provide range selectivity. This process involves **Bipolar Phase Shift Keying (BPSK)** encoding to focus the Doppler signal evaluation to a certain range while at the same time improving the system's **Signal-to-Noise Ratio (SNR)**. In order to reduce costs, Heide et al. favoured low-cost components such as the dielectric resonator oscillator and Schottky diode detector that were used[30]. The result was a system that was both highly accurate and affordable for large-scale deployment.

2.2 Discussion

This literature survey has outlined the extensive evolution of radar technology, from its historical military origins to widespread integration into everyday life. Its adaptability, and ability to function in almost all climatic conditions have allowed it to remain vital in applications such as air traffic control, weather monitoring, and military systems. Radar has also found a place in the automobile industry, being used for adaptive cruise control and collision avoidance systems. It has also shown promise for integration into smart cities, allowing for the monitoring and control of traffic and pedestrian movement.

The growing need for low-cost radar solutions in the context of traffic-calming radar has also been identified. Current commercial systems are relatively expensive, which opens an opportunity for innovations in the development of more low-cost solutions. Commercial companies are also reluctant to share any details as to the systems and processes implemented to produce the functionality that they have achieved. This gap in the available literature and the commercial market has given rise to some low-cost experimental systems. Several advancements have been made to this end as seen in the papers discussed in 2.1.5. These systems each provided a low-cost, innovative way to solve a particular challenge relevant to the research task. However, they were developed over 17 years ago, highlighting the need for newer technological advancements in vehicle speed identification and radar-based traffic calming.

2.3 Theory Development

2.3.1 Overview

In its most basic form, radar can be thought of as an transmitting a signal and recording and processing the received echo. In the same way that a voice would reverb off a mountain face, a piece of

Electromagnetic (EM) radiation produced by a transmitter could be 'heard' at some point later by the receiver after bouncing off its target. This phenomenon can be seen in Fig. 2.5[47].

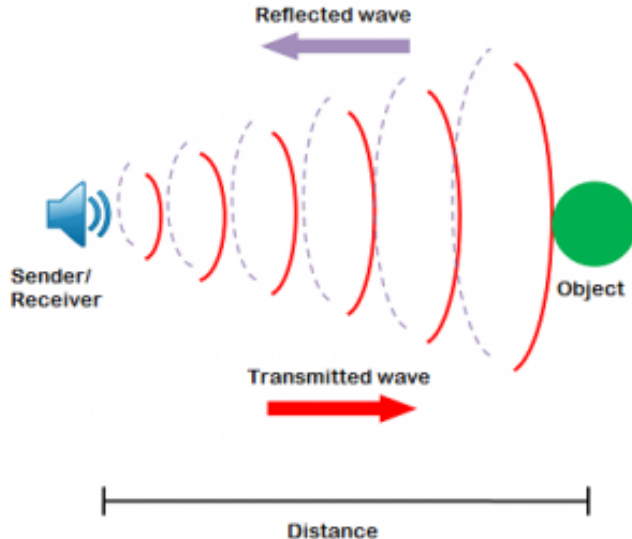


Figure 2.5: Basic Radar Concepts

More similar still is that because the speed of sound is known when passing through particular mediums, EM radiation is known to travel at the speed of light, $c = 3 \times 10^8 \text{ m/s}$ [8]¹, and it is this detail that makes radar possible, just as the speed of sound makes the likes of sonar possible. In its most simple case, the range to a target can be calculated using the following formula:

$$R = \frac{c \cdot \Delta T}{2} \quad (2.1)$$

Here c is the speed of light, ΔT is the change in time between the signal being sent and then received and R is the range to the target. It is necessary to divide by 2 because the time taken encompasses the time to and from the target, doubling the distance.

The range equation 2.1 only provides a portion of the possible information that radar can produce, so to unlock the next piece one has to understand a little more about EM radiation and the Doppler effect, discussed below.

EM radiation waves are electric and magnetic field waves oscillating perpendicularly through space at a defined frequency. The spectrum of possible frequencies ranges from roughly $1 \times 10^0 \text{ Hz}$ all the way up to $10 \times 10^{24} \text{ Hz}$, and includes visible light. This spectrum can be seen in Fig. 2.6a. Radar operates in the radio range region from 3 MHz to 300 GHz[6], with defined bands as can be seen in Fig. 2.6b below. The use of these bands has been sectioned according to international agreements as different frequencies provide varying functionality. In general, lower frequencies are better suited to longer-range applications whereas higher frequencies are preferred for finer-resolution applications such as angle sensitivity[6].

¹The true speed of light is 299,792,458 m/s, however for most radar applications this approximation is sufficient[48]

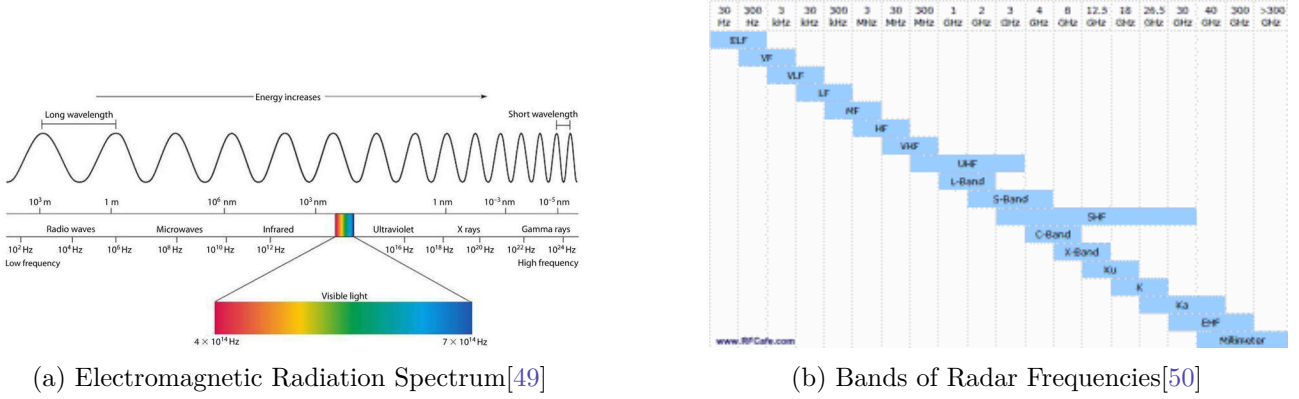


Figure 2.6: Overview of Electromagnetic Radiation and Radar Frequencies

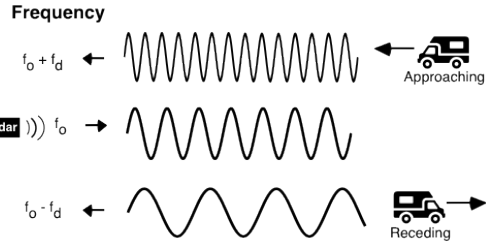


Figure 2.7: The Doppler Effect

On the other hand, the Doppler effect, being a cornerstone of radar, is the physical phenomenon whereby the frequency emitted from an observer will be 'heard' at a different frequency depending on the movement direction of the target[51]. Regarding Fig. 2.7[51] below, if the observer emits a signal at F_0 towards a stationary target, the received signal will be at an unchanged frequency. However, if the target is moving in relation to the observer, the received signal will be different frequency relative to the speed of the target, as expressed as $F_0 \pm F_d$. This change in frequency is known as the Doppler frequency (F_d) and can be used to obtain the target's speed as seen in equation 2.3. It must be noted that this equation only accounts for when moving directly towards or away from the observer

$$V = \frac{\lambda \cdot F_d}{2}, \quad \text{where} \quad \lambda = \frac{c}{F_0} \quad (2.2)$$

With this information, a useful tool (the spectrogram) can now be used to aid the visualisation of radar speed detection. A spectrogram plots a Time vs. Speed/Frequency graph, displaying the speeds of targets at a certain time interval on an intensity scale depending on the strength of the received signal. Imagine a car travelling down a straight road towards a speeding camera trap set slightly to the side, as seen in Fig. 2.8a below. The transmitted signal F_0 is rebounded off the car at $F_0 + F_d$. The receiver picks this up and through some signal processing extracts F_d . This frequency is then converted to a velocity using Equation 2.3. It is important to note that the vehicle's radial speed drops to zero when it moves directly in line with the radar device. This occurs because the Doppler effect depends on relative motion between the source and the observer. At the moment the vehicle passes directly in front of the radar, there is no longer any relative radial velocity, resulting in no detectable Doppler shift. To account for this angular component, Equation 2.2 is amended to only solve for the linear velocity, as seen in 2.3. Fig. 2.8b gives a visualisation of this effect where a target starting at an initial

distance, R_0 , of 25 metres is seen to be travelling at a speed, V_0 , of 5m/s. At this point, the detected speed, V_0 , is essentially the same magnitude as the car's actual speed, V_x . As the car approaches the radar device, the radial speed detected by the device begins to drop to 0m/s due to the speed of the vehicle being entirely tangential, as θ tends towards 90°.

$$V = \frac{f_d \cdot c}{2f_0 \cos(\theta)} \quad (2.3)$$

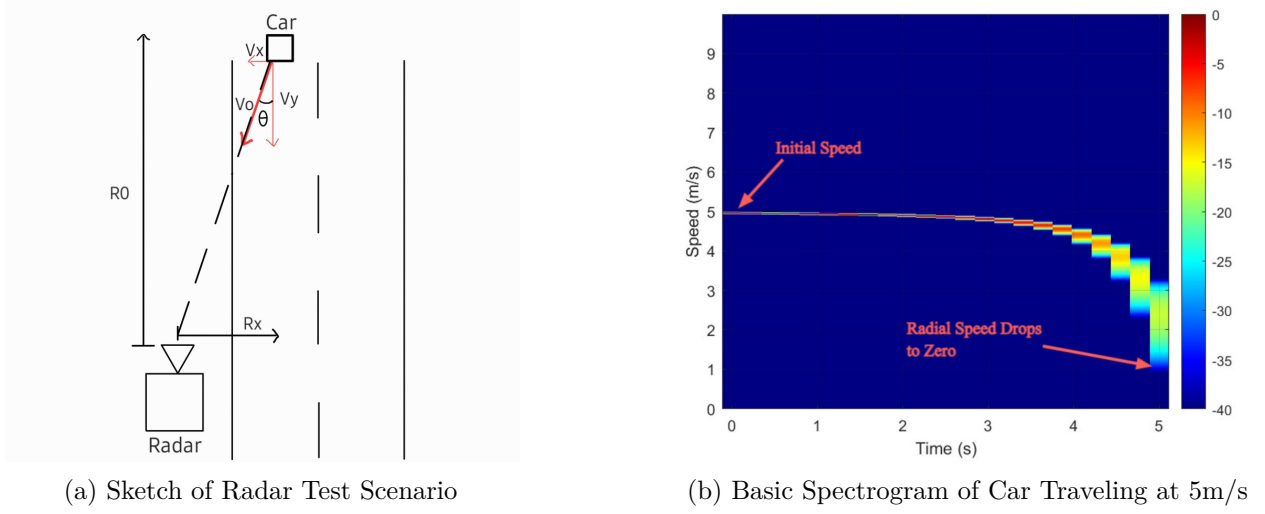


Figure 2.8: Test Scenario and Associated Simulated Spectrogram

2.3.2 Radar Theory

Now that the basic radar principles have been outlined, a breakdown of the steps needed to form the spectrogram of a moving target needs to be made. This next section outlines the radar theory in greater depth than was used throughout this report.

Radar Principles

Fig. 2.9[6] shows the fundamental workings of almost all radar devices. Application and design may vary between different devices, but the basic block components remain the same, those being: a

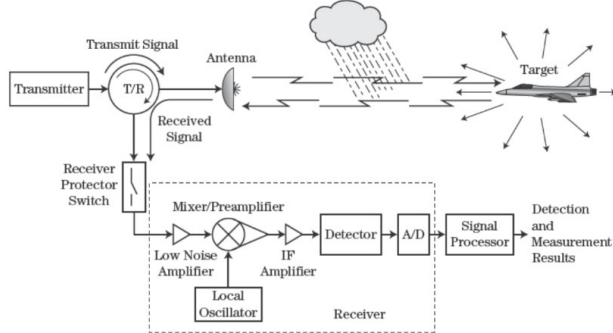


Figure 2.9: Basic Radar Block Diagram

transmitter and receiver, antenna and signal processor[6]. In general, a transmitter generates a signal that is radiated out into the atmosphere via the antenna. This signal is reflected off the objects it encounters with an intensity relative to the size, shape and structural components of the object. This term is known as the **Radar Cross Section (RCS)** and each target is assigned a value denoted by ' σ ' in mathematical computations. The **RCS** of a typical small vehicle varies between -12 dBsm and 25 dBsm.[52] The receiver then picks up these reflected signals which include both that of the desired target and the clutter from the undesirable objects. This signal is then passed through a series of filters and amplifiers in an attempt to isolate the desired signal and remove noise. The signal is then digitalised through an analogue-to-digital converter, before being passed through some form of signal processor to extract the relevant information in a usable format.

The diagram in Fig. 2.9 defined the components needed to build a radar device, but understanding how to quantify its performance is in most cases a judge of range ability. The Radar Range Equation, as seen in Equation 2.4 below relates the aspects of the physical radar device and the target as well as factoring in various losses to determine the maximum range at which a device can detect a target. Losses are generally caused by either system losses in the circuitry or components used or through propagation and environmental losses that result from attenuation of the signal caused by the medium through which the wave travels[8].

$$R_{\text{det}} = \left[\frac{P_t G_t G_r \lambda^2 \sigma n_p}{(4\pi)^3 \text{SNR} k T_0 F B L_s} \right]^{\frac{1}{4}} [8] \quad (2.4)$$

- P_t : Transmitted power.
- G_t and G_r : Transmitter and Receiver antenna gain respectively.
- λ : Wavelength of the radar signal ($\frac{c}{F_0}$).
- σ : **RCS** of the target.
- n_p : Processing Gain.
- **SNR**: Signal-to-noise ratio (SNR).
- k : Boltzmann's constant, $1.3807 * 10^{-23}$ Joules per Kelvin.
- T_0 : Standard noise temperature (usually 290 Kelvin).
- F : Noise figure of the radar system, noise introduced during signal processing.
- B : Bandwidth of the radar signal.
- L_s : System losses in the radar.

A key element of this equation is the SNR which represents the ratio of the power of the received signal to the power of the noise in the system. Each device has a minimum detectable **SNR** (SNR_{min}) which represents the lowest distinguishable signal power that is recognisable by the device[8]. This factor will also relate to the minimum **RCS** (RCS_{min}) needed for a given target to be detected at a given range.

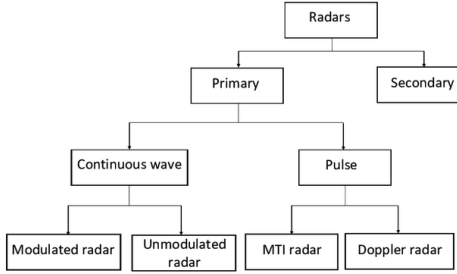


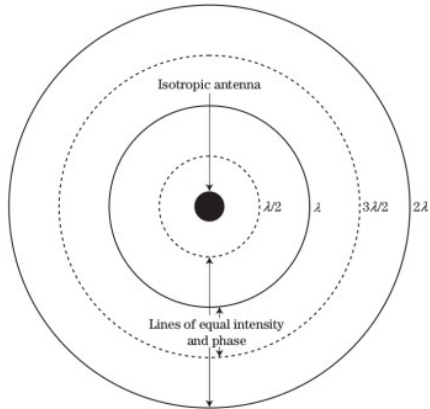
Figure 2.10: Radar Modulation Techniques

However, these factors and details cannot be explored further without first discussing the different types of radar devices and the processes they utilise.

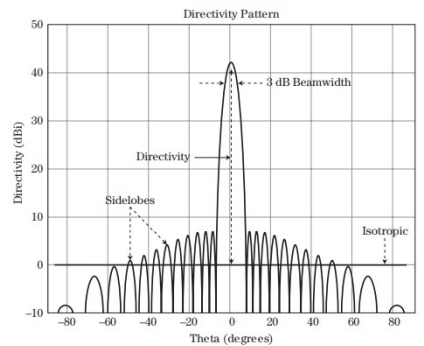
Radar Types

There are two main types of waveforms that a transmitter can produce, **CW** and Pulsed radar. These each have their own subbranches and categories of waveforms that can be emitted, as seen in Fig. 2.10[53], depending on the modulation techniques used. Each of these has its own set of advantages and limitations. **CW** radar is generally more limited in its application than Pulsed Radar, only being used for speed, and object detection with some variations able to be used for ranging as well. Pulsed radar can accomplish this and can be used for long-range targeting and precise distance measurements, as well as having applications in weather forecasting and high-resolution imaging for medical processes.

Additionally, the radiation pattern used by a radar device can greatly affect its performance and functionality[8]. To gain some perspective here, an isotropic antenna will be considered. This unrealisable radar pattern acts as a point source from which it can transmit in all directions equally. The propagation pattern can be seen in Fig. 2.11a below.



(a) Isotropic Radiation Pattern



(b) Directive Radiation Intensity

Figure 2.11: Comparison of Radiation Patterns

In this case, the power density (W/m^2) measured at a distance R (m) away from the antenna would be:

$$Q_t = \frac{P_t}{4\pi R^2} \quad (2.5)$$

where P_t is the total power radiated.

In contrast, if the radiation pattern is directive, a radar device can achieve greater performance, but will be limited to its field of view[8]. This is demonstrated in Fig. 2.11b where the power density is concentrated into a beam focused in the direction of the antenna.

Radar systems can also be classified by the structural makeup of their transmitter and receiver antenna. Simply, a radar device is known as monostatic if both the transmitter and receiver antennas are collated, often being the same antenna[6]. Bistatic radar devices, on the other hand, have these antennas separated, as was the case in the Dowding System used by Britain during the Second World War, seen in Fig. 2.1. Additionally, antennas have, over the years, been developed to optimise their performance in certain areas of application. Two common antenna types are the Reflector Antenna, which uses its parabolic shape to emanate or converge incident rays in such a way as to achieve a highly directional beam for long-range communication, and the Phased Array Antenna, which electronically steers the beam by adjusting the phase of the signal at each element, allowing for rapid beam direction changes without physically moving the antenna. These can be seen in Figs. 2.12a and 2.12b below.



(a) Parabolic Radar Antenna[54]



(b) Phased Array Radar Antenna[55]

Figure 2.12: Comparison of Radar Antennas

CW Radar

As this study involved two CW radar devices, some time was taken to understand them in greater detail.

CW radar is designed to emit transmit and receive continuously from its antennas. Because of this, they often embody a bistatic design[8] and have a continuous output transmission power equal to that of their peak power[6]. This power level is often also limited in magnitude due to the signal leakage that occurs between the transmitter and receiver[8]. This fact enables CW radar devices to be less expensive but also reduces their performance abilities in range detection. It is for this reason that CW radar is well-suited to low-cost applications.

In its standard form, CW radar devices can only be used for speed determination because there is no way to calculate the elapsed time of a round trip. Frequency Modulation (FM), a tool typically used to get around this, effectively marks a section of the EM wave, allowing for range determination during signal processing[8]. Other modulation techniques, as seen in Fig. 2.10, provide CW radar with further functionalities. Whatever the case, understanding and making meaning from the received radar

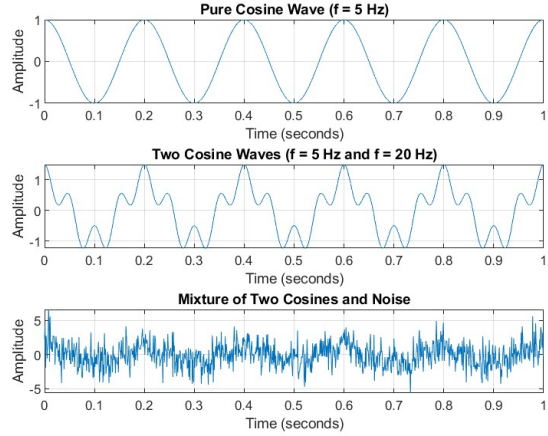


Figure 2.13: Simulation of Various Forms of Continuous Time Domain Return Signals

wave is only possible due to the deep mathematical understanding of the signal theory that has been developed and applied to radar.

2.3.3 Signal Theory

CW Radar Signal Modeling

In radar theory, a signal refers to a varying quantity, such as a voltage or current, that can encapsulate information[8]. For glsCW radar, this is a continuous sinusoid, represented in the time domain as:

$$x(t) = A \cos(2\pi f_c t + \phi) \quad [6] \quad (2.6)$$

Where:

- A : amplitude of the signal,
- f_c : carrier frequency,
- ϕ : phase, and
- t : time.

However, signals seldom resemble this perfect form as elements of noise and distortion are present in all real-world applications. This is compounded by the fact that in glsCW radar applications, multiple return signals are all received simultaneously causing the target signal to be unidentifiable. For a visual representation of this, look to Fig. 2.13 where three variations of a return signal of a 5 Hz wave have been plotted with diminishing identifiable characteristics.

For instance, a real-life recording example of multiple cars travelling past a radar device might look like Fig. 2.14.

In this form, there is no way to identify the Doppler Frequency (F_d) or to extract useful speed information. Therefore, the [Discrete-Time Fourier Transform \(DTFT\)](#), as seen in Equation 2.7. must be used to represent a given signal in the Frequency Domain.



Figure 2.14: Example Time-Domain Recording of Cars Travelling Passes a Radar Device

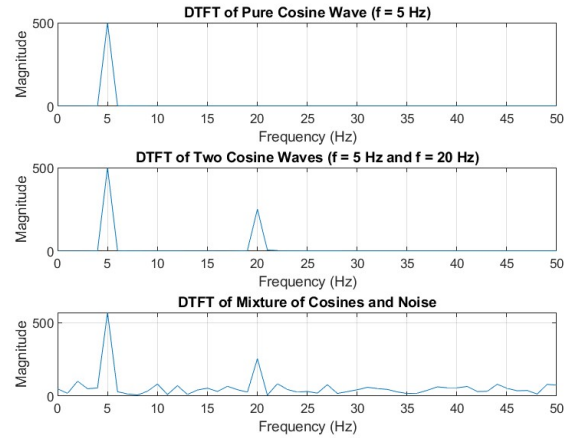


Figure 2.15: Discrete Time Fourier Transforms of Simulated Return Signal

$$X(f) = \sum_{n=-\infty}^{+\infty} x[n]e^{-j2\pi fnT_s} \quad [8] \quad (2.7)$$

This powerful tool represents the frequency components of a signal along with their magnitude[8]. This enhances the 'readability' of a return signal, making it easier to analyse and extract useful data. This can be seen in Fig. 2.15 which plots the corresponding Fourier Transforms to the signals seen in Fig. 2.13. In this form, the target frequency of 5 Hz is visible in all three plots.

This gives the overview of how signal processing is achieved, but in this form, the DTFT is limited in its usability as it plots the full spectrum of a signal. For radar applications, it is necessary to understand and record the time instances at which different signals are received, and therefore an adapted version of the DTFT is needed.

The Short-Time Fourier Transform

The **Short-Time Fourier Transform (STFT)**, seen in Equation 2.8, provides temporal information as to when frequencies occur during a received signal[56]. It does so by dividing the signal into small, overlapping time windows and performing the DTFT on each segment. This technique introduces time localisation, allowing for the analysis of how the frequency content of a signal evolves[56].

$$STFT(m, \omega) = \sum_{n=-\infty}^{\infty} x[n]w[n-m]e^{-i\omega n} \quad [8] \quad (2.8)$$

Where:

- $w[n-m]$: is a windowing function that defines the portion of the discrete signal being analysed

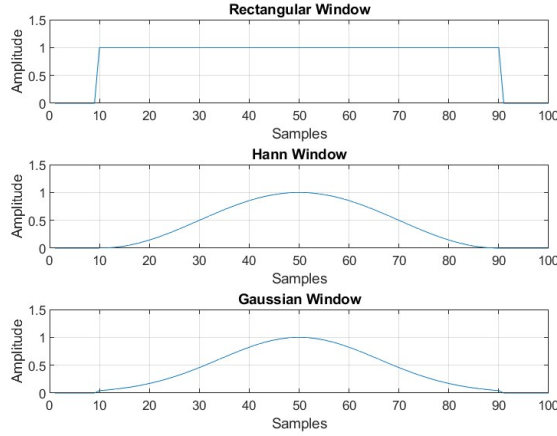


Figure 2.16: Plot of Three Types of Window Functions

in each time segment.

- n : discrete-time index at which the Fourier Transform is calculated.
- m : is the shift or position of the window, moving over the signal in discrete steps.

The windowing function is critical to the functioning of the **STFT** as it segments the signal into sections to which the Fourier Transform is applied independently[56]. It is this function that allows for the time and frequency information to be captured together.

Two main factors define the windowing function. The first is the window length. This parameter determines how much of the signal is analysed during each iteration[8]. Short windows allow for better time resolution, where a target can be more accurately located and its speed determined at any given moment. Longer windows, on the other hand, allow for improved frequency resolution as frequencies that exist on the frequency spectrum of the signal can more easily be distinguished. This trade-off in performance needs to be accounted for when deciding the window length as it is not possible to have both resolutions optimised at the same time.

The second parameter is window shape, where the most simple is the rectangular window as seen in Fig. 2.16. This function assigns a value of 1 to all the samples in the window duration[8]. However, this window shape results in spectral leakage due to the sharp discontinuities at its edges. This effect can spread energy across a wide range of frequencies, making it difficult to identify the true frequency components of a signal accurately[8]. This can be seen in Fig. 2.17, where a rectangular windowing function was used on a spectrogram plot of a car travelling at 5 m/s. Therefore other window shapes such as the Hann or Gaussian are preferred as they do not possess the same discontinuities[8]. The shape of these windows can be seen in Fig. 2.16.

The Hann Windowing Function, defined in Equation 2.9, is commonly used in radar signal processing to analyse Doppler shifts and measure velocities[57]. As both ends of the function taper to zero, there is less chance of discontinuities between subsequent frames, and as such, less spectral leakage occurs. This function was used to produce the plot in Fig. 2.8b, where no spectral leakage can be seen. Further, this function is symmetric about its centre which helps improve the accuracy of frequency component estimations. For these reasons, the Hann function was used in this report.



Figure 2.17: Visual Representation of Spectral Leakage on Spectrogram Plot

$$w(n) = 0.5 \left(1 - \cos \left(\frac{2\pi n}{N-1} \right) \right), \quad 0 \leq n \leq N-1 [57] \quad (2.9)$$

Where:

- N : length of the window,
- n : index of the sample in the window, ranging from 0 to $N-1$.

The **STFT** provides time information for when frequency elements are received during a radar signal, and a windowing function allows the frequencies to be processed without leakage between frames. With this, a spectrogram can now be plotted showing a visual display of how target frequencies vary over time during a signal recording. However, speed estimation is possible after targets are declared and therefore a target detection mechanism is needed.

Cell-Averaging Constant False Alarm Rate

In this report, **Cell-Averaging Constant False Alarm Rate (CA-CFAR)** was used as a means of target detection on spectrograms. This was done because spectrograms only give a visual indication of where a target signal exists, and to be able to extract useful target speed averages, a form of target detection was needed. It is also one of the most frequently used CFAR techniques and is simple to implement.

CA-CFAR is performed on each column of a spectrogram that the **STFT** created. In its operation, there are two critical parameters: the Guard Cells and the Reference Window Cells. A visual representation of these cells can be seen in Fig. 2.18[58]. In each column, this function considers each cell in turn, known as the **Cell Under Test (CUT)**, and declares if a target is present or not. Adjacent on either side of the **CUT**, are the set number of guard cells which are used to isolate the **CUT** from the surrounding signal intensity level[8]. On each side of the guard cells are a set number of reference window cells.

During the **CA-CFAR** processes, these cells' intensity levels are averaged to create a detection level which is then scaled by a scaling factor to set a dynamic detection threshold[8]. The **CUT** is then compared to this threshold to determine if it is a target, ie: has a signal intensity above that of the dynamic threshold. If it is, it is marked with an 'X'. The key advantage of this process is that the threshold level adjusts based on the average noise level in the signal and so, is robust to changes in environmental conditions[8]. This helps prevent false detections. This concept of a moving average can be seen in Fig. 2.19[6]. In this example, a single detection can be seen where the signal's power

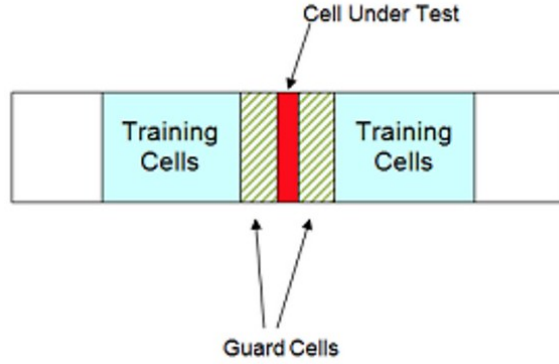


Figure 2.18: CA-CFAR Cell Diagram

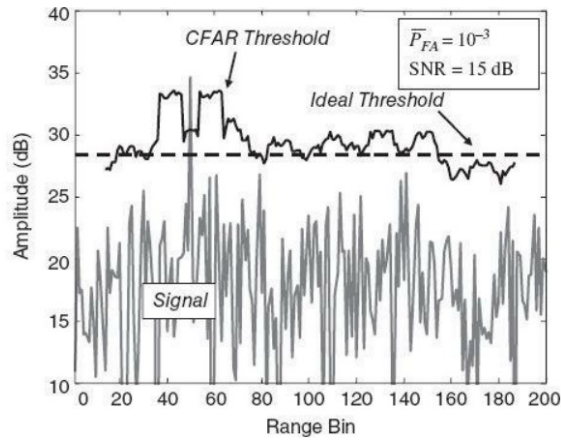


Figure 2.19: CA-CFAR Detection Threshold Example

exceeds that of the CFAR level.

A key metric in this process is the Probability of a False Alarm (P_{fa}), which is used to set the detection threshold limit[8]. It represented the probability that a noise level alone exceeded the threshold, leading to a false detection. It was important to set this variable at the correct level for a given data set as a value too could have created multiple false detections whereas a value too low might have meant that the target is not detected at all.

In this report, the formula to set the scaling factor for the detection threshold is shown in Equation 2.10, as provided by the derivation in Fundamentals of Radar Signal Processing, Second Edition[6].

$$\alpha_{CA} = (2N) \left(P_{FA}^{-\frac{1}{2N}} - 1 \right) [6] \quad (2.10)$$

Where:

- α_{CA} : The scaling factor in CA-CFAR.
- N : The number of reference cells on one of the sides of the CUT used for noise estimation.
- P_{FA} : The desired probability of false alarm.

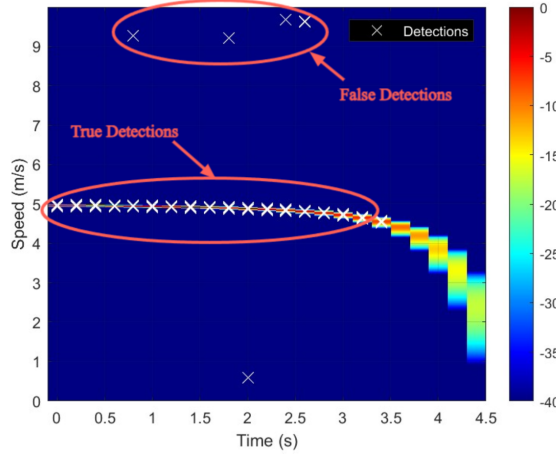


Figure 2.20: Example of CA-CFAR Applied to a Spectrogram

When applied to a spectrogram, the result should contain detections where the target signal is most intense, as well as a few false detections. This can be seen in the example Fig. 2.20.

2.4 Conclusion

Along with placing radar in its historical context and identifying its modern applications, the fundamentals of radar theory and signal processing have now been defined. The radar theory defined above was used to guide an understanding of the radar devices used in this process. From this, it was necessary to understand the different types of radar devices available, as well as the basic radar principles such as the Doppler Effect and how the ranging ability of a radar device can change due to external factors. The signal theory provided a guide for how to approach the writing and testing of the functions created to process the radar recordings made. Here, the importance of the [STFT](#) was made clear, along with how target detection can be achieved through [CA-CFAR](#). These techniques were integral to the processing and code development phase.

Chapter 3

Processing Pipeline

Following the theory development on radar signal processing, the following processing pipeline was envisioned and created to compute and plot the necessary spectrograms of the data that would be recorded. This was done with the knowledge that all radar recordings would be made using the Asus Xonar U5 sound card, and recorded in a Wav (Waveform Audio) file format. This Xonar sound card was used because of its high 24-bit [Analogue-To-Digital Converter \(ADC\)](#), which provided high resolution on the sampled signals, and its maximum sampling frequency of 192 kHz, which ensured the Nyquist criterion was met. The goal was to optimise the plots to have adequate resolution on both the frequency and time axis, ensuring that any possible targets could be identified. This would require the correct parameter values, settings, and normalisation techniques. This process was broken down into isolated steps, as identified and explained below.

3.1 Overview

Fig. 3.1 depicts the full code pipeline of how a radar recording was processed into a functional Spectrogram. Broadly speaking, the code consisted of two functions, a function to compute the STFT and a function to perform [CA-CFAR](#), that could be called when needed. Outside of these functions, the script was able to import the desired .wav signal file, perform a normalisation technique on the data and plot spectrograms, both including and excluding the [CA-CFAR](#) detections, as well as perform other necessary computations and initialise variables. All the necessary code can be found on [GitHub](#).

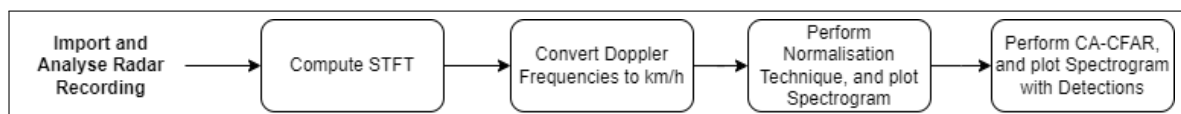


Figure 3.1: Full Code Process

3.2 Recording Import and Analysis

This section of the script was responsible for importing the radar recording and extracting the relevant data from in preparation for computing its [STFT](#). This was done using the Matlab function `'audioread()'`. This allowed for a sampled version of the signal to be extracted, along with the sampling frequency (F_s).

This section also defined all the necessary constants to be used in subsequent processing steps, such as c , the speed of light, and F_c , the centre frequency of the radar module. Once these initial steps were

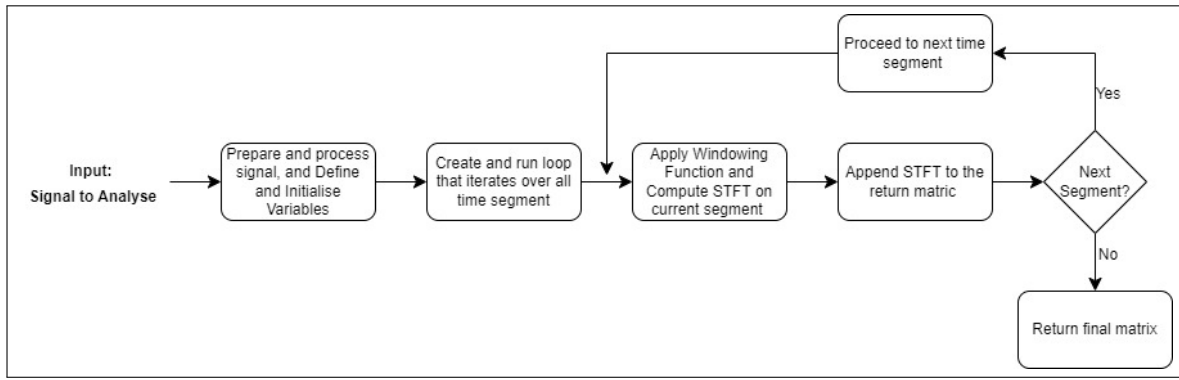


Figure 3.2: Flow Diagram of STFT Function

completed, the STFT of the signal needed to be calculated.

3.3 STFT

This piece of code was created as a function to be called when needed. Its purpose was to compute the **STFT** of any given input signal using a given set of parameter values. It returned this as a matrix, as well as the time and frequency vectors that would be needed to plot a spectrogram. The Flow Diagram can be in Fig. 3.2, where an overview of the step-by-step process is outlined. These are further defined below.

Inputs and Signal Preparation

The signal recording to analyse acted as the input to this function. as well as the sampling frequency, window length, and overlap percentage. Once imported, the signal was turned into a column vector to ensure all data entries beyond this point in the script were the same type.

Initialising Variables and Optimising Parameters

This step was crucial to the functioning of the Fourier Transform as the variables initialised here greatly affected the visualisation of the subsequent Spectrogram plot. Most notably was the windowing function to be applied to the window length. The Hann windowing function was used due to its ability to reduce spectral leakage through the smooth tapering on either end of the function that prevent discontinuities between subsequent segments.

The parameters the 'window length' and 'overlap percentage' were used to calculate the number of total segments that the signal would be divided into. The number of segments affects the time resolution of a resulting spectrogram, and as such, these parameters would need to be optimised to a given data set.

The final set in this section was to create an empty matrix for which the Fourier Transform of each segment would be appended.

Performing the Fourier Transform

To compute the **STFT**, a loop was created to iterate over each segment in turn. To do this, the windowing function was first applied to the section of the signal that was to be processed, then the

Fourier Transform was applied to the windowed signal as per Eq. 2.8. The resulting frequency spectrum was then appended to the final matrix. This process was until all the segments had been processed, at which point the function would return the full STFT matrix, marking the end of the function. This process can be seen in Fig. 3.2.

3.4 Conversion From Doppler Frequencies to Speed

As the STFT function returned a matrix of frequencies, the next set in the pipeline was to convert the frequencies into a correlating speed. This would then need to be filtered to ensure that only the relevant speeds were plotted in a spectrogram.

Using Eq. 2.3, the frequencies in the STFT matrix could be converted into speeds in metres per second (m/s). These were then multiplied by a conversion rate of 3.6¹ to obtain the speeds in kilometres per hour (km/h). The code then filtered the speed indices to retain only those within a specified range. Speeds below 5 km/h were excluded to reduce low-level noise, while speeds above 80 km/h were removed since they exceeded the national speed limit of 60 km/h for vehicles on public roads in urban areas. The expectation was that no vehicle would have been travelling at a speed beyond this in the environment specified in Sec. 1.6. This processed matrix of the STFT was named S_ofInterst.

At this point the only step left to do before a spectrogram could be plotted was to normalise the data into a usable scale.

3.5 Normalisation and Plotting

Spectrograms are designed to plot the magnitudes of a set of frequencies contained within a data set based on an intensity scale. In general, a Fourier Transform of a signal returns data that is complex, containing both an amplitude and phase, and that varies drastically in magnitude from one data point to the next.² Without normalisation, it can be difficult to distinguish between the different signal components when plotted as the large values tend to dominate the plot, suppressing the smaller, potentially significant, components.

In Matlab, spectrograms are usually plotted on a Decibel (dB) scale where 0 dB is the maximum value. This use of a logarithmic scale helps manage the large variations in magnitude that exist in most signals, reducing its dynamic range. Fig. 3.3a and 3.3b show why this is.

Fig. 3.3a shows a real-life example where a car travelled towards a radar device at 30 km/h for 20 seconds. At 20 seconds the car passed the device. This plot was made using no normalisation technique and on a linear scale adjusted to the largest magnitude found in S_ofInterst. As can be seen, the Spectrogram displays very little detail with only the last few seconds showing any sign of detection,

¹

$$v_{\text{km/h}} = v_{\text{m/s}} \times 3.6$$

²To calculate the Magnitude of a signal from its amplitude and phase use:

$$|X(f)| = \sqrt{\text{Real}(X(f))^2 + \text{Imaginary}(X(f))^2}$$

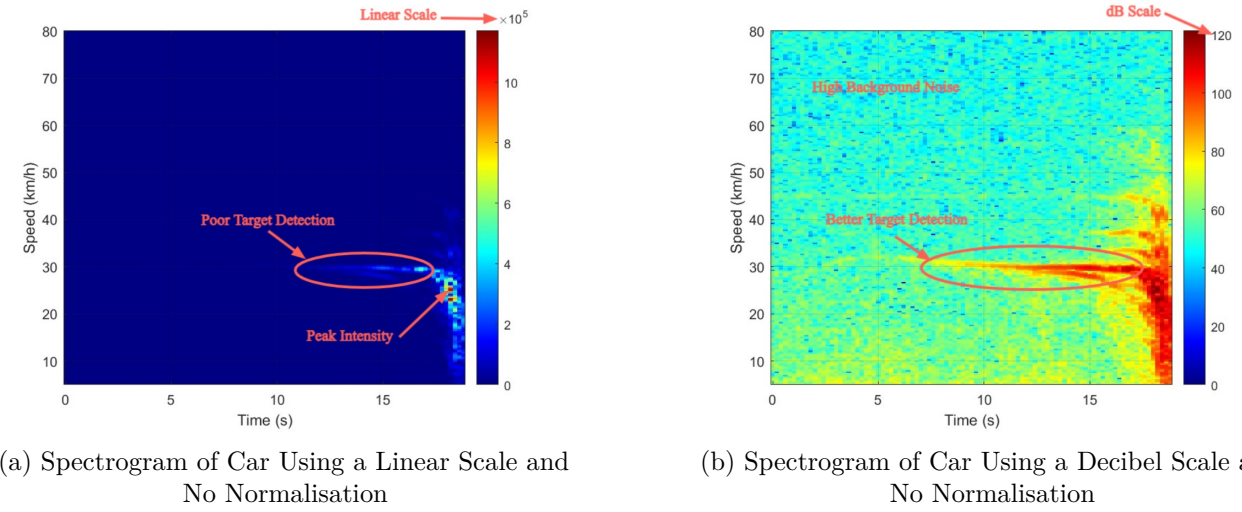


Figure 3.3: Comparison of Scaling Techniques for Plotting Spectrograms

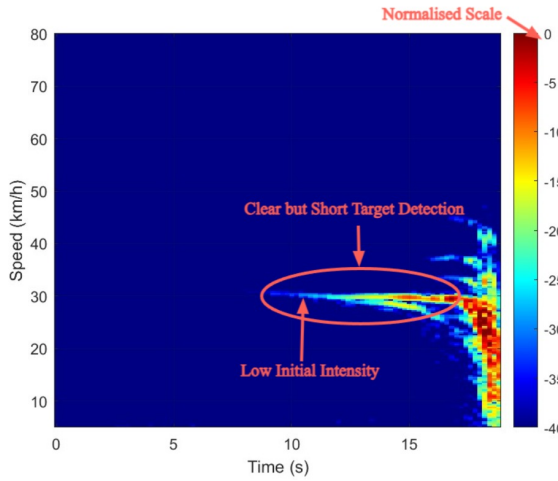


Figure 3.4: Spectrogram of Car Using N1 Normalisation

on a scale that ranges from 0 to 1×10^5 . However, only a speck of the detection displays this large intensity (the deep red), whereas most of the plot is a dark blue corresponding to a scaling of nearly 0.

Fig. 3.3b plots the same recording except using a decibel scale adjusted to the largest decibel contained in S_ofInterest. Here the scale ranges from 0 dB to 120 dB and as a result far more of the target detection is illuminated in the darker red. The target can also be observed for much longer, even though the background is far more noisy. This is, therefore, a better version of the spectrogram, however, maximum detection magnitudes can vary greatly between recordings, and therefore, normalisation is necessary to ensure uniformity and comparability between different spectrogram plots.

For this report, three normalisation techniques were considered.

N1 Normalisation

This form of normalisation simply normalised the entire S_ofInterest matrix to the largest magnitude detected within the matrix. This gave the largest magnitude a value of 1 (0 dB), with everything else adjusted accordingly.

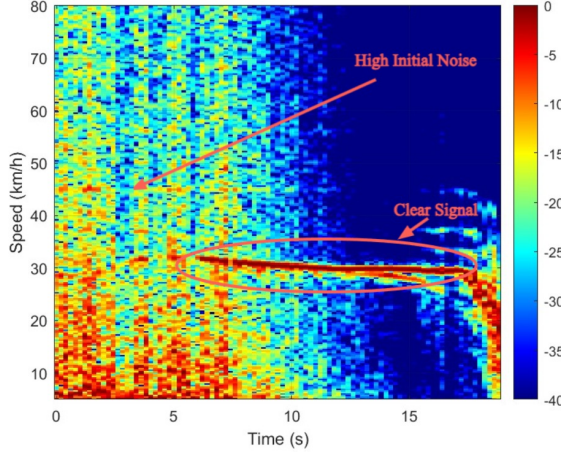


Figure 3.5: Spectrogram of Car Using N2 Normalisation

Fig. 3.4 shows the same data set with N1 normalisation. This plot shows no background noise, allowing the target to stand out very clearly against the dark blue background. The deepest reds occur when the car passes closest to the radar device, as this is where the target detections should be strongest due to the car's proximity to the radar. Further, the target can be clearly identified for 10 seconds before it passes the radar which is longer than that of Fig. 3.3a and about the same as Fig. 3.3b.

N2 Normalisation

This form of normalisation normalised each column of $S_{\text{ofInterest}}$ to the largest magnitude found in that column. The benefit of this method was that even if only a small amount of the target signal was present at any given moment in $S_{\text{ofInterest}}$, if it was greater in magnitude compared to the surrounding noise, it would be scaled to the highest possible decibel level, 0 dB. This made the signal detectable for longer periods but fell short when no signal was present as it would normalise the largest magnitude of noise in a column to 0 dB. This, as seen in Fig. 3.5 between 0 and 5 seconds, made the sections without a detectable target messy and cluttered unlike the dark blue observed in Fig. 3.4. However, the noise did diminish as the target moved closer to the radar, increasing its detection magnitude.

N3 Normalisation

This was the most computationally heavy form of normalisation attempted. It relied on a detection level being set and a noise level estimate being calculated. These values were both based on the first column of $S_{\text{ofInterest}}$ as it can be assumed that no detectable target will be in the frame at this point. The detection level was set as the max value found in that column and could be scaled as necessary, and the noise level estimate was taken as a mean value calculation of the column. With these values determined, this form of normalisation would iterate through all the columns of $S_{\text{ofInterest}}$, first removing the noise through a simple subtraction of the noise level estimate, and then a check would be made to see if the maximum magnitude of the signal in that column was larger than the detection threshold. If it was larger, that column would be normalised to the max level of that same column, as in N2, and if the max value was lower, the column would be normalised to the detection threshold.

This form of normalisation relied on the maximum value in a column when a target was present to be

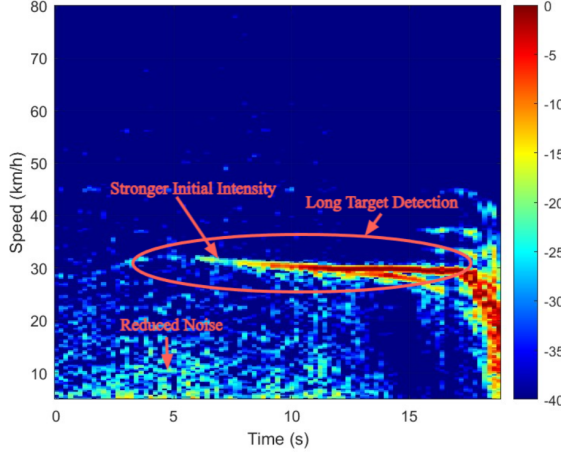


Figure 3.6: Spectrogram of Car Using N3 Normalisation

larger than the scaled detection threshold, but also ensured that the scaled detection threshold was far larger than the noise present in the system. This would ensure that the target stands out clearly while the noise gets suppressed as much as possible throughout the entire plot.

Fig. 3.6 is an example of this. It is clear that the target is visible for as long as in Fig. 3.5 but unlike that plot, there is far less noise present during the first 10 seconds. Further, when compared to Fig. 3.4, the target is detectable for close to 5 seconds longer, and the intensity of the detection during that time is far stronger, indicated by the deeper red colour.

During the processing of the results obtained for this report, the best-suited form of normalisation for a given data set was used. This was judged by observing how long the target was detectable for, and how much noise and clutter were present in the final plot. Another contributing factor for choosing a normalisation technique to use on a data set was how well the [CA-CFAR](#) function performed, as the more reliable the normalisation used was, the better the target detection algorithm performed.

3.6 CFAR

To ensure that a target could be detected in a plotted spectrogram, a [CA-CFAR](#) algorithm was implemented as per Fig. 3.7. The goal of this function was to analyse each cell in each column of the data and assess if it was a target or not based on its intensity level compared to a dynamic threshold based on an average of the cells around it multiplied by a scaling factor. If a target was declared, a cross (X) would be placed over that cell to indicate a target. If implemented correctly, the resulting spectrogram plot should have crosses over most of the area where the target is visible, with only a few false detections. An average of these detections could then be taken to calculate the vehicle's speed as the locations of these crosses were known.

Calculating the Detection Threshold

The first step to calculate the detection threshold was to average the intensity of the reference window cells on either side of the CUT. The second was to calculate the scaling factor which was accomplished by using the Eq. 2.10. The threshold was then set by multiplying the window cell average and the

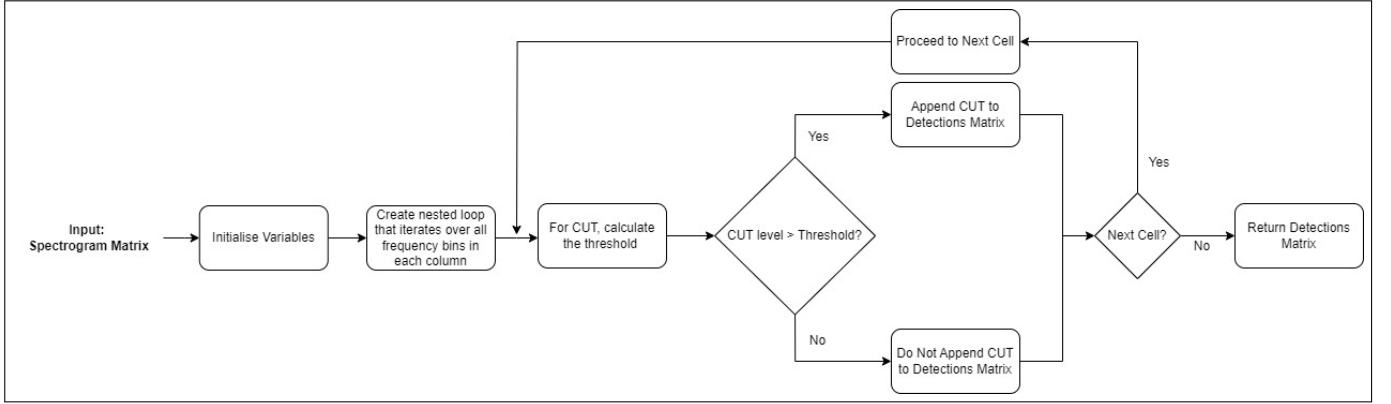
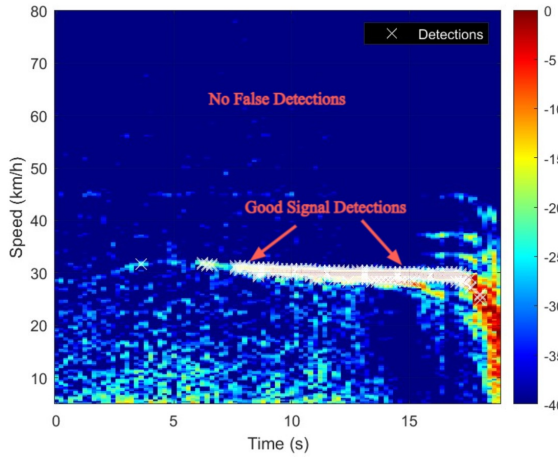


Figure 3.7: Flow Diagram of CA-CFAR Algorithm

Figure 3.8: Optimal Target Detection with High Probability of Detection
 $P_{FA} = 10^{-7}$, $N = 20$, $N_G = 6$

scaling factor together.

Variable Optimisation

Three variables affected how the [CA-CFAR](#) function performed: P_{FA} , Number of Reference window cells (N), and Number of Guard Cells (N_G). These would need to be optimised when applying this function to a given data set. Fig. 3.8 demonstrates an optimal tuning of the CA-CFAR parameters as the full target is detected and there are no false alarms.

P_{FA} controls the trade-off between false alarms and missed detections. A high P_{FA} increased the function's sensitivity, meaning that it tolerated more false detections while at the same time being able to detect small signals. This can be seen in 3.9b where the function made multiple false detections while still correctly detecting the target. Decreasing this value would have the opposite effect, as seen in 3.9a, where there are no false, but the signal is only partially detected. In both these cases, the probability of detection is reduced.

N affects the surrounding noise level estimation. The larger the window, the more accurate the estimation would become, decreasing the number of false detections. This can be seen in Fig. 3.10b where a large window was used, resulting in no false detections. However, a smaller window would

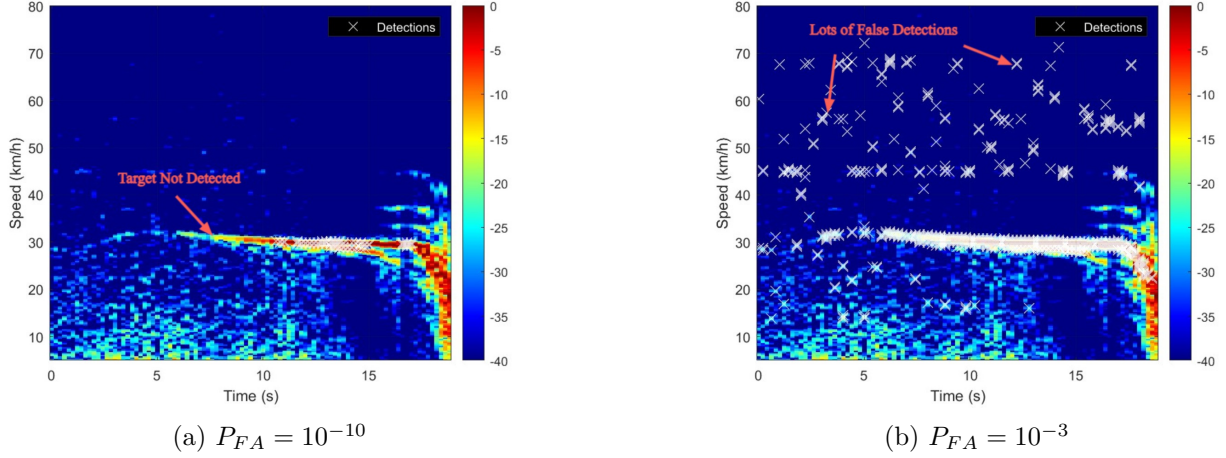


Figure 3.9: Comparison of Different P_{FA} Values
 $N = 20, N_G = 6$

enable the system to detect smaller targets. This is not evident in Fig. 3.10a, because there were no smaller targets, although, the function did make some false alarms indicating a heightened sensitivity to sudden fluctuations. Both these functions would however have a high probability of detection.

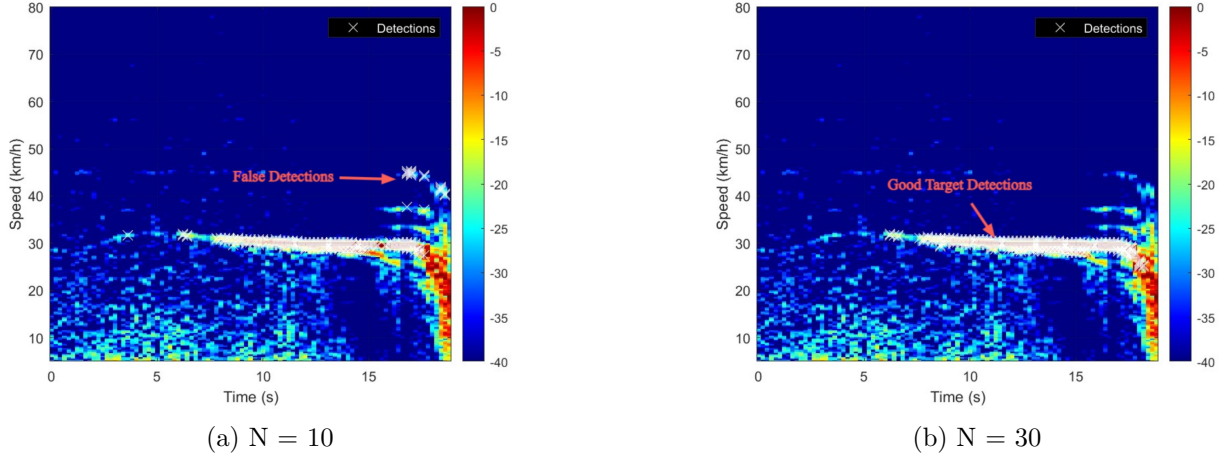


Figure 3.10: Comparison of Different Numbers of Reference Window Cells
 $P_{FA} = 10^{-7}, N_G = 6$

N_G helps to isolate the CUT from the immediate surrounding cells. This reduces the possibility of the target's energy affecting the reference window average. In general, a large number of guard cells helps to improve detection accuracy, however, this may reduce the number of reference window cells available, which would decrease the noise level estimate accuracy. Fig. 3.11b is an example where a large number of guard cells were used. In this case, there were more accurate detections made due to the prominence of the signal resulting from its high SNR. Fig. 3.11a shows an example of where a small number of guard cells were used. In this case, the resulting plot had fewer true detections caused by the signal leaking into the reference window, disrupting the average. In this case, Fig. 3.11b would have a higher probability of detection.

As seen, these parameters have a dramatic effect on the target detection capabilities of the CA-CFAR

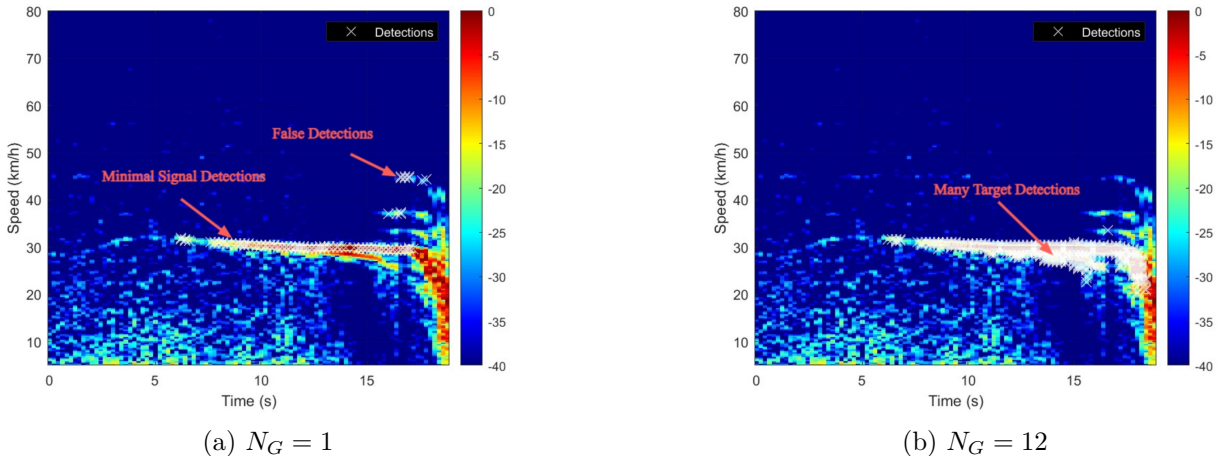


Figure 3.11: Comparison of Different Numbers of Guard Cells
 $P_{FA} = 10^{-7}$, $N_G = 6$

function. When used in this report, the parameters were optimised for the entire data set of one of the radar devices to produce the best target detection possible.

As the CA-CFAR function was the last step in the processing pipeline, time was then spent testing these functions on simulated data to assess their functionality.

3.7 Simulated Results

In order to assess if the processing pipeline was implemented correctly, simulations of cars passing a radar device were run on Matlab. Further, once confirmed that the functions were correct, the results acted as ground truth data for the actual experiments. These simulations established reliable spectrogram detection patterns that helped confirm whether the radar devices were functioning as intended in the real world.

3.7.1 Code Alterations for Simulated Data

To account for simulated results, a simulation time was set, along with the target's initial distance (R_0), the 'cars' initial speed (V_Y), and the radar device's horizontal distance from the centre of the 'road' (R_X), as per Fig. 2.8a.

Then for a given velocity pattern, the total distance (R_t) to the target could be calculated for the duration of the test by using the Pythagorean Theorem. This in turn was then used to calculate the phase shift, ϕ in the return signal using Eq. 3.7.1. Finally, the targets could be calculated using Eq. 2.3, which would be used in the same manner as in the subsequent processing steps defined in the pipeline above.

$$\phi = \frac{4\pi R_t}{\lambda} \quad (3.1)$$

3.7.2 Results

Having restructured the code to accommodate simulated data, two types of tests were conducted at various motion profiles. The first was a single-car test, in which the car started at an initial distance, R_0 , of 25 m.

Results Simulating a Single Car

For the single-car test, two motion profiles were used:

- Constant Velocity: 5 m/s
- Constant Acceleration: 0.6 m/s

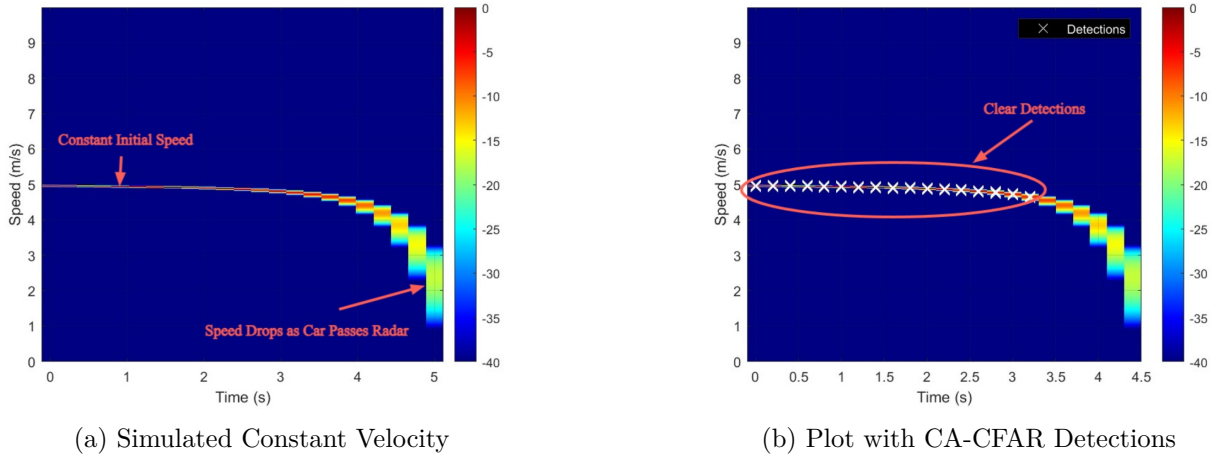


Figure 3.12: Simulated Spectrogram of a Car at a Constant Velocity

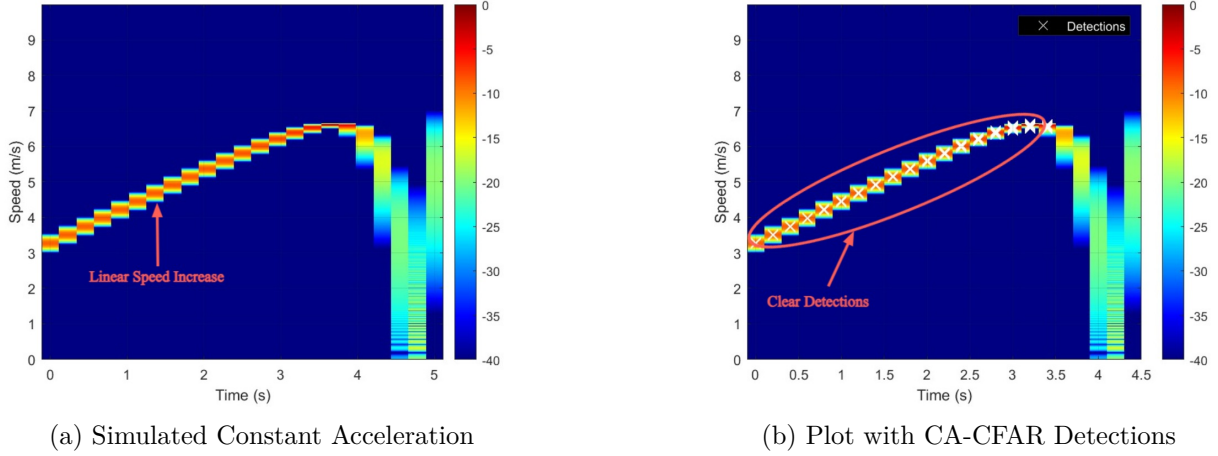


Figure 3.13: Simulated Spectrogram of a Car at a Constant Acceleration

The spectrograms in Figs. 3.12a and 3.13a demonstrate that the STFT function was able to accurately detect the speeds of the vehicles in the simulated data. Fig. 3.12a shows the vehicle travelling at a constant velocity of 5 m/s (V_0), while Fig. 3.13a shows the speed linearly increasing. As the vehicles

in both plots begin to pass the radar device, the detected (radial) speed dropped to zero, however, due to the angle between the devices approaching 90° , as outlined in Equation 2.3.

The CA-CFAR function applied to Figs. 3.12b and 3.13b also worked as intended, identifying the correct areas of the spectrogram with no false detections. These can be seen by the white 'X' marks. The function was not able to detect the speeds as the vehicle passed the radar due to the vertical spread of the frequencies being too large. This sets the window average too high, meaning that no detection can be made.

Results Simulating Two Cars

For this test, two cars were simulated travelling at different speeds, with the second car two seconds behind the first.

- Car 1: $V_I = 5 \text{ m/s}$
- Car 2: $V_I = 8 \text{ m/s}$

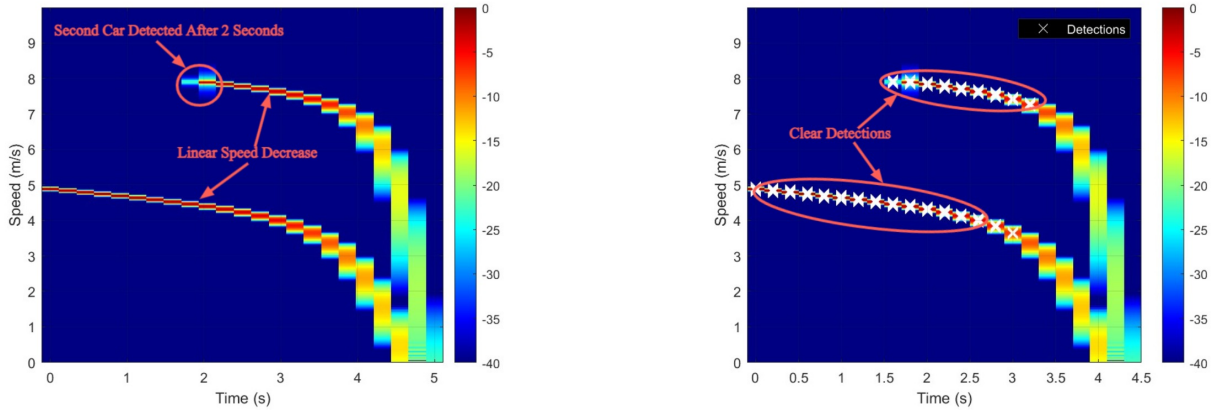


Figure 3.14: Simulated Spectrogram of Two Cars Travelling at Different Speeds

This test was designed to show how a vehicle, travelling behind another, could be detected later in the recording. As seen in Fig. 3.14a, car 2 is detected 2 seconds after the first car. It also shows this car travelling at a faster speed towards the radar. Both vehicles show the same linear speed decrease, but because the second car was travelling at a higher initial velocity, they travelled passed the radar at almost the same time.

Further, the CA-CFAR produced clear detections on both vehicles as indicated in Fig. 3.14b. This plot also contains no false detection indicating a high accuracy. Further, it should be noted that due to the simulation not considering the signal losses involved in radar detection, especially that of range to the target as defined by Equation 2.1 both vehicles are detected with the same signal strength.

The plots shown above indicate that the processing pipeline created to analyse the data recorded functions as intended. The STFT function was able to accurately portray how detected frequencies change over time when used on simulated data, enabling the generation of spectrograms. This step was crucial in understanding the temporal evolution of the frequency components in the signal. The

3.7. Simulated Results

CA-CFAR function performed effectively, maintaining sensitivity to detections while minimising false alarms. This indicates that the function was able to adjust its detection threshold based on the surrounding environment ensuring that the targets were identified.

The combination of these two functions provided the basis for which recorded data could be analysed and manipulated for effective visualisation. This was done in order to understand the data that was recorded using the two radar devices involved in this report, the likes of which are outlined in Chapter 4 below.

Chapter 4

Experiments and Testing Plan

4.1 Systems Overview

For this report, the two systems under test were the MIT Coffee-Can and the IPM-165_F, as defined in Section 1.5. These systems were not only low-cost, as required by the problem statement Section 1.4, but also chosen for their low power ratings, small size and transportability, as well as being accessible through UCT.

4.2 MIT Coffee-Can

The MIT Coffee-Can radar system, as seen in Fig. 4.1, was developed as part of an open course to help teach fundamental radar concepts using simple, accessible components. In doing so, a low-cost, low-power device was created, capable of measuring range, Doppler shifts and even gathering SAR images [59].

4.2.1 Working Principles

This device operates as a continuous wave radar. It has two configurations depending on the nature of the data that is looking to be collected. For target speed detection, the device is configured to emit an undulated waveform at a centre frequency (F_C) of 2.4 GHz. In this mode, the Doppler principle is used, (Equation 2.3), to determine the relative speed between the target and the device. However, when target range information is required, the device is configured to emit a FMCW. This allows for a time delay between the transmission and reception of a waveform section to be found, which is proportional to the distance to the target as per Equation 2.4.

4.2.2 Block Diagram

The system's block diagram, as seen in Fig. 4.2, outlines the processes necessary to generate, transmit and receive signals.

The left channel (top row) is responsible for the signal generation and transmission. This includes a modulator (Modulator1) which would generate a modulating waveform if this is required. The oscillator (OSC1) is the signal source, generating a continuous wave at F_C . The attenuator (ATT1) and Power Amplifier (PA1) are responsible for controlling the signal's power level and amplitude. This step ensures that the signal is ready for transmission. The splitter (SPLTR1) creates two pathways

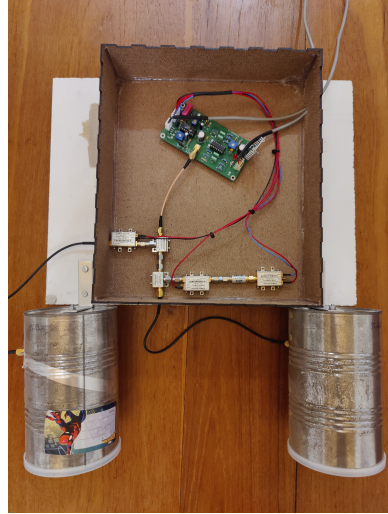


Figure 4.1: MIT Coffee-Can System

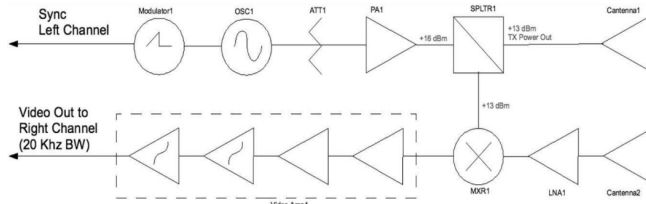


Figure 4.2: MIT Coffee-Can Block Diagram

[60]

for the signal. One is fed to the antenna (Cantenna1) for transmission, and the other is sent to the receiver to be used in the mixing process for frequency shift determination.

The right channel (bottom row) is responsible for receiving and processing the return signal. The second antenna (Cantenna2) receives this signal containing the Doppler shift information. The low noise amplifier (LNA1) ensures that the signal's strength is amplified without increasing the noise level. The Mixer (MXR1) then generates the Doppler frequency by mixing the original signal with the return signal. Lastly, the video amplification process (Video Amp1) further processes and amplifies the signal, ensuring it is ready for analysis.

4.2.3 System Specifications

The system specification can be seen in Table 4.1 below[60, 61].

4.3 IMP-165

The IMP-165 is a low-cost, K-band radar chip, designed and manufactured by InnoSenT. It is compact, with a top surface measuring only 25 mm x 25 mm, and is very energy efficient. This radar chip was combined with other components to create a functional module.

Table 4.1: MIT Coffee Can Radar System Specifications

Specification	Value/Details
Frequency Range	2.4 GHz - 2.5 GHz
Transmit Power	20 mW
Antenna Type	Circular Waveguide (Coffee Can) Monopole
Antenna Gain	7.2 dBi (measured), 8.0 dBi (theoretical)
Antenna Beamwidth	70° Half-power beamwidth (HPBW)
Power Supply	12V
Bandwidth	80 MHz (RF Design)
Antenna Isolation	50 dB
Waveform Type	CW / FMCW
Antenna Voltage Reflection Coefficient	-15.7 dB (return loss)
Antenna Effective Aperture	Diameter of coffee can: 9.9 cm
Cutoff Frequency	1.8 GHz for circular waveguide
Maximum Cost	R 6 317

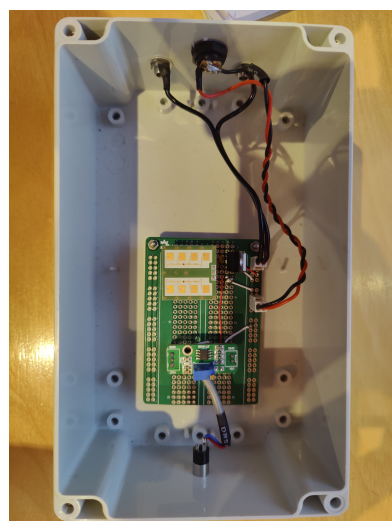


Figure 4.3: IPM-165 System

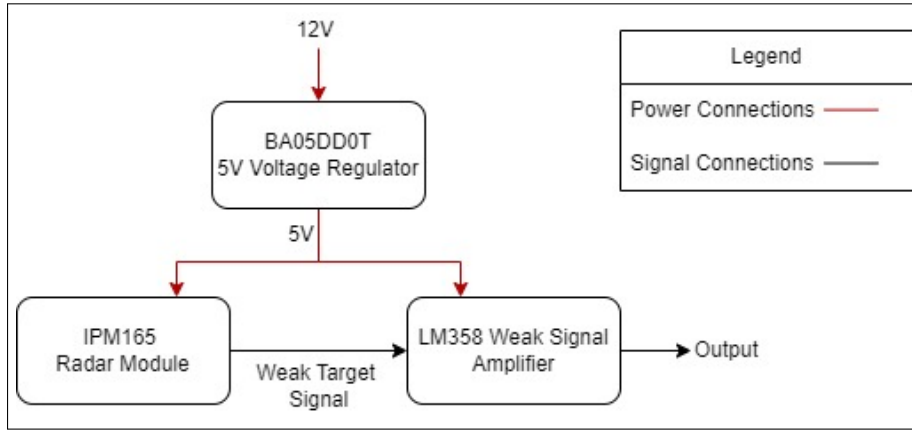


Figure 4.4: IPM165 Radar Module Block Diagram

4.3.1 Working Principles

Similar to the MIT Coffee-Can, this system emits a continuous waveform, but with a centre frequency of 24 GHz. It can only work in this mode of operation which limits its functionality to motion detection and speed determination. Other than that, it operates on the same working principles as the MIT Coffee-Can, employing a Doppler shift calculation to determine the speed of a target.

4.3.2 Block Diagram

The block diagram seen in 4.4 outlines the components needed to create a functional radar device using the IPM165 radar chip.

A 12 V input is used to power the system. The 5 V Voltage regulator ensures the radar chip is supplied with the correct voltage input as it is a sensitive component with strict voltage limits (4.75 V - 5.25 V). This radar module is capable of the creation, transmission, reception and processing of the radar signal. The weak output signal was passed to the low-signal amplifier which was also powered by the 5 V regulator. Here the signal was amplified to a usable voltage level that can be passed out of the device for further processing.

4.3.3 System Specifications

The system specifications can be seen in Tables 4.2[62], 4.3[63], and 4.4[64] below.

Table 4.2: 5V Regulator Specifications

Parameter	Value
Output Voltage	5.0 V
Input Voltage Range	7 - 25 V
Output Current	1A (Max.)
Ripple Rejection Ratio	55 dB
Operating Temperature Range	-40°C to 125°C
Package	TO252-5
Cost	R53.52[65]

Table 4.3: LM358 Weak Signal Amplifier Module Specifications

Parameter	Value
Supply Voltage	3-32 V
Output Current	40 mA (Max.)
Voltage Gain	1000 (Max.)
Operating Temperature Range	-40°C to 85°C
Package	DIP
Cost	R32.63 [66]

Table 4.4: IPM-165 Radar Module Specifications

Parameter	Value
Transmit Frequency	24.050 - 24.250 GHz
Output Power	16 - 20 dBm
IF Output Voltage	563 - 1819 mV
Supply Voltage	4.75 - 5.25 V
Supply Current	18 - 40 mA
Operating Temperature	-20°C to +60°C
Antenna Beam Width (Azimuth)	80°
Antenna Gain	9.5 dBi
Cost	R135.10 [67]

4.4 Test Procedure

The testing phase aimed to gather data aligned with the project objectives defined in Sec. 1.5. Most Notably Objective 1:

Objective 1: Test two low-cost radar systems, the MIT Coffee-Can radar system and the IPM165 radar chip, in their ability to estimate the speed of moving vehicles.

The data gathered also had to apply to the low-traffic, slow-speed environment in which the systems were expected to operate. Further, the device's performance needed to be evaluated on a range of car size classes. This led to the development of the following test plan.

4.4.1 Test Plan

Three classes of vehicles were used, a small hatchback, a larger pick-up truck (bakkie), and a bus, as shown in Fig. 4.5. This was done to observe the possible change in performance due to the varying **RCS** of the different-sized vehicles. A larger **RCS** should improve the detectable range of a target as per Equation 2.1.

Two types of tests were conducted. Controlled tests encompassed situations where the number of cars, and their speeds and directions were predetermined. Uncontrolled tests were performed on roads where this level of control was not possible and so the speed of the vehicles under test could not be set. Uncontrolled tests represented a real-world scenario in which the devices would have to work. Controlled and uncontrolled tests were performed on the hatchback and bakkie, while only uncontrolled experiments were performed on the bus due to limited vehicle access.



(a) Vehicle 1: Small Hatchback



(b) Vehicle 2: Bakkie



(c) Vehicle 3: Bus

Figure 4.5: Comparison of the Three Vehicle Classes Used

Controlled Tests

The following controlled tests were conducted on both the hatchback and the bakkie. All tests were performed with the radar device 1.5 m above the ground and the vehicle travelling towards the radar.

1. Speed tests at:

- (a) 10 km/h
- (b) 30 km/h
- (c) 60 km/h

2. Varying speed tests:

- (a) Accelerating while travelling past the radar device
- (b) Braking while travelling past the radar device

3. Range tests at a height of 1.5 m above the ground:

- (a) Vehicle travelling towards the radar device
- (b) Vehicle travelling away from the radar device

4. Range tests at a height of 0 m above the ground:

- (a) Vehicle travelling towards the radar device
- (b) Vehicle travelling away from the radar device

5. Two car tests:

- (a) Vehicles travelling in the same direction at the same speed
- (b) Vehicles travelling in opposite directions at the same speed

- (c) Vehicles travelling in the same direction at different speeds
- (d) Vehicles travelling in opposite directions at different speeds

Uncontrolled Tests

The following uncontrolled tests were performed:

1. Range test with the bus travelling towards the radar device
2. 'Real-life' test where multiple cars were travelling past the radar device

4.4.2 Experimental Methodology and Setup

The following procedure was followed to conduct the radar-based measurements:

1. The radar device was placed on a table positioned 2 meters perpendicularly from the central trajectory of the vehicle's path, ensuring alignment for optimal detection.
2. Proper connections were made between the radar device and the sound card, with the sound card connected to the computer. Verify that Audacity is correctly configured to read input from the 'Line - Zonar' channel, and is recording using two channels.
3. Begin recording using Audacity.
4. Conduct a test as defined above.
5. Upon completion, stop the Audacity recording.
6. Save the recorded file in '.wav' format, ensuring it is stored in the designated folder for subsequent processing and analysis.

Further, three test sites were used, as seen in Fig. 4.6. The criteria for the test site was a straight, unobstructed road, at least 200 m long.

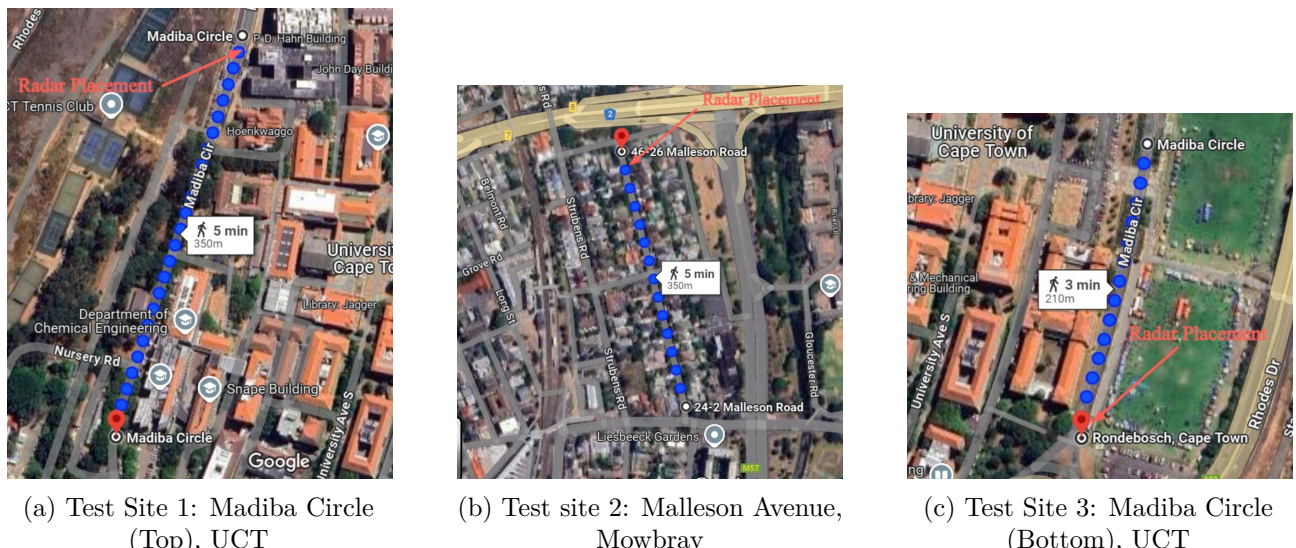
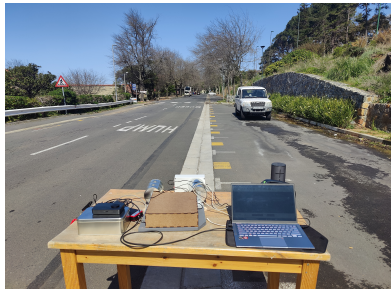


Figure 4.6: Maps of the Test Sites Used

4.4. Test Procedure

Fig. 4.7 appears here to visually identify the test set-up, and sites where radar recordings were taken.



(a) Test Site 1



(b) Test Site 2



(c) Test Site 3

Figure 4.7: Images from Testing

With this testing protocol defined above, the following results were obtained.

Chapter 5

Results and Discussion

The following results were obtained from the experiments described in Section 4.4.1 above. These tests were designed to comprehensively test the MIT Coffee-Can and IPM-165 systems to evaluate their ability in vehicle speed detection in both a controlled and uncontrolled environment, in alignment with the project's overall goals. To this end, a SNR of above 15 dB was considered sufficient to obtain an adequate probability of detection, while maintaining an acceptable probability of false alarm.

In the control tests, speed detection was evaluated in two vehicle classes, small hatchbacks and a larger bakkie. The purpose of these tests was to evaluate performance in ideal conditions where every test parameter was standardised and constant. This included the number of vehicles present, the speed and direction of the vehicles, their proximity to the radar device and the type of vehicle. The purpose of assessing different vehicle sizes was to assess the impact that RCS has on detection capabilities.

These systems were also tested in uncontrolled environments. This was a way to simulate real-world data where there may be multiple vehicles travelling towards the radar device, and their speeds may not be predictable. Additionally, buses were tested in this manner as, due to limited access, they could not be tested in a controlled environment.

All three normalisation techniques were trialled on the different datasets recorded. As each technique had its advantages and disadvantages it was important to see which performed best for which radar device. After analysing the results, it was clear, as per the guiding principles seen in Sec. 3.5 that the N1 normalisation technique worked best for the IPM-165 radar and the N3 technique worked best for the MIT Coffee-Can system. The following outlines the results that were obtained, with side-by-side comparisons of the two systems.

5.1 Controlled Tests

5.1.1 Constant Speed Tests

Constant speed tests were performed to collect data for different vehicle speeds. Due to the nature of the study being focused on low-density, slow-moving traffic, only speeds up to 60 km/h were tested. Three speed ranges were tested, between 10 km/h - 20 km/h representing a slow speed, between 30 km/h - 45 km/h for a medium speed, and between 50 km/h - 60 km/h for a fast speed.

As seen in Fig. 5.1 above, the majority of the SNR for the detected target is above 30 dB, represented by the difference between the dark blue of the background and the deep red in the target signal. However, the SNR is only around 10 dB when the signal is first detected on all the plots. This indicated

5.1. Controlled Tests

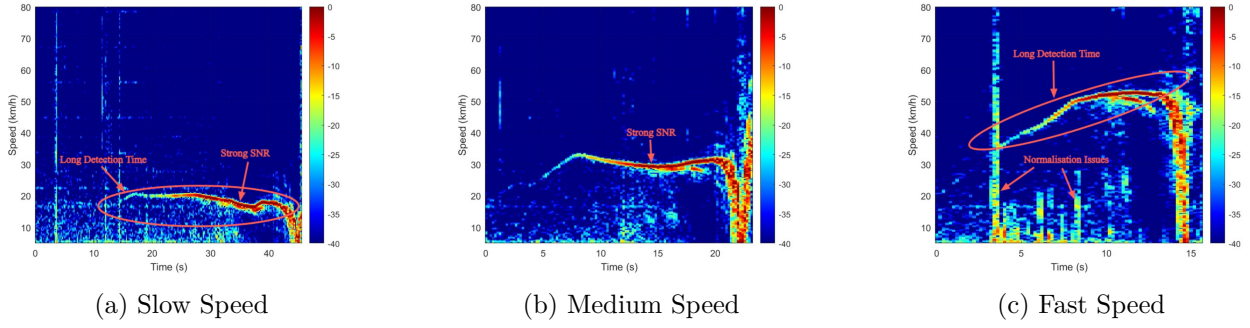


Figure 5.1: MIT Coffee-Can System Tracking the Bakkie at Set Speeds

that the normalisation technique used, N3, is working as intended, and the radar device is capable of detection in these speed ranges.

To calculate the detection range for each plot, the average speed was first found. This was done by averaging the CA-CFAR detections on the subsequent spectrogram plots seen in Fig. 5.1. It should be noted that these are unfiltered detection plots and so do contain false detections. However, as the number of true detections far outnumbers the number of false detections, these averages represent a good estimate of the vehicle's average speed during detection. The average slow speed was 20.09 km/h with a detection time of 30 s. The medium speed was averaged at 30.54 km/h with a detection time of 18 s, and finally, the average fast speed was 48.40 km/h with a detection time of 11 s. This corresponded to a detection range of 167 m, 152.7 m and 147.9 m for the slow, medium and fast tests respectively.

For the IPM-165 device, the N1 normalisation technique performed best, producing the plots in Fig. 5.2. The detection range for these tests was found to be 181.2 m (12.08 km/h for 54 s, Fig. 5.2a), 108.5 m (26.03 km/h for 15 s, Fig. 5.2b), and 41.13 m (49.36 km/h for 2 s, Fig. 5.2c). Further, the SNR for the slow and medium speed tests was around 13 dB, with only the last few seconds of detection being higher at around 20 dB. This was still better than the fast speed test where at its highest, the SNR was only around 10 dB. This can be seen by the light blue speckled background in Fig. 5.2c. In this plot, it is clear that the target was not identified until just before it passed the radar device which resulted in the short detection range.

The car produced similar results for this test, the spectrograms for which can be found in Appendix .2.

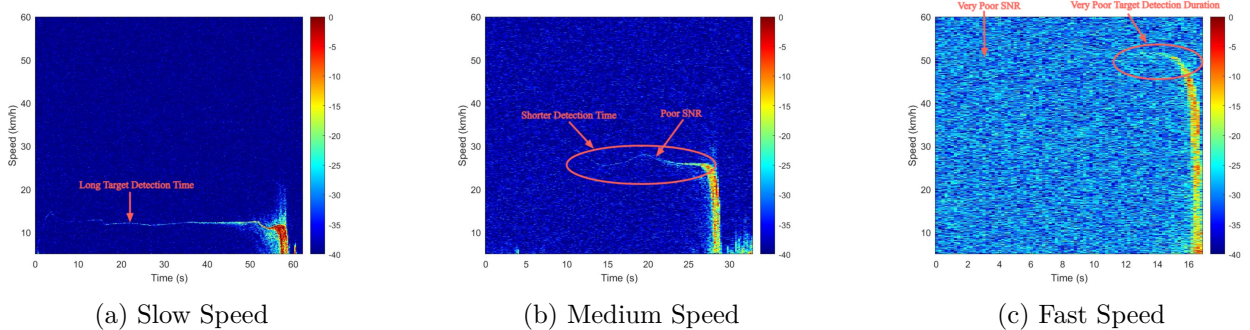


Figure 5.2: IPM-165 System Tracking the Bakkie at Set Speeds

5.1.2 Varying Speed Tests

These tests were carried out to evaluate the radar devices' performance under more complex and dynamic vehicle motion scenarios. Performance in this regard was required for these devices to be considered for applications in traffic calming as velocity profiles of motorists are likely to vary more than the targets seen in Figs. 5.1 and 5.2 above.

Fig. 5.3 shows the spectrograms of the car accelerating and braking while travelling past the IPM-165 radar device. Both these plots offer roughly 5 s of target detection time, and display a SNR of a little below 10 dB. In Fig. 5.3a it is especially difficult to distinguish the signal from the background noise during its acceleration phase.

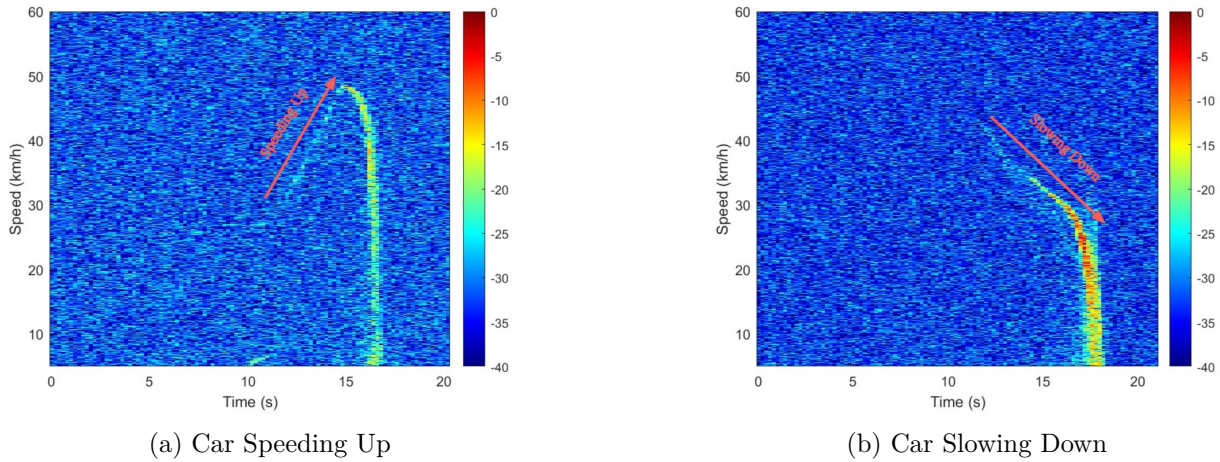


Figure 5.3: IPM-165 System Tracking the Car at Changing Speeds

The MIT Coffee-Can system produced a slightly longer detection time of around 7 s - 8 s, when compared to the IPM-165. However, the most noticeable difference between the two systems was the SNR. The MIT Coffee-Can produced a SNR close to 30 dB, which is far higher than the goal of 15 dB.

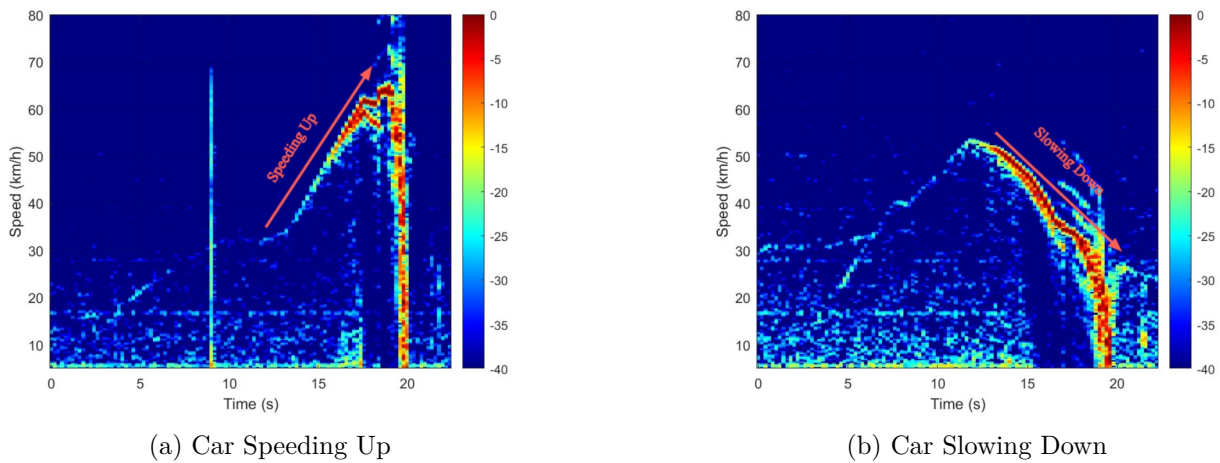


Figure 5.4: MIT Coffee-Can System Tracking the Car at Changing Speeds

5.1.3 Range Tests

Range tests were performed to investigate the impact that the radar's height above the ground would have on the device's detection range. A common cause of radar interference is multipath, which refers to the phenomenon whereby signals take multiple paths to return to the receiver[68]. This can distort the return signal and can be caused by a radar device being situated too close to the ground[68]. For this test, two heights were considered, the height of the table used for testing which sat at 1 m, and 0 m where the device was placed on the ground.

Range Tests at a Height of 1 m

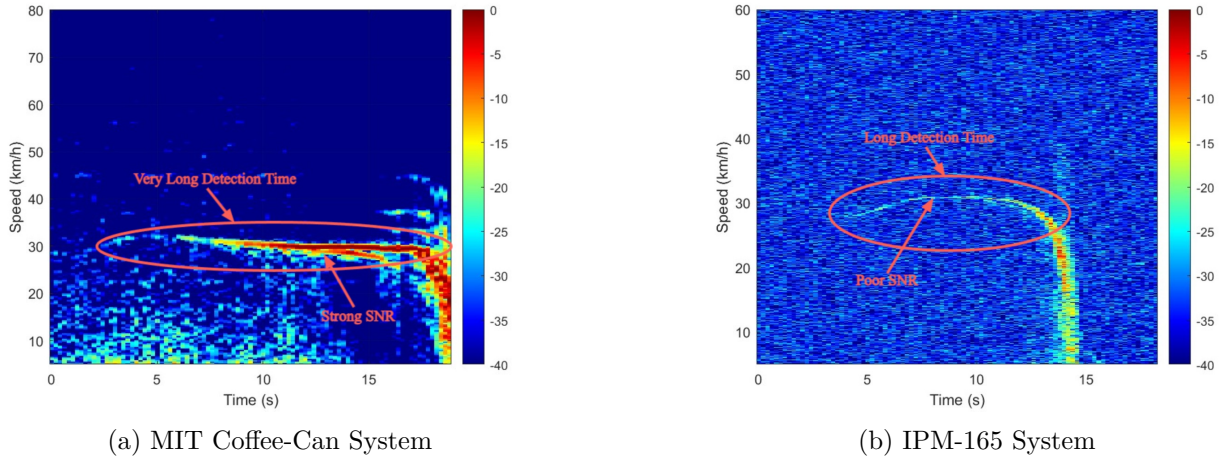


Figure 5.5: Comparison of the Two Systems at a Height of 1 m, Tracking a Car

As seen in Fig. 5.5a, this recording made by the MIT Coffee-Can system produced a plot with a long detection time of around 15 s and a high SNR of again around 30 dB. At an average speed of 30.68 km/h, this recording displays a detection range of 127.8 m.

Fig. 5.5b, on the other hand, shows the spectrogram of the recording made by the IPM-165. This plot has a detection time of just over 10 s, at a speed of 29.63 km/h. This correlates to a detection range of 82.3 m. Additionally, it has a far lower SNR, showing only around 10 dB for most of the detection.

Range Tests at a Height of 0 m

Both devices produced similar results when tested at 0 m, as seen in 5.6. Both struggled to overcome multipath interference from the ground, as well as the reduction in line of sight to the target, resulting in short, 2 s - 3 s, detection times.

5.1.4 Two Car Tests

Two-car tests were performed to see if the radar devices would be able to distinguish between targets. Ideally, the closer target would be detected first and return a stronger signal while in view in accordance with the power density equation or a radar signal, Equation 2.5. However, for this test, the second car was the bakkie which has a larger RCS. Therefore, from this test, it would be possible to see whether

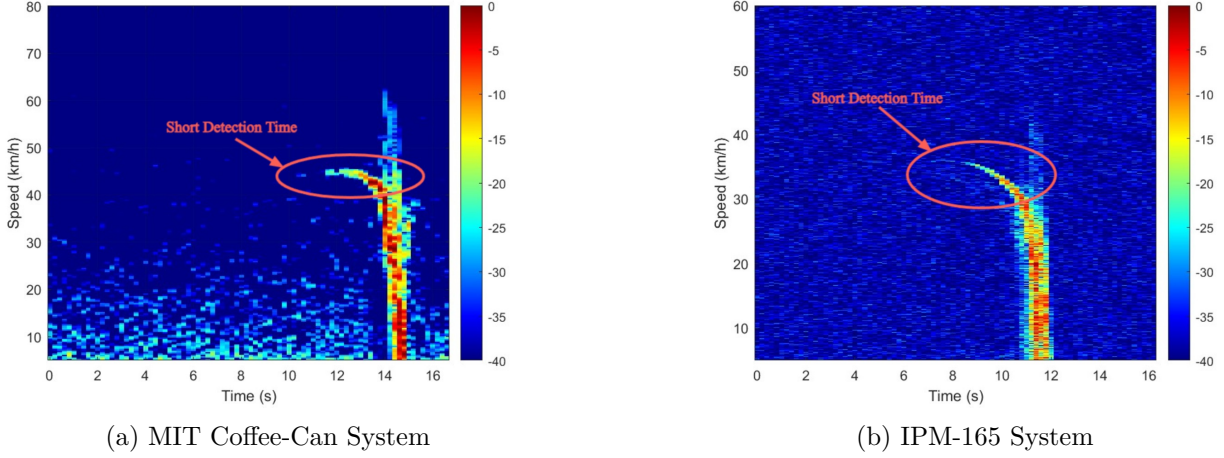


Figure 5.6: Comparison of the Two Systems at a Height of 1 m, Tracking a Car

the radar systems performed better with shorter relative proximity to targets, or for targets with larger RCS.

For this test, two cars were made to follow one another, with the second driving at roughly the same speed, or a slower.

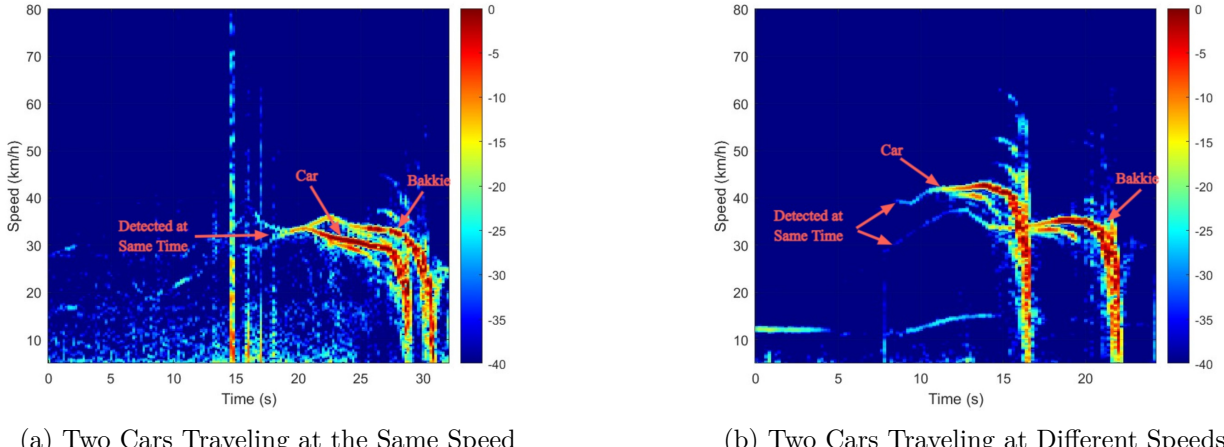


Figure 5.7: MIT Coffee-Can System Tracking Two Cars

In Fig. 5.7a and 5.7b it is clear that both vehicles have a SNR greater than 15 dB at the same time, as indicated. Both the car and the bakkie are visible on the spectrogram, with a strong SNR, and are distinct in both timing and speed. Further, it is also evident that the car produces a stronger detection signal than the bakkie. This is seen in the deep red detections from the car for the few seconds before it travels past the radar.

Fig. 5.8 shows the detections made by the IPM-165 radar module. Again, the two vehicles are distinct and easily recognisable. In these spectrograms, it is clear that the device detected the two vehicles at different times. The car, being the first vehicle, was detected first, and in the case of Fig. 5.8a, at least 10 s earlier than the bakkie. These plots also display a consistent SNR of around 20 dB.

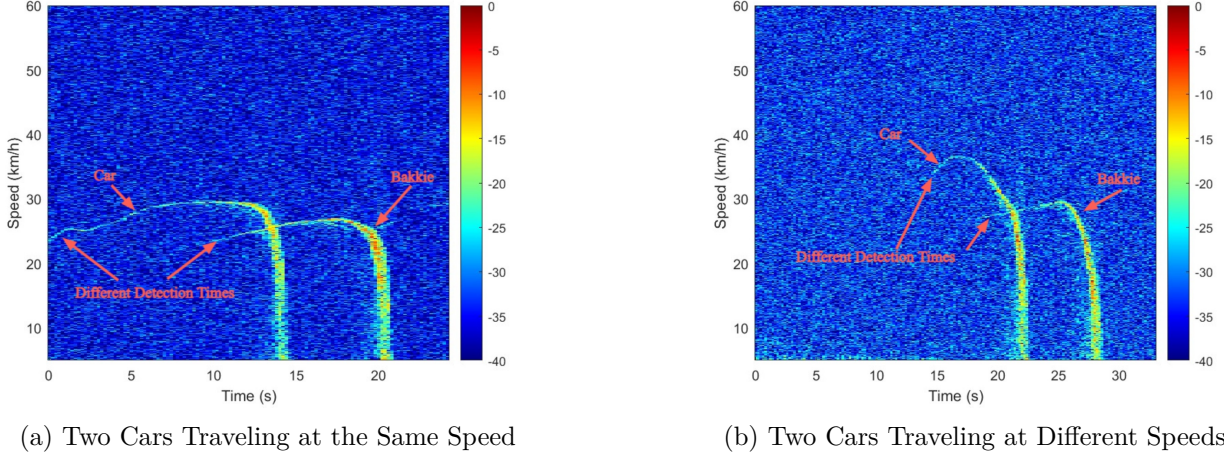


Figure 5.8: IPM-165 System Tracking Two Cars

In these plots, it is not obvious that the second car had a larger RCS. In Fig. 5.8a the two detections appear to have the same SNR, whereas in Ref. 5.3 it appears that the bakkie produces a weaker SNR. A larger RCS contributes to a larger detection intensity, however, that is not seen in these plots.

These controlled tests comprehensively showed the detection and ranging abilities of the two radar systems. Only some of the spectrogram plots of some of the tests were shown, as these best represented the gathered data. However, to view the other spectrograms of the different cars undergoing different tests, please refer to Appendix .2.

5.2 Uncontrolled Tests

Uncontrolled tests were a means to test the radar devices in real-world scenarios, as well as get access to a larger class of vehicle than what was otherwise available. The UCT Shuttle was used in this regard.

5.2.1 Large Vehicle Test

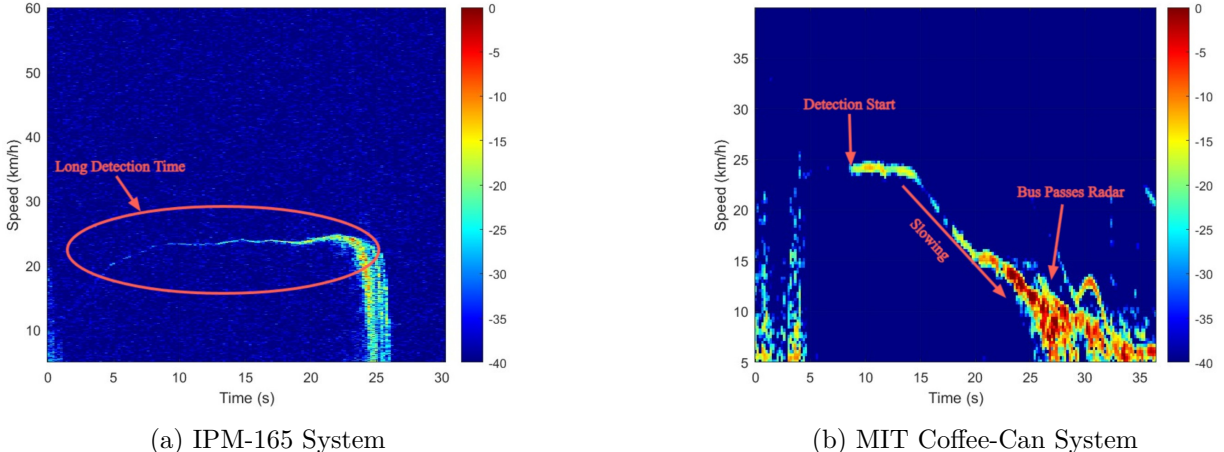


Figure 5.9: Comparison of Both Systems Tracking a Large Vehicle

Due to the uncontrolled nature of these tests, there was no way to regulate the speeds of the UCT shuttles driving towards the radar systems. In Fig. 5.9a, the velocity profile stayed constant throughout the recording, resulting in a familiar plot with a long detection time and SNR of around 10 dB. Further, because the velocity remains fairly constant at 22.48 km/h, the detection range can be calculated as 124.9 m for a detection time of 20 s.

The velocity profile in Fig. 5.9 shows the UCT Shuttle slowing as it approached the MIT Coffee-Can system. The detection time is roughly 18 s, as indicated. Due to the uncontrolled nature of the test, there was no way to ensure that a certain velocity was maintained. This resulted in a spectrogram plot where it was not possible to accurately determine the detection range due to the inconsistent speeds. The SNR for the initial 10 s of the detection is also lower compared to the other MIT Coffee-Can spectrograms, sitting at around 15 dB.

5.2.2 Multiple Vehicle Tests

This test was conducted to assess how these devices would perform if there was no limitation placed on the number of cars present, or the speeds they were travelling at. For this test, the radar systems were left to record for an extended period, allowing for multiple vehicles to travel passed.

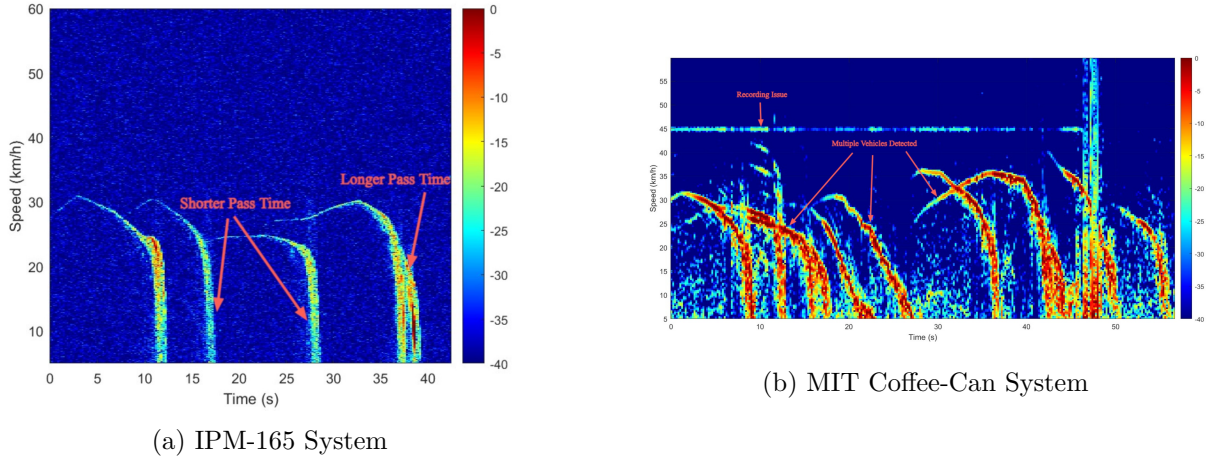


Figure 5.10: Comparison of Both Systems Recording a Busy Road with Multiple Targets

As seen in Fig. 5.10, both devices were able to observe multiple targets during the recording.

5.3 CA-CFAR

The results presented in this section focus on the performance of the **CA-CFAR** algorithm implemented to detect targets on the spectrogram plots from both radar devices. This section aimed to ensure that the target received maximum detection coverage while limiting any false detections. This was achieved by adjusting the key parameters of the **CA-CFAR** function, to set the detection threshold at a level high enough to not allow for many false detections, while at the same time ensuring that no targets are missed. The effects that each of these parameters has on the resulting detections as outlined in Sec. 3.6.

The detection threshold is set by multiplying the average of the reference window cells by the scaling factor. This scaling factor is defined by Equation ?? and is dependent on the [Probability of False Alarm \(PFA\)](#) and number of reference cells (N). This level determined whether a cell was denoted as a target or not and so it was vital to ensure that the parameters were adequately set. Furthermore, the parameters used needed to be consistent for each spectrogram plot from each of the radar devices. This meant that parameters could not be tailored to one single spectrogram, but rather to the full dataset of one of the radar devices. The parameters could however vary between devices as the data recorded by each produced results that favoured different normalisation techniques, leading to different spectrogram characteristics as described in Sec. 5.1 above.

5.3.1 Setting the PFA

The PFA represents the probability that a detection will be incorrectly declared. Typical values for this range from 10^{-6} to 10^{-2} , depending on the application. Lower values favour a higher accuracy with minimal false detections at the expense of sensitivity to weaker targets.

Because most of the experiments were designed to only include a limited number of vehicles, and because vehicles in general have a large RCS compared to sports balls or humans, a lower value, 10^{-6} , was initially chosen for both radar devices. The assumption here was that the signal recording would in general have a high SNR, which should allow for a detectable target once the spectrogram was plotted.

As seen, the MIT Coffee-Can system consistently produced spectrogram plots with a [SNR](#) of over the required 15 dB, producing clearly defined targets. The IPM-165 system struggled in this regard and only produced targets with a SNR of around 10 dB. Due to this discrepancy, different PFA values were investigated on each of the systems as seen in Figs. 5.11 and 5.12 below.

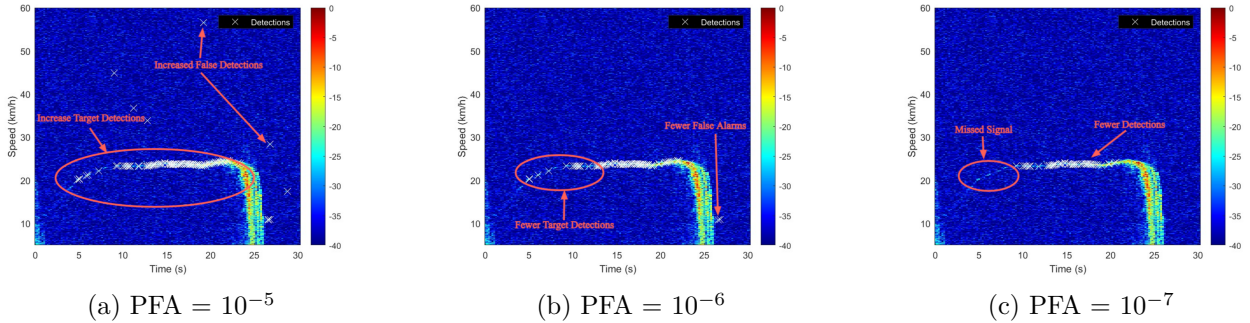


Figure 5.11: Comparison of Different PFA Values on an IPM-165 Spectrogram Plot

Fig. 5.11a, which used a higher PFA of 10^{-5} , showed improved target detections compared to the other plots, especially at the start of the detection where the signal is weakest. However, this plot also contained the most false detections. Fig. 5.11c showed no false detections but also missed large portions of the visible signal which would result in the probability of detection decreasing. Fig. 5.11b, with a PFA of 10^{-6} showed a balance between the two extremes.

As seen in Fig. 5.12, a higher SNR resulted in many more target detections compared to the IPM-165 system in Fig. 5.11. All PFA values trialled demonstrated adequate target detection abilities covering

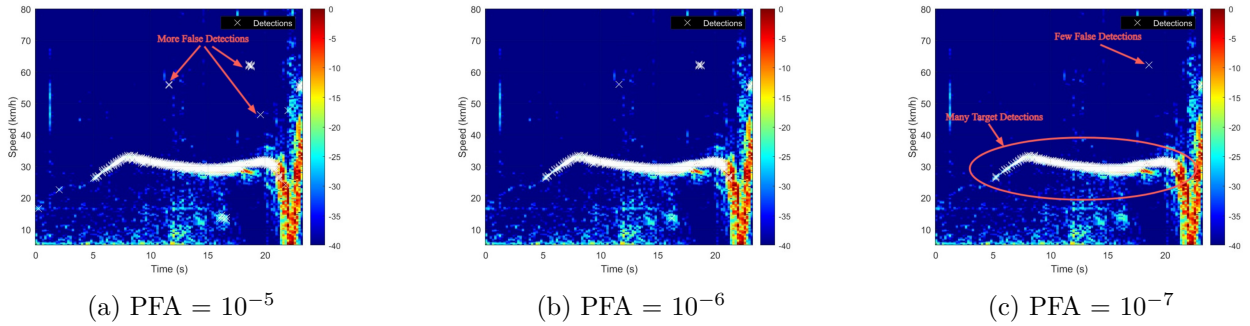


Figure 5.12: Comparison of Different PFA Values on an MIT Coffee-Can Spectrogram Plot

the full range of the detection. As expected though, a lower PFA value resulted in fewer false detections, improving the accuracy of the algorithm.

After testing these values on different test recordings it was determined that a PFA of 10^{-7} worked best for the MIT Coffee-Can system, whereas a value of 10^{-5} produced better signal detections for the IPM-165 system. This higher value was chosen for the IPM-165 system because even though the plots contained more false detections, the coverage of the actual signal was much improved. This fact demonstrated the need for a tracking algorithm to be implemented to reduce the number of false detections while still maintaining true detections. This work fell outside of the scope of this investigation, however, and was not implemented.

5.3.2 Setting the Number of Reference and Guard Cells

Reference cells are used to estimate the noise intensity level around the CUT. A higher number of reference cells, for instance over 30 cells, provides a more reliable estimate but also slows the algorithm's responsiveness to rapid changes in the noise levels. However, having too few would lead to an unrealistic estimate which could produce unwanted false detections in noisy environments.

Guard cells, on the other hand, protect the noise level estimate from being influenced by a target signal. The number selected depended on the expected size of the target present in the spectrogram plot. The target size differential between the two systems can be clearly seen in Fig. 5.13b where the target from the MIT Coffee-Can system is many cells thick and the one from the IPM-165 system, Fig. 5.13a, is only a couple of cells thick.

This detail resulted in the MIT Coffee-Can system requiring more guard cells to reduce the target leaking into the reference window. A value of 6 guard cells was found to be best suited to the majority of the spectrogram plots. This number was coupled with a 20-cell-wide reference window allowed for the moving average of the CA-CFAR algorithm to be more dynamic to changes in the spectrogram plot. The thinner target displayed in the IPM-165 system plots needed fewer guard cells to ensure that no target leakage occurred. It was found that 2 guard cells produced the best results, along with a reference window of 30 cells. The larger reference window helped account for the limited SNR produced as it gave a more accurate average of the surrounding cell's intensities. The final values chosen were summarised in Table 5.1.

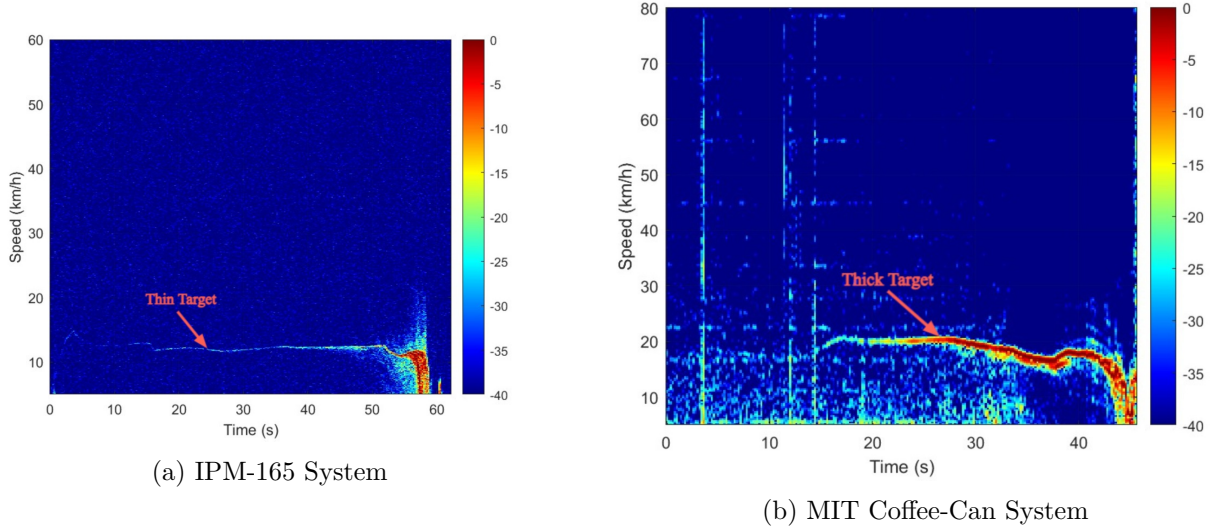


Figure 5.13: Comparison of the Thickness of the Visible Target in Both Radar Systems

Variable	MIT Coffee-Can System	IPM-165 System
Probability of False Alarm (PFA)	10^{-7}	10^{-5}
Number of Guard Cells	6	2
Number of Reference Cells	20	30

Table 5.1: Comparison of CA-CFAR Parameters for MIT Coffee-Can and IPM-165 Systems

5.3.3 CA-CFAR Comparison Between Systems

The following plots containing the CA-CFAR detections were created to demonstrate the functionality of this function on multiple test types of the two radar systems. The tests shown below were selected to demonstrate the consistent strengths and shortfalls experienced while attempting target detection. However, not all the plots from the various tests are shown. To see more examples from the different tests and vehicle types refer to App. ??

Single Vehicle Speed Tests

The following plots were obtained from some of the speed tests on the Bakkie. They were selected to demonstrate how the function performed on spectrograms at varying speeds with different SNRs and detection times.

As can be seen in Fig. 5.14, from the MIT Coffee-Can system, the CA-CFAR function performed well both at a lot and high speed, creating multiple detections on both targets. It is clear that the full target is correctly identified for the duration of its visible detection. These plots also contain very few false alarms, indicating a high detection accuracy, and further, a high probability of detection of the target.

Fig. 5.15 shows the CA-CFAR function used on the spectrograms obtained from the IPM-165 system. In Fig. 5.15a, the algorithm works well, clearly identifying the target for the majority of the time it is visible. The signal is completely detected, although, only a few detections are made per column due to the thin nature of the target. There are also many false detections present, reducing the probability of

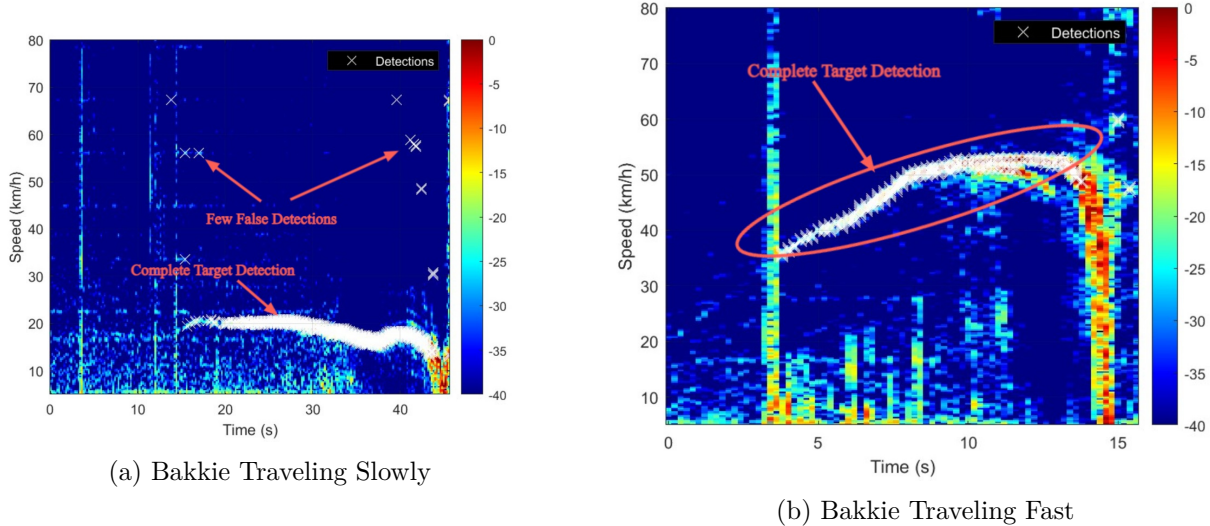


Figure 5.14: Comparison of the CA-CFAR Algorithm Performed on Various Speed Recording from the MIT Coffee-Can System

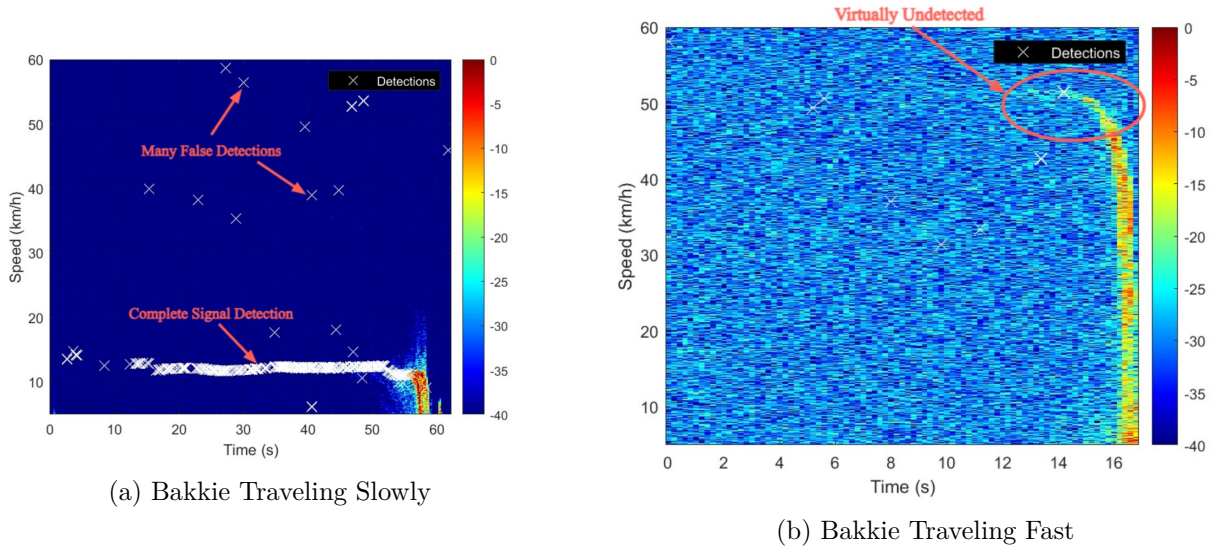


Figure 5.15: Comparison of the CA-CFAR Algorithm Performed on Various Speed Recording from the IPM-165 System

detection.

Fig. 5.15b demonstrates a recording where the CA-CFAR algorithm struggled to detect the target present. Due to the target only being present for a short period, and the SNR being below 10 dB for the majority of the detection, the function failed to identify it. Further, there were still several false detections made.

Multiple Vehicle Tests

Tests incorporating multiple vehicles were included in this investigation, to simulate real-world scenarios that these devices would experience if used as part of a traffic-calming radar system.

The optimal result from a target detection algorithm in this test scenario would be to have it able to identify the closer target with more certainty than that of another because it would be the closer vehicle whose speed would need to be displayed in a traffic-calming scenario. However, this was not accounted for in the CA-CFAR function created but would need to be included if this device was to be used in this capacity. This would most likely need to be in the form of a filtering system, capable of target tracking.

Fig. 5.16a shows the detection of two targets using the MIT Coffee-Can System. In general, the CA-CFAR algorithm performs well here, producing multiple, correct target detections per column on both targets. Further, the targets are identified separately from one another, with very few detections being made on the second target while the first is still visible. There are however multiple false detections present in the plot.

Fig. 5.16b shows the plot of multiple targets with detections included, obtained using the IPM-165 system. The CA-CFAR functions here at a high level of accuracy, correctly identifying each of the targets with multiple detections. However, due to the thin spectral spread of the target frequencies, only a few detections are made in each column of the data. Further, due to the device detecting one vehicle at a time with little overlap between the end of one target and the start of another, the CA-CFAR function seldom detected multiple targets in the same column.

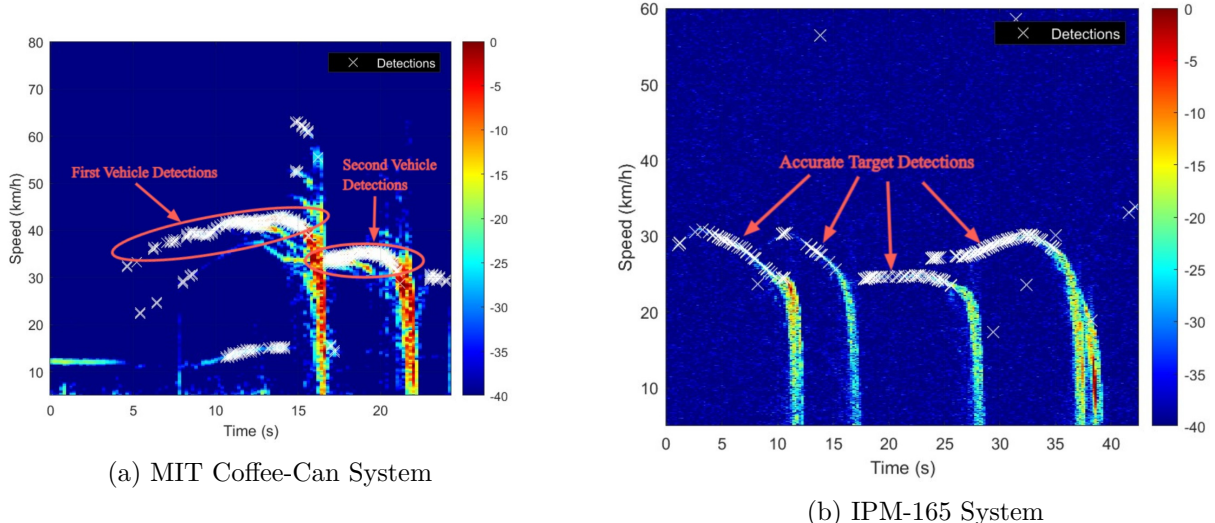


Figure 5.16: Comparison of the CA-CFAR Algorithm Performed on Recordings of Multiple Targets from Both Systems

5.4 Discussion

The tests conducted were designed to assess the feasibility of integrating these low-cost radar systems into a traffic-calming device capable of acting in real-time to alert motorists to the speeds they are travelling in a low-traffic environment. To this end, it was necessary to understand the detectable range limits of both of these devices, as well as to investigate if there was a change in performance when tested using varying motion profiles. The uncontrolled tests also aimed to simulate real-world

scenarios containing multiple vehicles moving at unpredictable speeds, to understand if the devices could produce the same level of performance in a more challenging environment. These factors would determine whether a trade-off exists between low-cost systems and the available performance necessary to be used in the application described. This fact would dictate whether widespread integration of low-cost systems would be preferable compared to the more expensive, commercially available products.

In order to evaluate this, each radar device had to be matched with the normalisation technique that best suited its recording characteristics. It was found that the MIT Coffee-Can system best suited N3 normalisation whereas the IPM-165 system best suited N1 normalisation, resulting in the spectrogram plots seen in the sections above. Once this was completed, the variables for the CA-CFAR algorithm had to be tailored to each device to ensure optimal target detection abilities.

Having completed this, it was possible to analyse the results and draw some conclusions.

5.4.1 Speed Estimation Performance

The performance in speed estimation abilities varied greatly between the two systems. The MIT Coffee-Can system demonstrated superior adaptability to varying speed profiles, producing consistently clear targets with a high SNR. Further, in most of the tests, the detection time that this system is capable of exceeded 10 s, as identified by the time where the SNR present was over 15 dB. This can be seen in Fig. 5.1, where for even the fastest speed, the detection time was still 10 s. A long detection time is preferable as it would allow enough time for a traffic-calming device to display the vehicle's speed before it travels past the device, ensuring that the driver would be alerted. This was consistent with the varying speed tests seen in Fig. 5.4, which both displayed a detection time of around 7 s.

The IPM-165 radar device faced challenges in maintaining speed accuracy. It performed better for slow target speeds, managing just under 60 s for the slow speed test of the Bakkie as seen in Fig. 5.2a. However, as the speeds increased its detection time decreased rapidly to only a couple of seconds in the fast test in Fig. 5.2c. Further, it only managed around 5 s of detection time in the speed-varying tests seen in Fig. 5.3. This may not provide the system with enough time to alert the driver when used in areas of faster-moving traffic, but may still have value for low-speed applications.

5.4.2 Detection Range Comparison

The detection range of the radar devices was closely linked to the detection time that they were capable of. It stands to reason that the longer a device can observe a target moving towards it, the greater the detectable distance becomes.

It is therefore no surprise that the MIT Coffee-Can performed better in this regard than the IPM-165 system. For the slow, medium and fast speed tests seen in Fig. 5.1 it achieved a detection range of 167 m, 152.7 m and 147.9 m respectively. For the explicit range test, Fig. 5.5a, it achieved a detection range of 127.8 m. This relatively low variation in detection ranges, along with the long detection times for the varying speed tests mentioned above, provided evidence that this device was able to detect targets at roughly the same distance regardless of their speed.

The IPM-165 system did not perform as consistently as the MIT Coffee-Can in this regard, although it did achieve a further detection range of 181 m in the slow speed test seen in Fig. 5.2a. As mentioned

previously, this device struggled to output data with a vehicle SNR of greater than 15 dB for a sufficiently long time, only managing a detection range of 41 m in its fast speed test. However, it managed similar detection ranges for both the medium speed test (108.5 m) and the range test conducted at a height of 1 m (82.3 m). Both these tests were conducted at around the same speed (30 km/h), which shows that there is some consistency in the results obtained which would be important for real-world applications.

The MIT Coffee-Can systems, as well as the IPM-165 system, struggled to perform when placed on the ground. This can be seen in Figs. 5.6a and 5.6b, where both radar recording produce very similar results. This was likely due to the limited line of sight available, as well as the effects of multipath obstructing the target from being detected. This test highlighted the importance of ensuring that any device integrated into a traffic-calming device would need to be positioned at least 1 m above the ground to obtain acceptable results.

5.4.3 CFAR Comparison

The CA-CFAR algorithm was applied to both systems in an attempt to identify targets in a plotted spectrogram. The effectiveness of this function varies based on the inherent characteristics of both radar systems. This resulted in the parameters of the function needing to be tailored for each of the systems in order to ensure optimal target detection with minimal false alarms.

For the MIT Coffee-Can system, a PFA of 10^{-7} , 6 guard cells and a reference window of 20 cells produced the best plots. Due to the large SNR that this system produces, targets were easily identifiable, often presenting at near the maximum intensity of 0db, a deep red colour, for the majority of their detection time. This stood out in stark contrast to the deep blue of the background, allowing for the CA-CFAR function to easily identify the target. This large SNR also allowed the PFA to be set lower, reducing the number of false detections.

The use of 6 guard cells accounted for the thickness of the target, as explained in Sec. 5.3.2. Because the target appeared thicker, indicating a larger target spread over the nearby frequencies, more guard cells were required to prevent these cells from influencing the average intensity of the reference window. This thickness also ensured that multiple detections were made in each column of the spectrogram. This ensured that the majority of detections made were true detections, minimising the impact of the false detections. This, in turn, allowed for the reference window to be set smaller which enhanced the algorithm's ability to detect smaller variations in the signal, making it more sensitive to weaker signals.

The high concentration of target signal detections, and few false detections allowed for the speed estimate of the vehicle to become more accurate. This resulted in a more exact detection range ability, improving the validity of the calculated values.

As the IPM-165 systems did not benefit from the same large SNR, a less stringent PFA of 10^{-5} needed to be set. This resulted in more false detections being declared, influencing the overall accuracy of the algorithm. However, this was necessary to ensure that enough target detections were made across the full range of the target to extend the detection time as far as possible. With the use of a digital filter, these false detections could be removed to help further isolate the signal, although this work fell outside of the scope of this investigation.

The IPM-165 system also produced a target with a far thinner frequency band, as seen in Sec. 5.3.2. This reduced the number of detections possible per column of the spectrogram, often resulting in only one or two detections being made. This, compounded by the slightly elevated number of false detections caused by the increased PFA, resulted in less accurate averages being made, which affected the uncertainty associated with the detection range.

With that said, the CA-CFAR function still managed to detect targets in recordings made by the IPM-165 system. Some of these even included very few false detections. This demonstrated that, although not as robust as the MIT Coffee-Can system, the CA-CFAR function could still be implemented to accurately identify targets for this system.

The results shown above have identified the strengths and weaknesses of the systems investigated in an attempt to understand their performance abilities and limitations. Both systems underwent the same testing procedures to obtain comparable datasets. These datasets were analysed through the use of spectrograms utilising various normalisation techniques as well through a CA-CFAR algorithm to determine whether target detection on the recorded data was possible. The conclusions drawn from these results were compiled in Sec. 6 below.

Chapter 6

Conclusion

This investigation sought to evaluate the performance of two low-cost radar systems, the MIT Coffee-Can and the IPM-165, in the application of vehicle speed detection. The motive behind this investigation was to assess whether modern, low-cost radar systems could be effectively integrated into a traffic calming device for use in low-traffic density areas such as housing complexes, schools, or university campuses. This was assessed through a series of controlled and uncontrolled tests where the detection time, detection range, and ability to adapt to varying speeds and number of vehicles were tested for each device. The results were assessed using spectrogram plots and a CA-CFAR function designed to identify targets. Further, this investigation aimed to provide insight into how experimental radar systems designed for vehicle speed detection have progressed, bridging a gap between the older, potentially outdated techniques and the advanced methodologies used in modern radar technology.

Direct comparisons were then made as per Sec. 5.4 to ascertain whether either of the systems performed well enough to warrant integration into a traffic-calming device. From this comparison, deductions could then be drawn as to whether this would be feasible when compared to the performance of already commercially available products outlined in Sec. 2.1.4.

Should the performance of these low-cost systems be below the standard set by the commercially available options, there would have to be a worthwhile trade-off between cost and performance to make a system suitable for integration into traffic-calming devices for applications in low-traffic density areas.

6.1 Coffee-Can

The MIT Coffee-Can system performed well in terms of detection range and ability to track vehicle speeds. It consistently managed to detect vehicles from around 150 m away regardless of the speed they were travelling, which would give enough time for a traffic-calming system to visually display the speed to alert the motorist.

This device also managed to produce plots with a strong SNR of around 30 dB for all tests, allowing for clear target identification. These plots were normalised using the N3 technique which set an intensity threshold based on a section of the recording which did not contain a target to which each column of data was compared to determine if a target was present. The received Doppler frequencies also had a large spread, creating a ticker target on the spectrogram plots. This all aided the CA-CFAR function in producing exceptionally accurate target detection with very few false detections once the function parameters had been tailored to the system.

This device also displayed abilities to identify targets of varying sizes. This demonstrated that the target's RCS did not significantly alter the performance of the device, making it suitable for use in areas where a variety of vehicle sizes would need to be detected.

6.2 IPM-165

The IPM-165 system produced results of varying performance. At slow speeds, it demonstrated an ability to detect targets at a further range than the MIT Coffee-Can (181.2 m compared to 167 m). However, at faster speeds, this performance dropped significantly. At an average speed of just under 50 km/h, this device was only able to detect the vehicle for two seconds, around 40 m, before the vehicle passed by. At this speed, there this would not give the traffic-calming device enough time to alert the motorist as to what speed they are travelling. This alone would make this system unsuitable for integration into areas where the maximum speed of motorists is 50 km/h.

The N1 normalisation technique, where the entire plot is normalised to the cell of the highest intensity, was most suited to the data recorded on this device. This was due to the limited SNR that the device was capable of producing which, on average, was around 10 dB. This is under the necessary benchmark of 15 dB, to assure a reasonable probability of detection. This result was further diminished by the fact that the Doppler frequency spread from the target recorded on this device was far more narrow than its counterpart. This resulted in fat thinner target detections. However, the CA-CFAR algorithm still managed adequate target detection on spectrograms where the target was visible, albeit with more false detections than desired.

6.3 Performance Comparison

From these results, it was clear that the MIT Coffee-Can had distinct performance advantages over the IPM-165 system. This was largely due to the elevated SNR level that the MIT Coffee-Can system was able to produce, making targets clearly visible for the duration of their detection time. This aided the CA-CFAR function to perform more reliably on this system, producing a higher probability of detection with fewer false detections and multiple target detections.

In this, the MIT Coffee-Can system fulfilled all of the investigation objectives as it is low-cost and able to accurately identify targets in a wide range of test scenarios. The IPM-165 system failed some of these objectives, being unable to reach the required level of accuracy during some of the tests.

6.4 Practical Implications

These results have demonstrated that a low-cost system is capable of the requirements for deployment as part of a traffic-calming device. For a total cost of R 6 317, this radar device drastically undercuts the price of the commercially available traffic-calming systems which can cost over R 50 000 per unit. However, it should be noted that this device would need additional components in order to function as a traffic-calming device, such as an LED display and microprocessor. Further, this device also produces a shorter detection range when compared to the commercial competitors which are capable of around 360 m when tested in a similar speed window.

The IPM-165 system on the other hand showed some promising results considering it is cheaper still than the MIT Coffee-Can, costing only R 221. At this exceptionally low price, it was still able to offer an acceptable level of performance at slower speeds. This indicates that this device could still find applications in low-speed vehicle detection, possibly where the aim is to simply identify target presence rather than obtain reliable speed information.

This research shows that while cost-effective experimental systems may be a viable alternative to commercially available ones, there exists a performance trade-off where both systems tested displayed limitations in detection range abilities.

6.5 Limitations and Recommendations

The focus of this study was on two low-cost radar systems, and their ability to detect vehicle speeds in a low-traffic environment. It did not consider the real-time implementation and extra components that would be necessary to create a functional traffic-calming device. It was also limited in its range of test subjects as testing pedestrians or motorbikes was not permitted as per the ethics clearance of the project. Further, no investigation into the efficacy of traffic-calming radar in slowing traffic was conducted.

The next step towards creating a functional traffic-calming device ready to be deployed would be to design a filter capable of target tracking. This would be a step beyond the CA-CFAR function and would allow for all false detections to be mitigated. Additionally, real-time target tracking would allow for speeds to be digitally displayed, which would be a crucial part of any functional device.

From this, further work is needed to automate the process of target speed detection. This would require some form of microprocessor, capable of computing real-time STFT consistently. This, combined with real-time target tracking, would then only require an LED display to fulfil all the functionality of traffic-calming radar.

6.6 Summary

In conclusion, the MIT Coffee-Can system outperformed the IPM-165 system, by fulfilling all of the requirements to make it suitable for integration into a traffic-calming device designed for low-traffic areas. It performed well in all the tests conducted, and is low-cost, although more expensive than the IPM-165.

The IPM-165 system did produce some promising results, however, its variation in performance at different speeds makes it unsuitable for use in this application. It could however be used for alternative environments with fewer demands on accuracy and detection range.

Finally, this project demonstrates that while low-cost radar systems can offer valuable insights and contributions, performance trade-offs must be carefully considered. The findings offer a strong foundation for further research in affordable radar technology and traffic management solutions.

Bibliography

- [1] A. Alive, “Traffic calming, speed calming and road safety,” <https://www.arrivealive.mobi/traffic-calming-speed-calming-and-road-safety>, 2024, accessed: September 17, 2024.
- [2] eBay Seller, “Product listing: TC-400 Portable Radar Speed Sign,” 2023, accessed: 2024-10-03. [Online]. Available: https://www.ebay.com/itm/296598426490?chn=ps&mkevt=1&mkcid=28&srsltid=AfmBOoqLMDUpw0LZ1zFx0KYZdUS6lFSkgoh1njrSL6SJr_9U39Eo0MybCL4
- [3] SupplyApp, “Led radar speed display sign - your speed,” 2023, accessed: 2024-10-03. [Online]. Available: https://supplyapp.com/led-radar-speed-display-sign-your-speed-p32no39.html?srsltid=AfmBOoq4ndjrmCWIsJMOjUxOUmAW_LtZLNBKkQGVfbvDDr6cCvwiFXgvCHU
- [4] D. Herald, “Are speed bumps causing more harm than good?” <https://www.durangoherald.com/articles/are-speed-bumps-causing-more-harm-than-good/>, 2022, accessed: September 17, 2024.
- [5] V. M. Fines, “Speed limits in south africa,” <https://viewmyfines.co.za/speed-limits-in-south-africa/>, 2024, accessed: September 30, 2024.
- [6] M. A. Richards, *Fundamentals of radar signal processing*, second edition. ed., ser. McGraw-Hill education books. New York: McGraw-Hill Education, 2014.
- [7] M. Skolnik. (2024) History of radar. Available: <https://www.britannica.com/technology/radar/History-of-radar>. [Accessed: 04 September 2024].
- [8] M. A. M. A. Richards, J. Scheer, and W. A. Holm, *Principles of modern radar*. Raleigh, NC: SciTech Pub., 2010.
- [9] J. Sánchez-Oro, D. Fernández-López, R. Cabido, A. Montemayor, and J. Pantrigo, “Radar-based road-traffic monitoring in urban environments,” *Digital signal processing*, vol. 23, no. 1, pp. 364–374, 2013.
- [10] P. J. Gómez-del Hoyo, N. del Rey-Maestre, D. Mata-Moya, M. P. Jarabo-Amores, and M. C. Benito-Ortiz, “Coherent detection and 3d tracking stages of a dvb-t based passive radar for terrestrial traffic monitoring,” *IOP Conference Series: Materials Science and Engineering*, vol. 524, no. 1, pp. 12 002–, 2019.
- [11] P. Samczynski, K. Kulpa, M. Malanowski, P. Krysik, and L. Maslikowski, “A concept of gsm-based passive radar for vehicle traffic monitoring,” in *2011 Microwaves, Radar and Remote Sensing Symposium*. IEEE, 2011, pp. 271–274.
- [12] Cybertrek, “Speed guns,” <https://cybertrek.co.za/speedguns>, 2024, accessed: September 17, 2024.
- [13] Sensortec, “Portable speed radar camera,” <https://sensortec-eu.com/product/portable-speed-radar-camera/>, 2024, accessed: September 17, 2024.

- [14] Cybertrek, “Pocket radar classic - for vehicles, rc athletes (not for ball sports),” <https://cybertrek.co.za/speedguns/pocket-radar-classic---for-vehicles-rc-athletes-not-for-ball-sports-853>, 2024, accessed: September 17, 2024.
- [15] ——, “Speedster 3 speed radar gun and screen kit with accuracy tuning fork & tripod,” <https://cybertrek.co.za/speedguns/speedster-3-speed-radar-gun-and-screen-kit-with-accuracy-tuning-fork--tripod>, 2024, accessed: September 17, 2024.
- [16] H. Security, “Bushnell velocity radar speed gun - basic,” <https://hmsecurity.co.za/product/bushnell-velocity-radar-speed-gun-basic/>, 2024, accessed: September 17, 2024.
- [17] Cybertrek, “Decatur scout 2 police quality directional handheld radar speedgun,” <https://cybertrek.co.za/speedguns/decatur-scout-2-police-quality--directional-handheld-radar-speedgun#review>, 2024, accessed: September 17, 2024.
- [18] Sensortec, “Portable speed radar camera,” <https://sensor-tec-eu.com/product/portable-speed-radar-camera/>, 2024, accessed: September 17, 2024.
- [19] N. Hardwares, “Axis 02420-001 surveillance network camera,” <https://www.networkhardwares.com/en-za/products/axis-02420-001-axis-02420001-surveillance-network-cameras-02420-001>, 2024, accessed: September 17, 2024.
- [20] Alibaba, “Signalway radar speed camera - smart traffic,” https://www.alibaba.com/product-detail/Signalway-Radar-speed-camera-Smart-traffic_1600924779994.html, 2024, accessed: September 17, 2024.
- [21] ClickMechanic, “How do speed guns and cameras work?” <https://www.clickmechanic.com/blog/how-do-speed-guns-and-cameras-work/>, 2024, accessed: September 17, 2024.
- [22] C. Keys, “What happens if a radar speed gun records you speeding?” <https://www.carkeys.co.uk/guides/what-happens-if-a-radar-speed-gun-records-you-speeding>, 2024, accessed: September 17, 2024.
- [23] V. Traffic, “Viasis speed displays,” <https://www.viatraffic.com/en/products/viasis-speed-displays/>, 2024, accessed: September 17, 2024.
- [24] TraffiCalm, “Radar speed signs,” <https://trafficalm.com/products/radar-speed-signs>, 2024, accessed: September 17, 2024.
- [25] A. G. Hagargund, R. Udayshankar, and N. Rashmi, “Radar based cost effective vehicle speed detection using zero cross detection,” *International Journal of Electrical, Electronics and Data Communication*, vol. 1, no. 9, pp. 1–5, 2013.
- [26] J. Fang, H. Meng, H. Zhang, and X. Wang, “A low-cost vehicle detection and classification system based on unmodulated continuous-wave radar,” in *2007 IEEE Intelligent Transportation Systems Conference*. IEEE, 2007, pp. 715–720.

- [27] L. Xu, J. Lien, and J. Li, “Doppler–range processing for enhanced high-speed moving target detection using lfmcw automotive radar,” *IEEE Transactions on Aerospace and Electronic Systems*, vol. 58, no. 1, pp. 568–579, 2022.
- [28] F. Alimenti, F. Placentino, A. Battistini, G. Tasselli, W. Bernardini, P. Mezzanotte, D. Rascio, V. Palazzari, S. Leone, A. Scarponi, N. Porzi, M. Comez, and L. Roselli, “A low-cost 24ghz doppler radar sensor for traffic monitoring implemented in standard discrete-component technology,” in *2007 European Radar Conference*, 2007, pp. 162–165.
- [29] R. Rasshofer and E. Biebl, “A direction sensitive, integrated, low cost doppler radar sensor for automotive applications,” in *1998 IEEE MTT-S International Microwave Symposium Digest (Cat. No.98CH36192)*, vol. 2, 1998, pp. 1055–1058 vol.2.
- [30] P. Heide, V. Magori, and R. Schwarte, “Coded 24 ghz doppler radar sensors: a new approach to high-precision vehicle position and ground-speed sensing in railway and automobile applications,” in *Proceedings of 1995 IEEE MTT-S International Microwave Symposium*, 1995, pp. 965–968 vol.2.
- [31] I. W. Museums, “What was the dowding system?” 2024, accessed: 2024-10-01. [Online]. Available: <https://www.iwm.org.uk/history/what-was-the-dowding-system>
- [32] ——. (2024) *What Was The 'Dowding System'?* [Online]. Available: <https://www.iwm.org.uk/history/what-was-the-dowding-system>. [Accessed: 04 September 2024].
- [33] ——. (2024) *How Radar Changed The Second World War* [Online]. Available: <https://www.iwm.org.uk/history/how-radar-changed-the-second-world-war>. [Accessed: 04 September 2024].
- [34] MVRSimulation, “An-mpq-39.us.camo,” <https://www.mvrsimulation.com/model/mpq-39uscamo>, 2024, accessed: 09 10, 2024.
- [35] Wikipedia, “An/fps-16 instrumentation radar,” https://en.wikipedia.org/wiki/AN/FPS-16_Instrumentation_Radar, 2024, accessed: 09 10, 2024.
- [36] I. Petrovic and M. Kankaras, “A hybridized it2fs-dematel-ahp-topsis multicriteria decision making approach: Case study of selection and evaluation of criteria for determination of air traffic control radar position,” *Decision Making. Applications in Management and Engineering (Online)*, vol. 3, no. 1, pp. 146–164, 2020.
- [37] J. Xia, X. Lu, and W. Chen, “Multi-channel deconvolution for forward-looking phase array radar imaging,” *Remote Sensing*, vol. 9, no. 7, 2017. [Online]. Available: <https://www.mdpi.com/2072-4292/9/7/703>
- [38] A. Franczyk, J. Bala, and M. Dwornik, “Monitoring subsidence area with the use of satellite radar images and deep transfer learning,” *Sensors*, vol. 22, no. 20, pp. 7931–, 2022.
- [39] Y. Peng, Y. Wu, C. Shen, H. Xu, and J. Li, “Detection performance analysis of marine wind by lidar and radar under all-weather conditions,” *Remote Sensing*, vol. 16, no. 12, 2024. [Online]. Available: <https://www.mdpi.com/2072-4292/16/12/2212>

- [40] M. Caffa, F. Biletti, and R. Maggiora, “Binary-phase vs. frequency modulated radar measured performances for automotive applications,” *Sensors (Basel, Switzerland)*, vol. 23, no. 11, pp. 5271–, 2023.
- [41] M. Ahmed, H. Chen, and N. Fisher, “Demo abstract: Multi-modal scheduling of radar-based cruise control system,” in *21st IEEE Real-Time and Embedded Technology and Applications Symposium*, 2015, pp. 331–331.
- [42] A. H. Eichelberger and A. T. McCartt, “Toyota drivers’ experiences with dynamic radar cruise control, pre-collision system, and lane-keeping assist,” *Journal of safety research*, vol. 56, pp. 67–73, 2016.
- [43] S. e. Song, S. d. Kim, Y. s. Jin, D. h. Lee, and J. h. Lee, “A new proposal of smart lighting system based on radar and camera sensors for smart city,” in *2018 International Conference on Computational Science and Computational Intelligence (CSCI)*. IEEE, 2018, pp. 1448–1449.
- [44] P. Nimac, A. Krpič, B. Batagelj, and A. Gams, “Pedestrian traffic light control with crosswalk fmcw radar and group tracking algorithm,” *Sensors (Basel, Switzerland)*, vol. 22, no. 5, pp. 1754–, 2022.
- [45] T. Global, “What is a smart city?” 2023, accessed: 2024-10-03. [Online]. Available: <https://www.twi-global.com/technical-knowledge/faqs/what-is-a-smart-city/#SmartCityDefinition>
- [46] RadarSign, “Tc-400 portable radar speed sign,” 2023, accessed: 2024-10-03. [Online]. Available: <https://www.radarsign.com/products/tc-400-portable-radar-speed-sign/>
- [47] HSAT, “Radar satellite basics,” 2024, accessed: 2024-09-30. [Online]. Available: <https://hsat.space/satellites-radar-satellite-basics/>
- [48] W. contributors, “Speed of light — wikipedia, the free encyclopedia,” 2024, accessed: 2024-10-01. [Online]. Available: https://en.wikipedia.org/wiki/Speed_of_light
- [49] Elevise, “Radar speed equation - physics gcse,” 2024, accessed: 2024-09-30. [Online]. Available: <https://www.elevise.co.uk/gap6j.html>
- [50] R. Cafe, “Frequency bands - rf cafe,” 2023, accessed: 2024-10-03. [Online]. Available: <https://www.rfcafe.com/references/electrical/freq-bands.htm>
- [51] CopRadar, “Doppler radar - the doppler effect,” 2024, accessed: 2024-09-30. [Online]. Available: <https://copradar.com/chaps/chapt3/ch3d1.html>
- [52] T. Schipper, J. Fortuny-Guasch, D. Tarchi, L. Reichardt, and T. Zwick, “Rcs measurement results for automotive related objects at 23-27 ghz,” in *5th European Conference on Antennas and Propagation (EUCAP)*. Karlsruhe, Germany: European Microwave Signature Laboratory, Joint Research Center of the European Commission, 2011, pp. 683–686. [Online]. Available: [file:///mnt/data/ERMTGSRR\(17\)030005_RCS_of_vehicles_24GHz.pdf](file:///mnt/data/ERMTGSRR(17)030005_RCS_of_vehicles_24GHz.pdf)
- [53] ResearchGate, “Different types of radars for detection, identification, and tracking of aerial vehicles,” 2023, accessed: 2024-10-03. [Online]. Available: <https://www.researchgate.net>

net/figure/Different-types-of-radars-for-detection-identification-and-tracking-of-aerial-vehicles_fig1_360772107

- [54] Antesky, “9m buy huge old big large satellite dish,” 2024, accessed: 2024-10-01. [Online]. Available: <https://www.antesky.com/project/9m-buy-huge-old-big-large-satellite-dish/>
- [55] COMSOL, “Designing a butler matrix beamforming network with rf modeling,” 2024, accessed: 2024-10-01. [Online]. Available: <https://www.comsol.com/blogs/designing-a-butler-matrix-beamforming-network-with-rf-modeling>
- [56] J. Allen, “Short term spectral analysis, synthesis, and modification by discrete fourier transform,” *IEEE transactions on acoustics, speech, and signal processing*, vol. 25, no. 3, pp. 235–238, 1977.
- [57] S. Braun, “Windows,” in *Encyclopedia of Vibration*, S. Braun, Ed. Oxford: Elsevier, 2001, pp. 1587–1595. [Online]. Available: <https://www.sciencedirect.com/science/article/pii/B0122270851000527>
- [58] T. Tsai, “Detect peaks with the cfar algorithm,” 2024, accessed: 2024-10-03. [Online]. Available: <https://tsaith.github.io/detect-peaks-with-cfar-algorithm.html>
- [59] M. OpenCourseWare, “Build a small radar system capable of sensing range, doppler, and synthetic aperture radar imaging,” 2011, accessed: 2024-10-03. [Online]. Available: <https://ocw.mit.edu/courses/res-ll-003-build-a-small-radar-system-capable-of-sensing-range-doppler-and-synthetic-aperture-radar-imaging-pages/projects/>
- [60] G. Charvat, “Mit iap 2011 laptop based radar: Block diagram, schematics, bill of material, and fabrication instructions,” [https://ocw.mit.edu/courses/res-ll-003-build-a-small-radar-system-capable-of-sensing-range-doppler-and-synthetic-aperture-radar-imaging-january-iap-2011/12391162c1f8fe2b3e2844a8c5794fde_MITRESLL003IAP11projn.pdf](https://ocw.mit.edu/courses/res-ll-003-build-a-small-radar-system-capable-of-sensing-range-doppler-and-synthetic-aperture-radar-imaging-january-iap-2011/12391162c1f8fe2b3e2844a8c5794fdeMITRESLL003IAP11projn.pdf), 2011.
- [61] A. Fenn, “Antenna design for the laptop radar project,” [https://ocw.mit.edu/courses/res-ll-003-build-a-small-radar-system-capable-of-sensing-range-doppler-and-synthetic-aperture-radar-imaging-january-iap-2011/fa61f02356be7fc88142b258d031110_MITRESLL003IAP11lec02.pdf](https://ocw.mit.edu/courses/res-ll-003-build-a-small-radar-system-capable-of-sensing-range-doppler-and-synthetic-aperture-radar-imaging-january-iap-2011/fa61f02356be7fc88142b258d031110MITRESLL003IAP11lec02.pdf), 2011.
- [62] R. Semiconductor, “Baxxdd0t, baxxcc0t, baxxcc0fp series: Power management,” <https://www.rohm.com/datasheet/BAxxDD0T,BAxxCC0T>, 2013, accessed: 2024-10-03.
- [63] L. Manufacturer, “Lm358 weak signal amplifier module datasheet,” <https://datasheet.lm358.com>, 2023, accessed: 2024-10-03.
- [64] I. GmbH, “Ipm-165 analog radar module datasheet,” <https://www.innosent.de/products/ipm-165/>, 2017, accessed: 2024-10-03.
- [65] DigiKey, “Ba05t - rohm semiconductor,” 2023, accessed: 2024-10-03. [Online]. Available: <https://www.digikey.co.za/en/products/detail/rohm-semiconductor/BA05T/658215>
- [66] AliExpress, “Electronics product - aliexpress,” 2023, accessed: 2024-10-03. [Online]. Available: <https://www.aliexpress.com/item/1005003318815976.html>

- [67] DigiKey, “Ipm-165 analog radar module - innosent,” 2023, accessed: 2024-10-03. [Online]. Available: <https://www.digikey.co.za/en/product-highlight/i/innosent/ipm-165-analog-radar-module>
- [68] K. Yan, W. Jin, Y. Huang, Z. Li, P. Song, and L. Huang, “Deep anomaly detection with attention (dada): A novel approach for identifying multipath interference in radar signals,” *IET Signal Processing*, vol. 2024, no. 1, p. 5026821, 2024. [Online]. Available: <https://ietresearch.onlinelibrary.wiley.com/doi/abs/10.1049/2024/5026821>

.1 Appendix A

GA	Requirement	Justification and section in the report
1	Problem-solving	Problem-solving ability was used to identify, outline and proceed to investigate the problem at hand as evidenced by Sections 1.4, 1.5, 1.6, and 1.7. These sections demonstrate an ability to approach a problem logically, breaking it down into pieces that can be handled individually.
4	Investigations, experiments and data analysis	As seen in Chapters 3, experiments were designed to validate the performance of each system. Chapter 4 then provides the analysis thereof, outlining the successes and limitations of each system. Further, Chapter 2 contains a detailed literature review placing these systems in the context of radar systems. This is followed by Theory Development which provides the mathematical and functional implications of radar.
5	Use of engineering tools	MATLAB was exclusively used for processing, data visualisation and analysis, as seen in Chapters 3 and 5. Audacity was used for the recording of the radar signals. Further, GitHub was used to store all necessary code.
6	Professional and technical communication (Long report)	Weekly meetings were held with Dr Abdul Gaffar to discuss aspects of the project that needed attention. Further, MS Teams was used as a secondary channel of communication. Further, the structure of this report is logical, equations are typed and numbers and all figures are inserted correctly. All figures and tables are referred to in the text and all acronyms clearly defined.
8	Individual work	Chapter 2 is evidence of individual research that was conducted in order to understand the topic. Further, all Matlab code, including the STFT and CA-CFAR functions were created from scratch. Further, this report was not plagiarised as per the signed declaration.
9	Independent learning ability	As per the initial submission on Amathuba, this report has a Turnitin of 11% which demonstrates independent work was conducted. Further, Chapter 6 represents the culmination of the full report and the in-depth understanding of the topic that has been developed throughout.

Table 1: Appendix A - GA Requirements

.2 Appendix B

The following are the spectrograms from the tests not shown above. They are here to show the consistency with the performance obtained from both systems, and the CA-CFAR function performed on each.

.2.1 MIT Coffee-Can Spectrograms

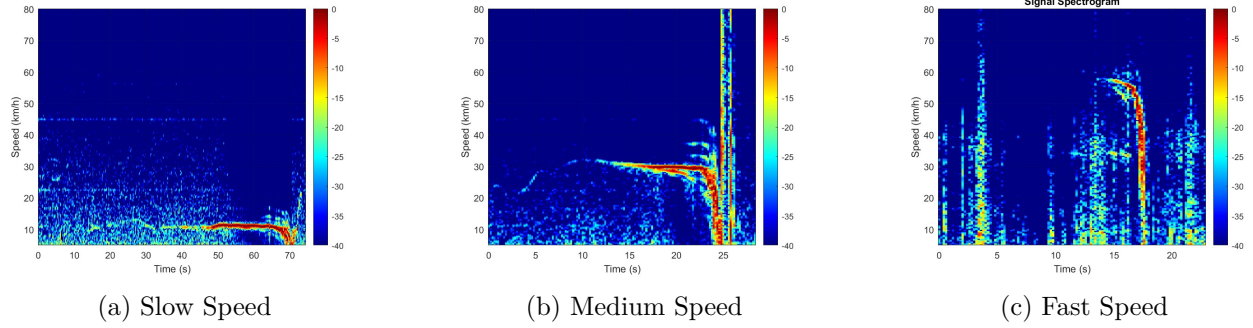


Figure 1: MIT Coffee-Can System Tracking the Car at Set Speeds

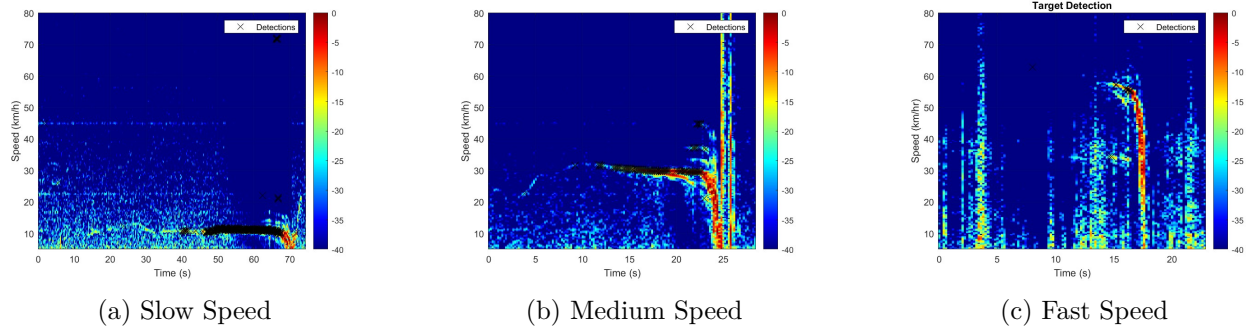


Figure 2: MIT Coffee-Can System Tracking the Car at Set Speeds

.2.2 IPM-165 System Spectrograms

2. Appendix B

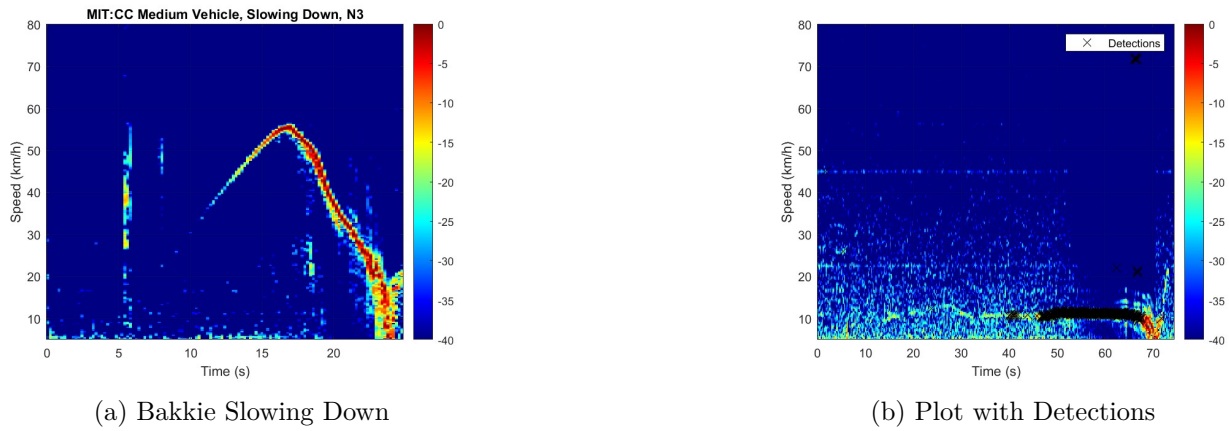


Figure 3: MIT Coffee-Can System Tracking the Bakkie Under Braking

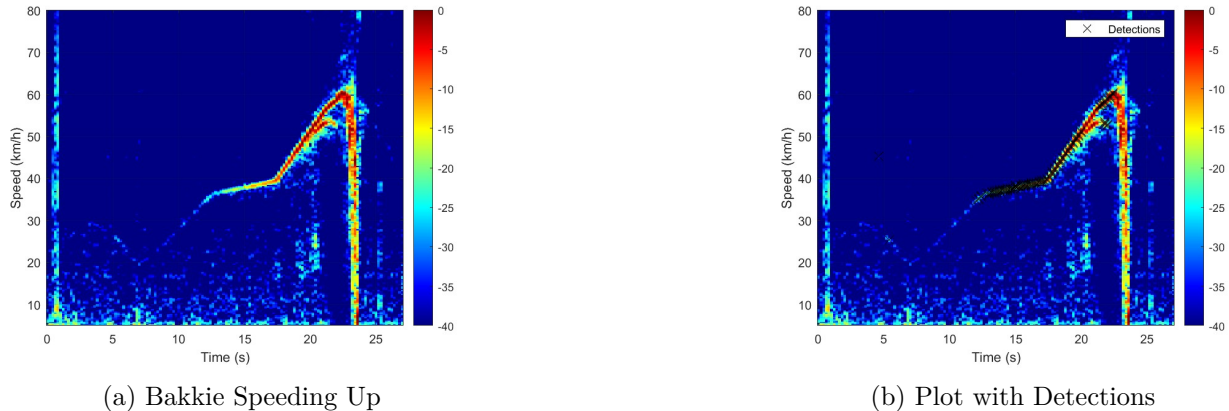


Figure 4: MIT Coffee-Can System Tracking the Bakkie While Accelerating

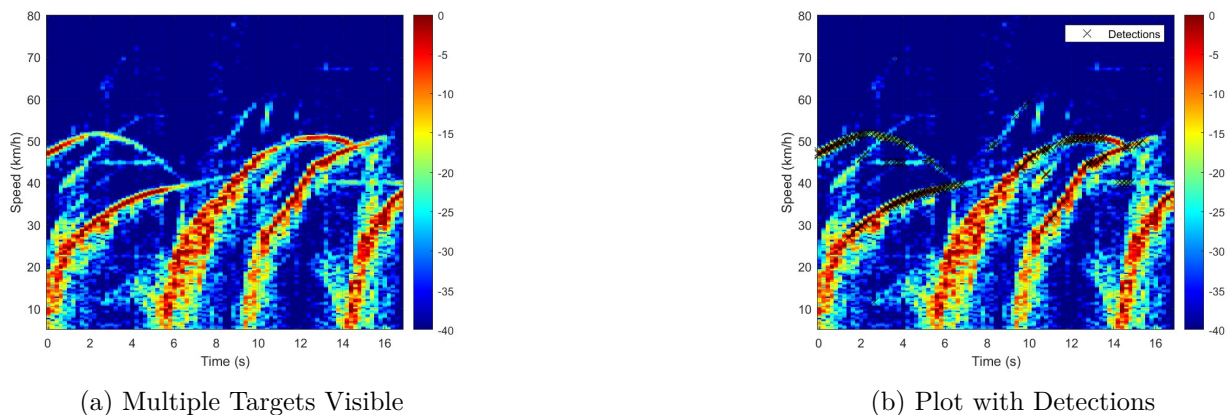


Figure 5: MIT Coffee-Can System Tracking Multiple Targets

2. Appendix B

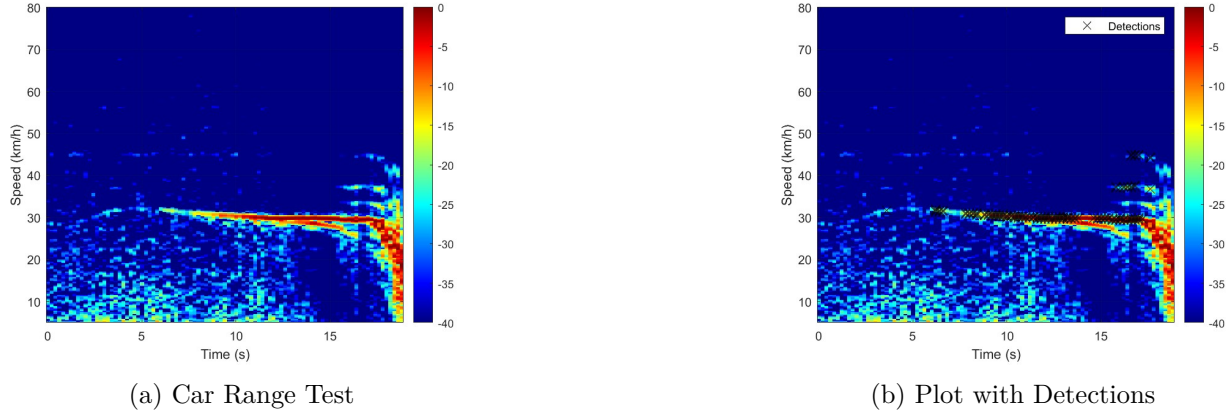


Figure 6: MIT Coffee-Can System Range Test Using the Car

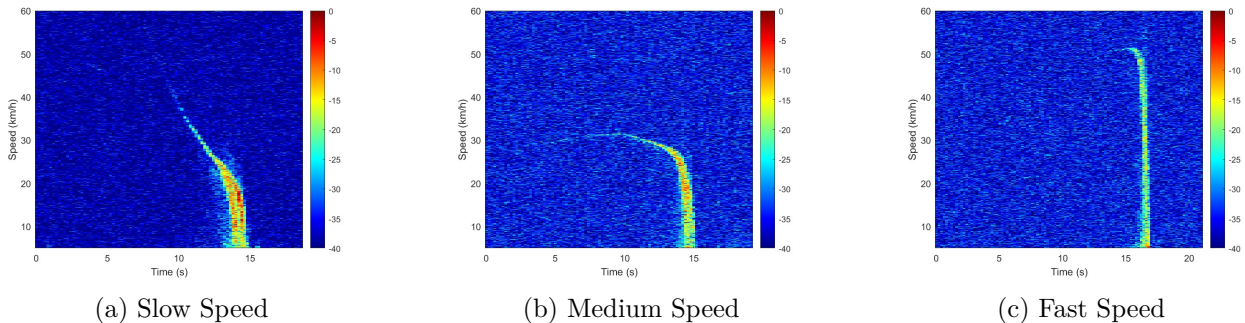


Figure 7: IPM-165 System Tracking the Car at Set Speeds

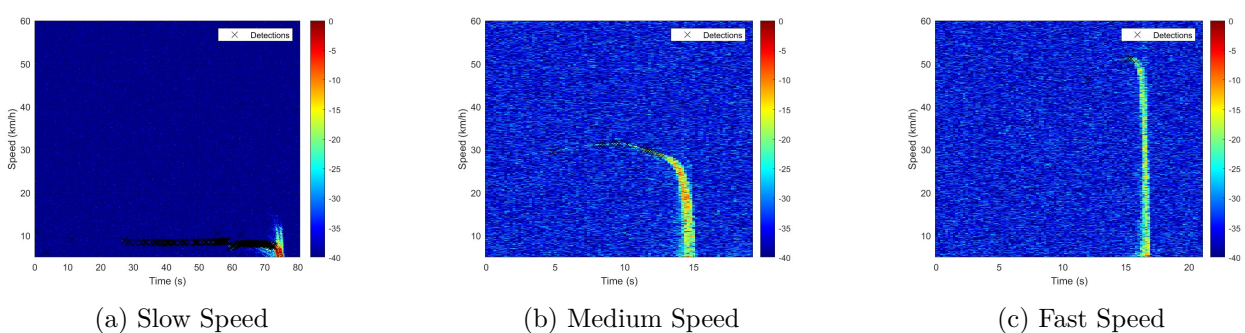


Figure 8: IPM-165 System Tracking the Car at Set Speeds

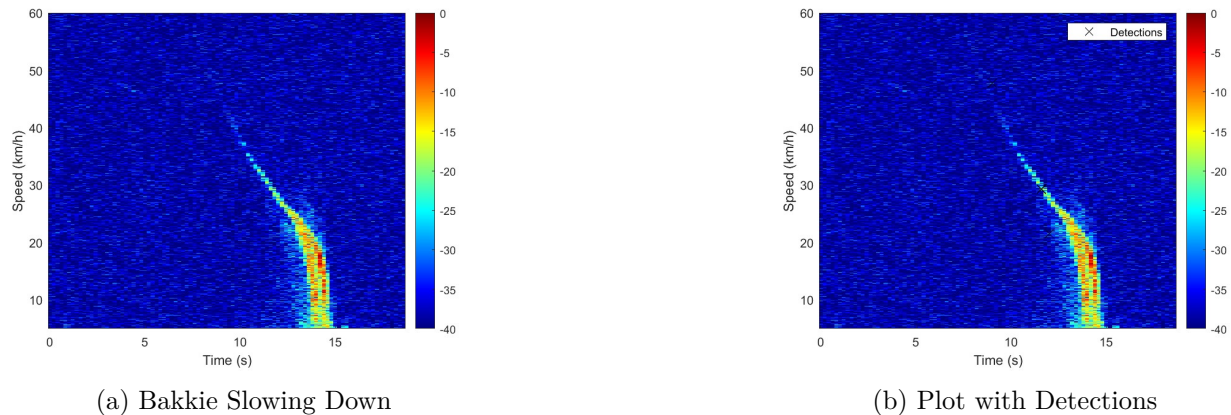


Figure 9: IPM-165 System Tracking the Bakkie Under Braking

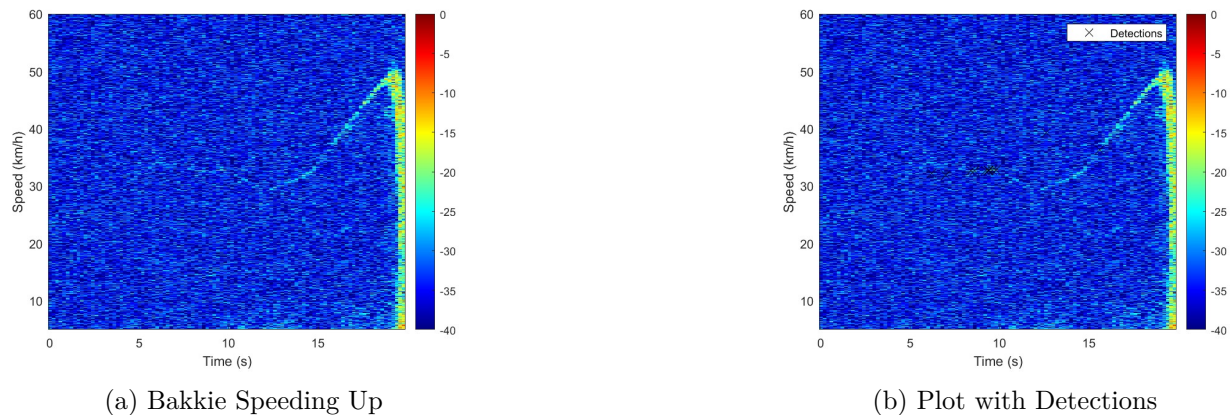


Figure 10: IPM-165 System Tracking the Bakkie While Accelerating

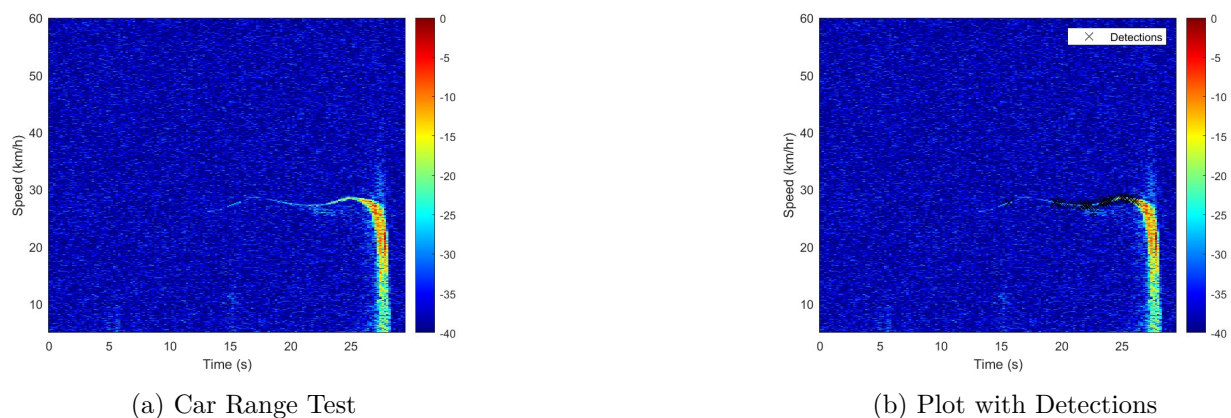


Figure 11: IPM-165 System Range Test Using the Car

.3 Appendix C

The following are screenshots of the questions that were asked to ChatGPT, and the responses given.

The screenshot shows a ChatGPT interface. At the top, there is a table titled "10.1 Appendix A" with two columns: "GA" and "Requirement". The requirements listed are: Problem-solving, Investigations, experiments and data analysis, Use of engineering tools, Professional and technical communication (Long report), Individual work, and Independent learning ability. Below the table, a user message asks, "could you please convert the image into a latex table". A response message follows, stating, "Here's how you can convert the table from the image into LaTeX code:" and provides the corresponding LaTeX code:

```

\begin{table}[htbp]
\centering
\begin{tabular}{|c|l|l|} \hline
& Requirement & Justification and section in the report \\ \hline
1 & Problem-solving & \\ \hline
4 & Investigations, experiments & \\ \hline
5 & Use of engineering tools & \\ \hline
6 & Professional and technical communication (Long report) & \\ \hline
8 & Individual work & \\ \hline
9 & Independent learning ability & \\ \hline
\end{tabular}
\caption{Appendix A - GA Requirements}
\label{tab:GA_requirements}
\end{table}

```

Figure 12: Use of ChatGPT

3. Appendix C

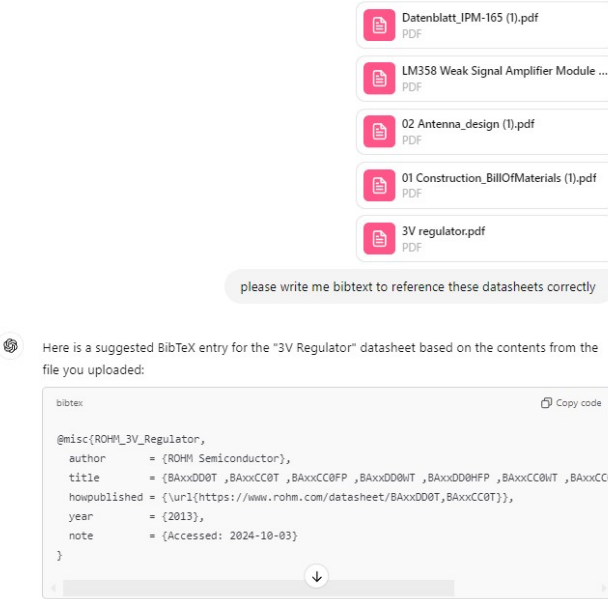
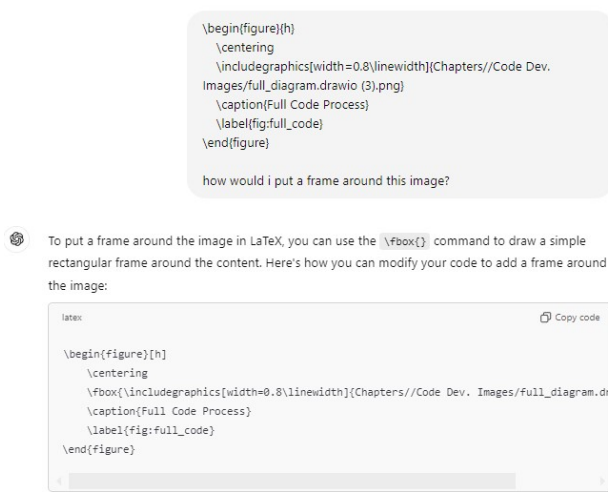


Figure 13: Use of ChatGPT



This will place a rectangular frame around the image. You can adjust the frame thickness or add padding inside the frame using additional commands if needed, such as `\setlength{\fboxsep}{value}` and `\setlength{\fboxrule}{value}`. For example:

Figure 14: Use of ChatGPT

3. Appendix C

Continuous STFT

$$STFT = X(\tau, \omega) = \int_{-\infty}^{\infty} x(t)w(t - \tau)e^{-i\omega t}dt$$

Discrete STFT

$$STFT = X(m, \omega) = \sum_{n=-\infty}^{\infty} x_n w_{n-m} e^{-i\omega t_n}$$

please write the discrete stft in latex for me

Here is the discrete Short-Time Fourier Transform (STFT) formula written in LaTeX:

$$STFT(m, \omega) = \sum_{n=-\infty}^{\infty} x[n]w[n - m]e^{-i\omega n}$$

This formula represents the discrete STFT, where $x[n]$ is the discrete input signal, $w[n - m]$ is the windowing function shifted by m , and the exponential term accounts for the Fourier transform.

please write them it in latex

Here is how you can write the continuous and discrete STFT in LaTeX:

```
latex
\textbf{Continuous STFT}
\[
STFT(\tau, \omega) = X(\tau, \omega) = \int_{-\infty}^{\infty} x(t)w(t - \tau)e^{-i\omega t}dt
\]

\textbf{Discrete STFT}
\[
STFT(m, \omega) = \sum_{n=-\infty}^{\infty} x[n]w[n - m]e^{-i\omega n}
\]
```

Figure 15: Use of ChatGPT

how do i ensure that my referencing order starts from 1 in the order in which they appear on latex?

To ensure that the references in your LaTeX document are numbered in the order in which they appear, you should follow these steps:

1. Use a proper citation management package: The most common package for managing references in LaTeX is `biblatex` or `natbib` for BibTeX. However, the simplest option for sequentially numbered citations is `biblatex`.
2. Insert citations in the correct order: The references will automatically be numbered based on the order in which you use the `\cite{}` command in your document. Be sure to insert the `\cite{}` commands in the order in which you want the references to appear in the text.
3. Ensure you are using the correct bibliography style: You can ensure correct numbering by using a numeric style in your bibliography, such as `numeric` or `plain`.

Here's an example of how to set this up:

```
latex
\documentclass{article}
\usepackage[style=numeric]{biblatex} % Use numeric style
\addbibresource{references.bib} % Your .bib file

\begin{document}

This is the first citation \cite{author2023firstpaper}, and here is the second citation \c

\printbibliography
\end{document}
```

Message ChatGPT

Figure 16: Use of ChatGPT

$$X(f) = \sum_{n=-\infty}^{+\infty} x[n] e^{-j 2\pi f n T_s}$$

please use thhis form of the dtft and write it in latex for me

Here's the DTFT formula from the image you provided in LaTeX form:

```
X(f) = \sum_{n=-\infty}^{+\infty} x[n] e^{-j 2 \pi f n T_s}
```

Where:

- $X(f)$ is the DTFT of the signal.
- $x[n]$ is the discrete-time signal.
- f is the frequency in Hz.
- T_s is the sampling period (1/sampling frequency).

Let me know if you'd like to adjust anything!

Figure 17: Use of ChatGPT

.4 GitHub

You can access the full repository containing the code and documentation for this project at the following GitHub link: [EEE4022S_Thesis_WSSCAR008 Repository](#).